SURVIVABILITY OF *D. RADIODURANS*, HALOBACTERIUM *SP. NRC-1*, CYANOBACTERIUM *CHROOCOCCIDIOPSIS SP. 029*, AND *ESCHERICHIA COLI* BACTERIA IN THEORIZED ATMOSPHERIC CONDITIONS ON THE SURFACE OF ANCIENT MARS

by

Mary Ewell

A Dissertation
Submitted to the
Graduate Faculty
of
George Mason University
in Partial Fulfillment of
The Requirements for the Degree
of
Doctor of Philosophy
Physical Sciences

Committee:

Michael E Summers — Dr. Michael Summers, Dissertation Director

B. Joseph Lieb — Dr. B. Joseph Lieb, Committee Member

Harold A. Geller — Dr. Harold Geller, Committee Member

Joseph C Weingartner — Dr. Joseph Weingartner, Committee Member

Timothy C Born — Dr. Timothy Born, Committee Member

John Schreifels — Dr. John Schreifels, Program Chairperson

Richard Diecchio — Dr. Richard Diecchio, Associate Dean for Academic and Student Affairs, College of Science

Vikas Chandhoke — Dr. Vikas Chandhoke, Dean, College of Science

Date: 12-3-10 — Fall Semester 2010
George Mason University
Fairfax, VA

Survivability of *D. radiodurans*, *Halobacterium sp. NRC-1* and its mutants, Cyanobacterium *Chroococcidiopsis sp. 029*, and *Escherichia coli* bacteria in theorized atmospheric conditions on the surface of Ancient Mars

A dissertation submitted in partial fulfillment of the requirements for the degree of Doctor of Philosophy at George Mason University

By

Mary Ewell
Master of Science
George Mason University, 2000
Bachelor of Science
George Mason University, 1994

Director: Dr. Michael Summers, Professor
Department of Physics and Astronomy

Fall Semester 2010
George Mason University
Fairfax, VA

Dedication

I dedicate this dissertation to my mother, Jayne D. Szaz, and my father, Dr. Z. Michael Szaz, who instilled in their children a desire to learn.

Acknowledgments

I would like to thank Dr. Joseph Lieb whose help and guidance getting started and working with the atmospheric model was invaluable.

I would like to thank my husband, Andrew Woodcock, for his endless patience and diligent housework that allowed me time to finish this work.

I would like to thank Dr. Harold Geller for always being ready to help and encourage me through this work.

Finally, I would like to thank my adviser, Dr. Michael Summers, who patiently waited and never pushed too hard while I worked on this thesis part-time.

Table of Contents

List of Tables

List of Figures

Abstract

SURVIVABILITY OF *D. RADIODURANS*, *HALOBACTERIUM SP. NRC-1* AND ITS MUTANTS, CYANOBACTERIUM *CHROOCOCCIDIOPSIS SP. 029*, AND *ESCHERICHIA COLI* BACTERIA IN THEORIZED ATMOSPHERIC CONDITIONS ON THE SURFACE OF ANCIENT MARS

Mary Ewell, PhD

George Mason University, 2010

Dissertation Director: Dr. Michael Summers

Life on the Martian surface today is unlikely due to its thin atmosphere, although the possibility of extinct and subsurface life is possible and therefore, life on ancient Mars is an open question. Martian morphology and mineralogy indicate that Mars had surface water and active volcanoes in the past, which together imply warmer climates. Sulfur species have been linked to an increased greenhouse effect and offer additional UV shielding. Previous studies have used pulsed inputs of atmospheric sulfur species modeling the ancient Martian surface during periods of volcanic eruptions but leaving open the effect of atmospheric sulfur species during quieter periods of surface outgassing. Using surface mineralogy data from landers and orbiters, total volcanic sulfur deposition was estimated and an averaged upward flux for sulfur species found for the lifetime of volcanic activity on Mars. Using a one-dimensional photochemical model, concentrations of plausible atmospheric constituents including sulfur species were calculated to model different atmospheric conditions in Martian

history. The amount of UV shielding obtained from the models determine UV survivability of Earth life. Earth bacteria *D. radiodurans* and cyanobacteria *Chroococcidiopsis sp. 029* and an Archaean halophile *sp. NRC-1* are shown as likely UV survivors in the modeled 350mbar atmosphere but questionable survival is found in thinner modeled atmospheres. Finally, reported surface data was used to determine likely surface locations on Mars for chosen microorganisms.

Chapter 1: Introduction of Problem

Mars surface mineralization data are rapidly expanding with the use of orbiting satellites and ground based rovers, see Appendix for listing of orbiters and their instruments. Minerals indentified are then tied to varying dated terrains and geologists can determine the environment in which the minerals formed. With these data, the atmospheric history of Mars is also emerging, as mineral growth is dependent upon the ambient climate. Using the geological data constraints to constrain atmospheric parameters and likely constituents, simulations were run to determine plausible atmospheric composition during the different mineralization epochs of Martian history. This allowed determination of UV shielding available in the early Martian climate. With a better understanding of the surface mineralization and plausible atmosphere constituents in ancient Mars, more knowledgeable assessments of possible extant or extinct life on the surface or near surface of Mars can be inferred.

Radiodurans, desiccant tolerant cyanobacteria, halophiles, and sulfate-reducing bacteria have been suggested to be likely homologues to bacteria that could survive in the past in or on the Martian regolith [12,15,19]. *D. Radiodurans* ability to withstand high levels of UV radiation, similar to UV dosages on the present day Martian surface, make these bacteria one of the few groups of bacteria present on Earth to be plausible Martian survivors if only less than 1 day. Certain cyanobacteria have been examined because of their ability to withstand extreme climates and desiccation. These bacteria would likely only survive within a rock pore, more than 1mm in depth [20] to shield it from the most intense UV flux on the Martian surface. Halophiles flourish in extremely salty environments. Squyers et al. [21] have examined the Eagle Crater in

Meridiani Planum and attribute the geology to be indicative of episodic inundation by shallow surface water, evaporation, and desiccation. Clark et al.[20] state that even now if the outcrop were to become infiltrated by liquid H_2O, it is predicted that [the] water would become hypersaline with soluble sulfates and chlorides. This high salinity environment would be ideal for halophiles that survive in such waters as the Dead Sea on Earth. The one cautionary note concerns the amount of free Cr. Although free chromium atoms are not likely to be extractable from the minerals, if they were, they would likely be toxic to even halophiles [20].

Using the two extremophiles, a cyanobacterium, and a reference bacterium E. coli one can analyze the likelihood of their survival using the model results for UV surface dosage for different epochs in Martian history obtained from the mineralization data of the various terrains. Although this will determine only the surface flux and therefore the most inhospitable environment for the life, it would stand as a lower bound for potential habitability with regard to UV flux since speculated life on Mars often includes additional protection either living in rocks or buried in the Martian regolith.

Chapter 2: Background-Martian Geological History

Martian atmospheric history has until recently not been well defined and many unsolved problems with atmospheric scenarios still exist. With current and recent instruments in orbit (Mars Reconnaissance Orbiter (MRO), Mars Express (ME), Mars Global Surveyor(MGS), and the Mars Odyssey (MO)) and on the surface of Mars (Mars Exploration Rover Mission (MER): Spirit and Opportunity rovers and Mars Scout Program Phoenix rover) much new geological information has been gathered and thus, by proxy, constraints on ancient atmospheric constituents.

The geological ages of Martian terrains have been estimated by the crater analysis method developed over the past several decades. Surface dating from crater analysis has developed from initial controversial measurements in the 1960s and 1970s to a robust analytical tool [22–24]. Todays surface dating has been improved by many additional analysis methods, such as the Moon/Mars cratering ratio [25–27]. The lack of tectonic activity on the planetary surface of Mars aids in terrain dating, as resurfacing must be accomplished by surface activity and not tectonics. Since the Martian surface is not recycled as is the Earths surface by plate subduction, inspecting crater impacts and other surface alterations throughout Martian history can help date surface terrains. The analyses of Martian meteorites also provide age and composition of the surface of Mars during different epochs to which the meteorites have been dated.

Relative dating data are gathered by crater analysis. Cross cutting features and erosion help geologists determine the order of formation of surface features which

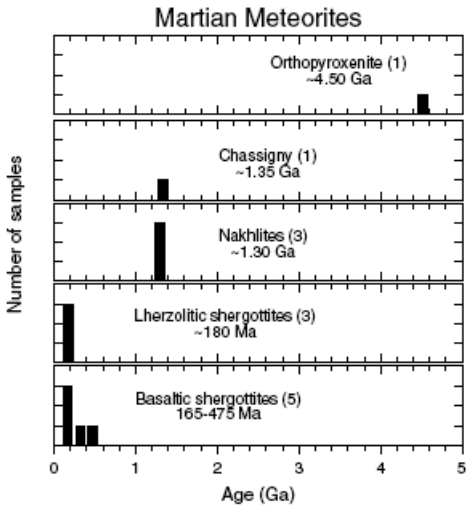

Figure 2.1: Martian Meteorite Ages from the review by Nyquist *et al.*, 2001

then aid in the determination of the absolute age for a particular terrain. Martian historical epochs have been analyzed in terms of crater density. The size and density of craters are then mapped to likely time periods through suppositions about the crater density on other planets and moons, when compared to Mars, and adjusted for its size and position in the solar system.

Meteorites are gathered and separated into groups according to composition and can be tentatively matched to likely surface origin locations. Dating of the meteorites is accomplished by radiometric analysis and crystallization after ejection shock analysis. Figure 2.1 shows analysis of meteorite families and age from Nyquist *et al.* [28].

Through these analyses of the surface of Mars geologists have separated the evolutionary history of the planet into three epochs determined by differentiated terrain: Noachian, Hesperian, and Amazonian, see Figure 2.3. The surface of Mars can be separated into the Northern Lowlands and the Southern Highlands, see Figure 2.2 on page 5. These regions also separate the epochs as the Southern Highlands form most

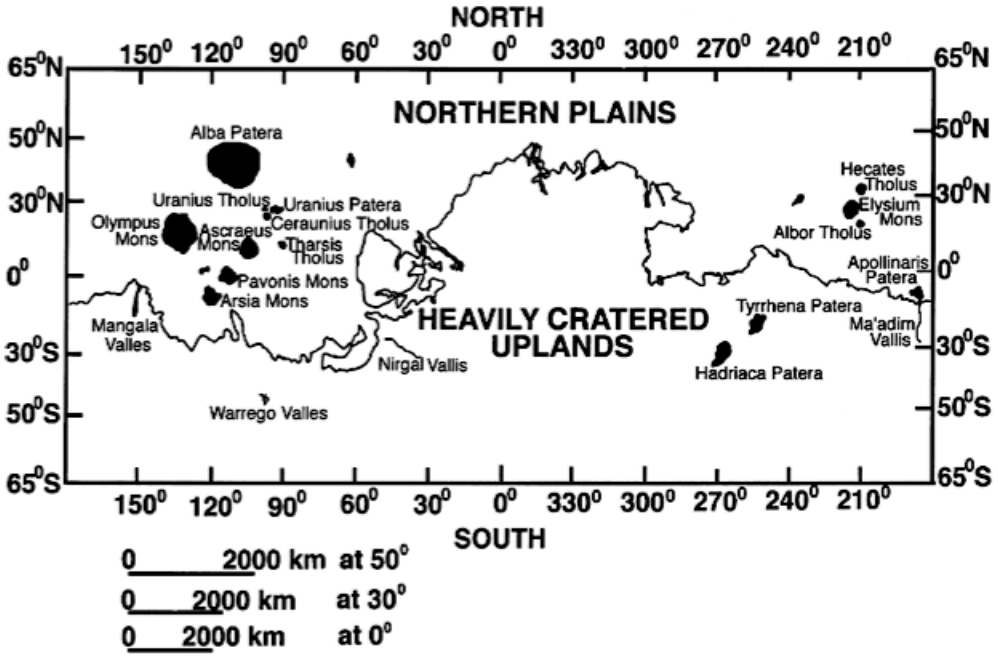

Figure 2.2: Map of Mars showing highland and lowland regions, Gulick *et al.*, 2001

of the Noachian aged surface while the Northern Lowlands are smoother and newer surfaces from volcanic, fluvial, and eolian resurfacing.

The oldest epoch, the Noachian, shown in Figure 2.3, extends from the early bombardment until the establishment of the Tharsis volcanic region. Crater impacts during the early part of the epoch were frequent when larger meteorites impacted the surface. Refer to Table 2.1 for resurfacing rates during this epoch. It is likely during the early Noachian that life, if it existed, would have been exterminated due to hot impact sites and rock vaporization [29]. During the later Noachian and Early Hesperian most of the valley network systems were formed. Valley networks are found more globally on Noachian dated terrain but not so for Hesperian age surfaces. Therefore the mechanisms for the creation of valley networks during these two epochs may well be different, although geologists agree that water either by flow or sapping created the valley networks. This implies that at least for some portion of the late

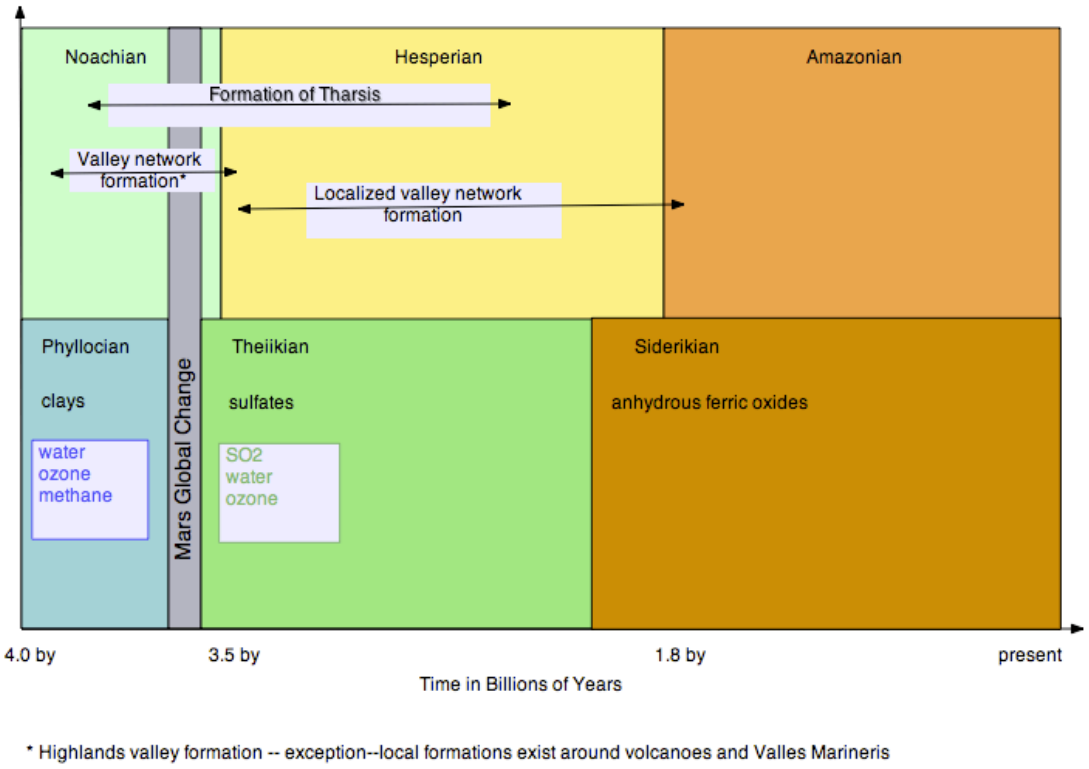

Figure 2.3: Crater Epochs vs. geological alteration Epochs with timing of major surface formations indicated and plausible atmosphere constituents that have UV shield implications (modified from diagrams found in Bibring*et al.* 2006) [8]

Noachian and early Hesperian water was on or near the surface.

The Hesperian epoch follows the Noachian. Volcanic activity continued throughout this epoch with the expansion of the Tharsis region with the addition of volcanoes such as Ceraunius Tholus [1, 25]. Crater forming impacts would lessen over time, see Table 2.1 on page 7, and the surface volcanic activity would have softened or covered craters near active volcanoes thus diminishing the visibility of impact sites[30]. With active volcanoes the atmosphere would likely see an increase in water and sulfur species (see Table 2.2 on page 13, Kilauea column). Valleys and outflow channels near some volcanic regions are found on Hesperian dated surfaces of Mars. The morphologies around these younger volcanoes are theorized to depend upon snow melt

Table 2.1: Extent of Resurfacing Areas (in $10^3 km^2$) Exposed on Mars According to Age and Process[a] (recreated from *Mars* [1])

Epoch	**Volcanic**	**Aeolian**	**Fluvial**	**Periglacial**	**Impact**[b]	**Total**	**%**
Late Amazonian	3280	4878	1245	322	574	10299	7
Middle Amazonian	7272	2076	326	1021	574	11269	8
Early Amazonian	12676	1569	354	394	574	155567	11
Late Hesperian	11503	983	7235	6501	574	26796	19
Early Hesperian	19267	1306	1099	209	783	22664	16
Late Noachian	7702	2432	5353	209	1130	16826	12
Middle Noachian	20019	320	3241	209	10766	34555	24
Early Noachian	2074	–	–	209	3741	6024	4
Total	83793	13564	18853	9074	18716	144000	–
Total %	58	9	13	6	13	–	–
[a] Data from *Tanaka et al. (1988)*							
[b] Only crater > 150 km in diameter were included in table.							

due to magmatic activity and subsequent drainage as well as sapping. [25] If in fact the water is from melting snowpack, this suggests at some point in Martian history water in the atmosphere led to snow fall on high volcano edifices [25, 31]. Warmer surface temperatures could then explain Snowpack or glacial accumulation on these high volcanic peaks during high obliquity. Forget *et al.* [32] proposed that high obliquity would cause water migration from the poles to high volcanic edifices. The view during the Hesperian is one of catastrophic water flow events rather than long term, slow, fluid flow. A global hydrological cycle is not likely due the non-uniform distribution of the valleys across the Martian surface, valley networks are found alone or in clusters [33]. These morphologies are therefore an indication of water flow during this epoch and indicative of warmer temperatures at least locally. Sulfur species as

well as water vapor are released to the atmosphere through volcanic activity here on Earth. Both gases can supply UV shielding directly or indirectly in the atmosphere. Therefore during this epoch it would seem at least one barrier to the formation of life would be minimized.

During the first billion years of Martian history, some time during the late Noachian or the early Hesperian epoch, it is believed that Mars lost much of its atmosphere [34, 35]. The timing of this loss is not well known as well as its cause. Many reasons have been postulated but no definitive data indicates which scenario dominated this loss process. Sequestering of carbonates is one hypothesis for the loss of carbon from the atmosphere. Carbonates are a component of Martian meteorite ALH84001 (dated to approximately 3.9 billion years old) found on Earth and therefore carbonates existed on Mars [36]. This idea is consistent with the lack of plate tectonics that recycle carbonates on the Earth. Once the carbon is sequestered in rocks on Mars surface, the carbon would be permanently trapped [37]. The problem today is a lack of identifiable carbonates on the surface of Mars. Whether the carbonates are somehow hidden below the surface or transformed by some as yet undefined process is a relevant unanswered question. Another atmospheric loss theory relies upon the end of the magnetic dynamo, which led to non-thermal atmospheric loss from processes such as the solar wind, sputtering loss of oxygen, and loss of hydrogen, or explosive loss due to asteroid impacts [38]. Since theories on the process are still being vetted this proposal will not attempt to answer this question. The models will simply simulate the loss of atmosphere by changing model parameters to those indicated by the geological record. Therefore, models will either address the before or after periods of major geological change and not delve into the processes of the change itself.

Finally, the Amazonian epoch which continues to the present day would have seen even fewer crater impacts, similar to Earth today, and a lessening of surface activity.

This epoch sees oxidation and erosion as primary processes on the surface although recent data suggests that glaciations due to high obliquity may have occurred in the late-Amazonian near Tharsis Montes volcanoes and small areas of possible water have been suggested by Shean *et al.* and Forget *et al.* [31,39]. During this period volcanic activity subsided and the dominant surface processes would be iron oxidation, wind erosion, and the transport of water vapor due to sublimation of polar ice into the atmosphere by winds to form glaciers [39].

Shean *et al.* [39] have suggested that the fan-shaped deposits around Tharsis Montes volcanoes are probable remains of Late-Amazonian glaciations. These fan-shaped deposits, earlier attributed to volcanic debris, have been reevaluated due to recent data from MGS and Odyssey and are supported by new glacier simulation data performed with high obliquities. The glacier simulations changed obliquity but otherwise kept much of Mars present day atmosphere unchanged. The obliquity simulations predicted glaciers where morphology also indicates glaciations in the Northern hemisphere, e.g. the Tharsis Montes volcanoes. Simulations were rerun supplying water to the southern region and areas within the Hellas basin area were found to form large glaciers. Both Tharsi Montes volcanoes and Hellas Basin locations coincide well with present morphological findings and suggest that the atmosphere may have been quite similar to that of the present day Mars, although with a different obliquity. The obliquity of Mars today, 25.2°, was replaced with approximately 41° in the models, found to be the most probable obliquity for Mars during the past 4 billion years [40].

Although glaciations would be indicative of water at least in the frozen state, iron oxidation during this period is dominantly anhydrous. It is not known how much of the Martian surface is oxidized. The precise processes for the oxidation are also not known with certainty. Several theories have been suggested. Yen *et al.* [41] proposed that super-oxide ions created when UV radiation strikes Martian type mineral surfaces

would yield results as seen in the Viking mission soil reactions. It would also produce the lack of organic material found at the Viking landing site. Hydrogen peroxide has also been proposed as a possible Martian surface oxidant. Atreya *et al.* [42] proposed that electrostatic fields due to dust devils and dust storms could create high levels of H_2O_2 in the atmosphere, much more than through photochemistry enough H_2O_2 that it could precipitate onto the surface and diffuse into the regolith. H_2O_2 will oxidize iron and has been found in simulations to be a surface chemical on Mars in small amounts (10-30ppb) in the lower Martian atmosphere [43] and seasonally variable, a maximum value found in morning at sub-solar latitude of 6 x 10^{15} cm^2 [44]. This proposed precipitated amount of H_2O_2 from storms would need to be larger than the amount destroyed by the UV radiation and transition metal oxide decomposition on the surface of Mars to influence surface iron oxidation [41]. This may not be a problem since the winds creating dust devils and storms can be great on Mars due to the thin atmosphere and therefore large horizontal temperature gradients and large changes from day to night.

More recently new epoch demarcations have been proposed that use geological alteration mechanisms on the surface and subsurface of Mars to separate Martian history into time periods. These periods may be more useful from an atmospheric standpoint since the mineralization of the surface is linked with atmospheric constituents. These epochs are named for the dominant processes during the time period: Phyllocian (phyllosilicate production), Theiikian (sulfur production), and Siderikian (iron oxidation). Figure 2.3 on page 6 shows the relationship between the epochs named for crater formation and the epochs named for mineral alteration processes. With the higher crater forming impacts rates during the early Phyllocian (Noachian), large amounts of volatiles would be supplied to the surface of Mars. As the Phyllocian epoch continued the impact would have lessened and a more stable environment would

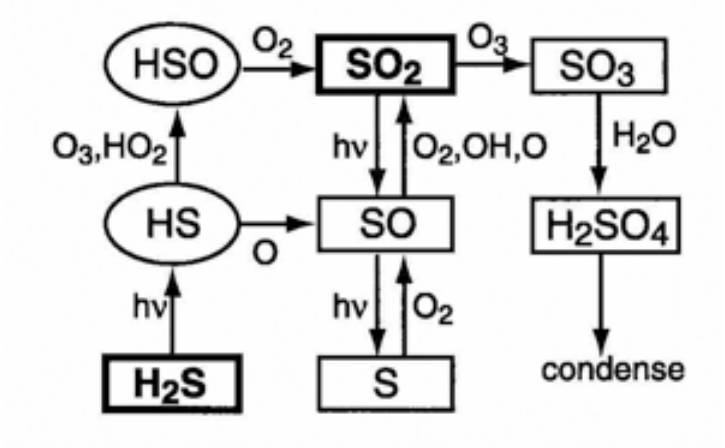

Figure 2.4: Proposed Sulfur Cycle reproduced from Wong *et. al.* 2004 [9]

have developed over time. The formation of clay minerals would have begun on the surface or near subsurface. Many of the phillosilicates (e.g. clay minerals), seen on the surfaces of ancient landscapes or exposed under newer mineralization and later revealed through surface erosion and viewed by the OMEGA imaging spectrometer on the Mars Express spacecraft, require the presence of water and alkaline environments such as nontronite, chamosite and montmorillonite [45].

If these clay minerals were formed on the surface of Mars, this would indicate a long-lasting wet episode [during the late Noachian and early Hesperian, or early Theiikian], with large surface aqueous reservoirs and alkaline water resulting from this chemical alteration [8]. Thus, a constraint on the atmospheric environment exists if these clay minerals formed on the surface. Unfortunately, it is not necessary that these minerals be due to surface processes as subsurface reservoirs also could have altered minerals producing clays. If these minerals were altered in subsurface reservoirs, when did surface water produce fluvial features that have long been attributed to the action of surface water? Data from the inside of Valles Marineris, a giant canyon, indicates no phillosillicates but the surrounding surface area does show clay minerals. If in

fact this channel was etched with water, it doesnt seem likely during the Phyllocian. This may indicate that water was on the surface in two distinct time periods, or that the early period was dominated by subsurface alterations where later periods were surface water dominated. Valley formations on Mars are globally dated to the later Noachian and early Hersperian. These valleys could have formed while phyllosilicate formation was dominant or during the time of global change between the Phyllocian and Theiikian. The large valley networks appear to be formed not by running water on the surface but by groundwater flow. This would support the subsurface formation of clay minerals and lead to surface water flow at least episodically when the surface soil collapsed, exposing the valley. [8,33] Between the proposed Phyllocian and Theiikian epochs Mars went through a large change in global climate. This transformed the surface from that of clay minerals to surface forming sulfates. Also during this period volcanic activity increased. Shield volcanoes on Mars are able to grow to much larger heights than Earth counterparts due to the smaller surface gravity. Although larger, Martian volcanoes are thought to have similar structures to Hawaiian shield volcano. Since volatile volcanic output of these volcanoes is approximately 37 % water and 12% sulfur species, see Table 2.2 on page 13, it is likely that the Martian atmosphere and surface saw a large influx of water and sulfur species. Sulfur species will react with water to form sulfuric acid, see Figure 2.4 on page 11. The acid would then condense out of the atmosphere and provide a likely source for the sulfur mineralization that dominates the Theiikian epoch. With volcanic activity continuing through much of the Theiikian, local waterways could exist even as the global valleys appear to have dried up. Looking closely at Figure 2.3 on page 6 one notices that the Theiikian closely mirrors the Hesperian epoch and such the processes described above for the Hesperian are true for the Theiikian. The Theiikian is named for sulfur species formation which occurs globally and then locally during the Hesperian.

Table 2.2: Examples of volcanic gas composition, in volume percent concentrations ([2] and USGS website [3])

Volcano	Kilauea Summit	Erta‘ Ale	Momotombo
Tectonic Style	Hot Spot	Divergent Plate	Convergent Plate
Temperature	1170 °C	1130 °C	820 °C
H_20	37.1	77.2	97.1
$C0_2$	48.9	11.3	1.44
$S0_2$	11.8	8.34	0.50
H_2	0.49	1.39	0.70
CO	1.51	0.44	0.01
H_2S	0.04	0.68	0.23
HCl	0.08	0.42	2.89
HF	—	—	0.26

Finally, again referring to Figure 2.3 on page 6, the Siderikian mirrors the Amazonian epoch. During this epoch anhydrous ferric oxidation dominates. Volcanic activity and fluvial features even in local areas become dormant. The surface is changed by wind erosion and the red color of iron oxides dominates the landscape, which turned Mars into the well-known red planet.

Chapter 3: A Review of the Present Atmospheric constituents of Mars

The present Martian atmosphere is mainly composed of carbon dioxide. Along with CO_2 many trace gases exist that influence the chemical and thermal structure of the Martian atmosphere; see Table 3.1 on page 15 for gas constituents percentages. Although present in only small amounts, trace gases can greatly influence the atmosphere. This can be seen by the importance of water vapor in the stability of CO_2 in the Martian atmosphere. In a completely CO_2 atmosphere, Reaction Pathway shown in Equation 3.0, high values of CO and O_2 would be present because of the UV photolysis of CO_2 ($r = 3 * 10^{-37} s^{-1}$ at 200K, [10]). Two free oxygen atoms can react with a third body and combine to form O_2. Thus, in a pure CO_2 reaction cycle the following is seen,

Equation 3.0: Pure CO_2 atmosphere Reaction Pathway

$$2\left(CO_2 + hv \rightarrow CO + O\right)$$

$$\underline{O + O + M \rightarrow O_2 + M}$$

$$2CO_2 \rightarrow 2CO + O_2$$

It should be noted that in this pure CO_2 atmosphere dissociation of O_2 due to photolysis will also occur, $O_2 + hv \rightarrow 2O$. This reaction produces free oxygen that

Table 3.1: Atmospheric Composition of Mars recreated from table by Moroz 1998 [4] with additional data from Formisano *et al.* 2004 [5]

Species	Fractional Abundance
CO_2	0.9532[1]
N_2	0.027
Ar	0.016
O_2	0.0013 [2]
CO	0.0007
H_2O	0.0003 [3]
Ne	2.5ppm
He	1.1ppm
Kr	0.3ppm
Xe	0.08ppm
O_3	0.04 to 0.2ppm [4]
CH_4	10.5ppb [5]
SO_2	0.1 ppm (upper limit)
H_2S	0.1 ppm (upper limit)

can then react with the molecular oxygen produced in Equation 3.0 and a third body (CO_2) to form ozone. Therefore, in a pure CO_2 atmosphere ozone is readily formed as well as O, O_2, and CO.

Reactions change with the introduction of water vapor, see Equation 3.1 CO_2 catalytic Reaction Pathway (I). The presence of water vapor in this majority CO_2 atmosphere efficiently produces OH and O through photolysis, $H_2O + hv \rightarrow OH + H$. The OH radials react with CO (from the photolysis of CO_2) to produce CO_2 and H, $OH + CO \rightarrow CO_2 + H$.

The free hydrogen can then react with O_2 and a third body to produce HO_2. HO_2 reacts with a free oxygen atom to produce O_2 and OH radicals that again can react with CO to continue the catalytic cycle. The catalytic Reaction Pathway (I)

[1] CO_2 varies seasonally by as much as 30%, value provided from Viking landing site with pressure of 7.5mbar.

[2] O_2 abundances vary with season and location.

[3] Annual global average of H_2O is 10x10^{-}3 kg m^{-}2 or 0.00016 by volume.

[4] O_3 abundances vary with season and location.

[5] Mars Express verifies Mummas measurement of several ppb [5]

in Equation 3.1 shows the net loss of CO and O to CO_2 in the presence of water vapor that through photolysis produces to OH + H to initiate the supply of OH to the pathway. Although this is not the only reaction pathway for net CO_2 production, in the present atmosphere (low H_2O abundance) it comprises about 77% of the CO_2 catalytic production [10]. Other cyclic reaction pathways use ozone, oxygen molecules, hydrogen peroxide, and nitrogen species to also reproduce CO_2. These pathways comprise the remainder of the CO_2 catalytic production pathways. A schematic of the reaction pathways for hydrogen species is shown in Figure 3.1. Notice that the supply and loss endpoints are water and molecular hydrogen, thus water is the driver for the reaction pathways of CO_2 and hydrogen species.

Initial photolysis reactions:

$$CO_2 + hv \rightarrow CO + O$$

$$H_2O + hv \rightarrow OH + H$$

Equation 3.1: CO_2 catalytic Reaction Pathway(I)

$$CO + OH \rightarrow CO_2 + H$$

$$H + O_2 + M \rightarrow HO_2 + M$$

$$\underline{O + HO_2 \rightarrow O_2 + OH}$$

$$CO + O \rightarrow CO_2$$

The presence of OH radials not only supplies the catalytic reaction pathway to produce CO_2, stabilizing it in the atmosphere, but also promotes the production of

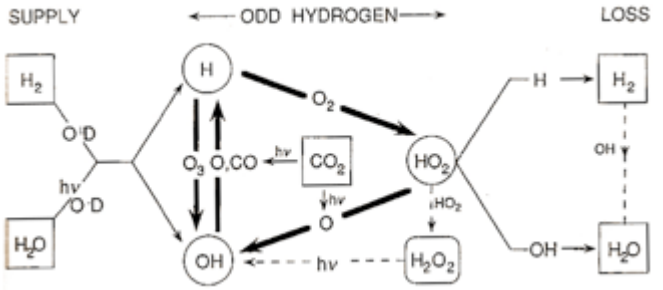

Figure 3.1: Principle pathways for Hydrogen Species from Yung and DeMore, 1999 [10]

O_2. This O_2 production pathway leads to the net loss of CO_2 and the formation of CO and O_2. In Reaction Pathway (II), Equation 3.2, CO and O_2 are produced rather than CO and free oxygen which is produced in Reaction Pathway (I).

Initial photolysis reactions:

$$H_2O + hv \rightarrow OH + H$$

Equation 3.2: CO_2 catalytic Reaction Pathway(II)

$$CO_2 + hv \rightarrow CO + O$$

$$O + OH \rightarrow O_2 + H$$

$$H + O_2 + M \rightarrow HO_2 + M$$

$$\underline{O + HO_2 \rightarrow O_2 + OH}$$

$$2CO_2 \rightarrow 2CO + O_2$$

The scheme in Equation 3.2 shows the production of O_2 and not atomic oxygen.

This in turn will limit the production of O_3 since it converts CO_2 into CO and O_2 and not CO and O, the O being needed to produce O_3 in the reaction $O + O_2 + M \rightarrow O_3 + M$. Additional loss of O_3 is seen through the reaction of O_3 with free hydrogen to produce not only OH but more molecular oxygen, $H + O_3 \rightarrow OH + O_2$. Therefore, in the presence of trace water as seen on Mars today, CO_2 and O_2 are produced preferentially and therefore a loss of O_3 is seen when compared to a pure CO_2 atmosphere where O_3 reaches concentrations sufficient to offer UV shielding.

In a high water content atmosphere (unlike present day Mars) Reaction Pathway (I) is not as important as the reaction pathway shown below, Equation 3.3, for CO_2 stability, this will be an important pathway when model parameters go well above the present atmospheric water content.

Equation 3.3: Important Reaction Pathway for high H_2O atmosphere content

$$2\,(CO + OH \rightarrow CO_2 + H)$$

$$2\,(H + O_2 + M \rightarrow HO_2 + M)$$

$$HO_2 + HO_2 \rightarrow H_2O_2 + O_2$$

$$\underline{H_2O_2 + h\nu \rightarrow 2OH}$$

$$2CO + O_2 \rightarrow 2CO_2$$

When viewing the reaction pathways shown in Equations 3.0, 3.1, 3.2 and 3.3, it is important to note a loss of hydrogen and oxygen to the upper atmosphere is therefore a loss of these species from the atmosphere of Mars and chemical reaction availability in the lower atmosphere.

Although H and O alone are reactive and unlikely to diffuse to the upper atmosphere, the molecular counterparts have a higher probability for transportation to the upper atmosphere where the molecules are separated through reaction pathways that allow for the escape of free H and O atoms. About 20% of the H_2 molecules produced in the lower atmosphere through the break up of two water molecules diffuse to the upper atmosphere and thermally escape. The atomic mass of the oxygen atom prevents thermal loss due to escape velocity but it can be lost in the upper atmosphere due to dissociative recombination with thermal electrons above the exobase [10]. Reaction pathways link the production of H_2 and O_2 such that the thermal loss of 2H balances the dissociative loss of O. Thus, in the present day atmosphere stability of CO_2, production of UV shielding O_3, and loss of H and O to the atmosphere are linked to the availability of H_2O in the atmosphere. Modeling the present day atmosphere with its stability of CO_2 resting on the presence of H_2O has been developing for decades in an attempt to match measured atmospheric species values [6, 46, 47].

Chapter 4: Computer Models of Present Day Mars

Models for the major atmospheric constituents have existed since the original work of McElroy and Donahue [46] that addressed the problem of CO_2 stability in the Martian atmosphere through the introduction of atmospheric water levels as discussed in Chapter 3. McElroy and Donahue presented an atmospheric model that included reactions with constituents: CO_2, CO, O, O_2, O_3, OH, HO_2, H_2O, H, and H_2. Parkinson and Hunten (1972) using Mariner 9 observational data predicted high levels of H_2O_2 that through photolysis provides reactive OH molecules which deplete levels of CO and O_2, and provide additional CO_2 stability. These models required simplifying assumptions and included inaccurate cross sectional data as well as atmospheric species measurements. Thus, obtaining matching measured values for atmospheric constituents was difficult. With the addition of updated trace species measurements and chemical kinetics data, Nair *et al.* in 1994 [6] tested a more complete photochemical model, adding nitrogen chemistry, more realistic eddy diffusion rates, and water vapor values, against the present measured levels of CO, O_2, and O_3 and found good agreement with atmospheric values without the addition of surface chemistry, relying totally upon gas phase chemistry. Krasnopolsky in 1993 [48] also published an updated model which was dependent upon heterogeneous chemistry to match CO and O_3 measured values. Krasnopolsky used collisions among atmospheric gases and surface rocks, dust particles, and ice to reduce the amount of H, OH, and HO_2 in the atmosphere, therefore reducing the efficiency of these odd hydrogen chemistries. Because Nair's model did not require additional heterogeneous chemistry it will be adapted in this paper with the additional chemistries to make it relevant to ancient

Mars and referred to in future writing as simply the Nair model. The updated chemistry added to the Nair model includes methane and sulfur chemistry via Summers *et al.*, Formisano *et al.*, and Wong *et al.* [5, 49, 50]. Since this model was adapted from the Nair model it is important to verify model results to those results reported initially by Nair *et al.* [6].

The Nair model, originated at Caltech/JPL, solves the one-dimensional continuity equation for steady-state conditions for the species listed in Nair *etal.* and the additional reaction species and equations shown in table 4 and table 5. The equation,

$$\frac{\partial n_i}{\partial t} + \frac{\partial \Phi_i}{\partial z} = P_i - L_i \tag{4.1}$$

is solved where n_i are the concentrations, Φ_i are the vertical diffusive fluxes, and P_i and L_i are the chemical loss and production terms for each indexed species. Since the steady state term leads to $\frac{\partial n_i}{\partial t} = 0$, the continuity equation can be solved with the indexed species vertical flux by the equation

$$\Phi_i = -D_i \left(\frac{\mathrm{d}n_i}{\mathrm{d}z} + \frac{n_i}{H_i} + \frac{n_i\,(1+\alpha)}{T} \frac{\mathrm{d}T}{\mathrm{d}z} \right) - K \left(\frac{\mathrm{d}n_i}{\mathrm{d}z} + \frac{n_i}{H} + \frac{n_i\,(1+\alpha)}{T} \frac{\mathrm{d}T}{\mathrm{d}z} \right) \tag{4.2}$$

where D_i is the molecular diffusion coefficient, K is the eddy diffusion coefficient, T is the temperature, α is thermal diffusion factor (which is taken to be zero), and H is the scale height of the background atmosphere [6].

The Nair (CalTech/JPL) model is a one-dimensional atmospheric model able to move forward in time steps in either diurnal or steady state modes. For all modeling proposed in this paper, the atmosphere will be run until a steady state is found

Table 4.1: Additional Species added to Nair model

CH_4	SO_2	$(3)CH_2$
CH_3	SO	CH
H_2S	HSO_3	SO_3
NH_3	H_2SO_4	HCN^+
NH_2	S	NH(a)
HCN	HSO	NH
CN	HSNO	HNO
H_2CO	CH_3ONO	N_2H
CH_3OOH	CH_2OOH	HCO
CH_3O_2	$CH_3O_2NO_2$	NCO
SH	$CH_3O_2CH_3$	H*
CH_3O	$(1)CH_2$	OH*
		O*

Table 4.2: Model Boundary Condition (key: FND = fixed number density, FMR = fixed mixing ratio, FV = fixed velocity, FF = fixed flux)

Element	Surface Boundary		Upper Boundary	
N_2	FND	5.813x10^{15} cm_{-3}	FF	0.00
O_2	FMR	1.30x10^{-3}	FF	0.00
O	FF	0.00	FF	1.20x10^8 $cm^{-2}s^{-1}$
H	FF	0.00	FV	3.08x10^3 cm s^{-1}
H_2	FMR	3.00x10^{-5}	FV	3.39x10^1cm s_{-1}
H_2O_2	FV	-1.00x10^{-1}	FF	0.00
CO	FMR	6.00x10^{-4}	FF	0.00
CO_2	FND	Varies with model runs	FF	0.00
CH_4	FMR	1.00x10_{-6}	FF	0.00

for the given input constituents and boundary conditions. The model divides the vertical atmosphere into 121 segments of 2 km each. Boundary conditions are set for transported species that maintain a specific concentration, mixing ratio, flux, or velocity at the surface or the upper boundary locations.

Determining appropriate boundary conditions requires knowledge of the processes controlling the species at lower and upper boundaries. For example, the rates of escape for H and O above the exobase are used to determine velocity and flux boundary

conditions respectively at the upper atmospheric boundary. These values follow Nairs O upper boundary flux of 1.2x10^8 cm^{-2}s^{-1} and the H upper boundary condition velocity of 3.08x10^3 cm s^{-1}. The CO_2 and N_2 boundary conditions are set to produce fixed column number densities that represent current measured values. The fixed column density for CO_2 will change depending upon the type of atmosphere modeled and will range from the standard model value of 2.05x10^{17} cm^{-3} at the surface to approximately 100 times this value. The N_2 lower boundary condition will remain constant. The type of boundary condition for N_2 is changed from Nairs work from a mixing ratio to a constant number density. This change was made for easier altering of atmospheric parameters as a mixing ratio for N_2 would lead to increases in N_2 for increases in CO_2, this will not occur for a number density boundary condition. CO, O_2, and H_2 surface boundary conditions are set to current observed values. H_2O_2 and H_2SO_4 condense out of the atmosphere at the surface and thus are given a velocity lower boundary condition in line with this downward transport and precipitation out of the atmosphere and onto the surface. Both velocities are set to -1x10^{-1}cm s^{-1}. All other boundary conditions for transported species are set to a flux value of zero at the lower and upper boundaries.

The 27 species used in Nair *et al.* [6] have been augmented by Summers *et al.* [49] with an additional 37 species shown in Table 4.1. The addition of these species required species relevant reactions to be added to the model. These reactions are listed in Table 4.3 along with associated rate constants. Where possible JPL photochemical data was used. For a complete discussion of parameter value settings used in the model see Nair *et al.* [6] and references within.

Results for major trace gases of the updated Nair model for present day atmosphere of Mars are seen in figure 4.1. Additional trace gases concentrations will be added for Early Mars modeling which presently are in very low levels, for example,

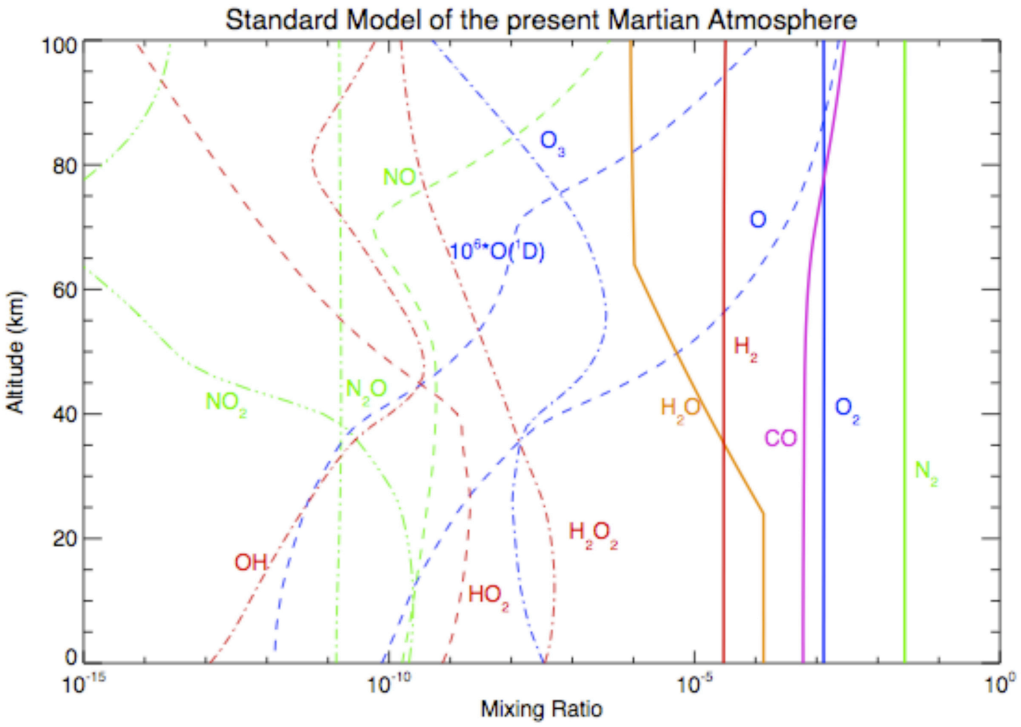

Figure 4.1: Model Results for Present Day Martian atmosphere

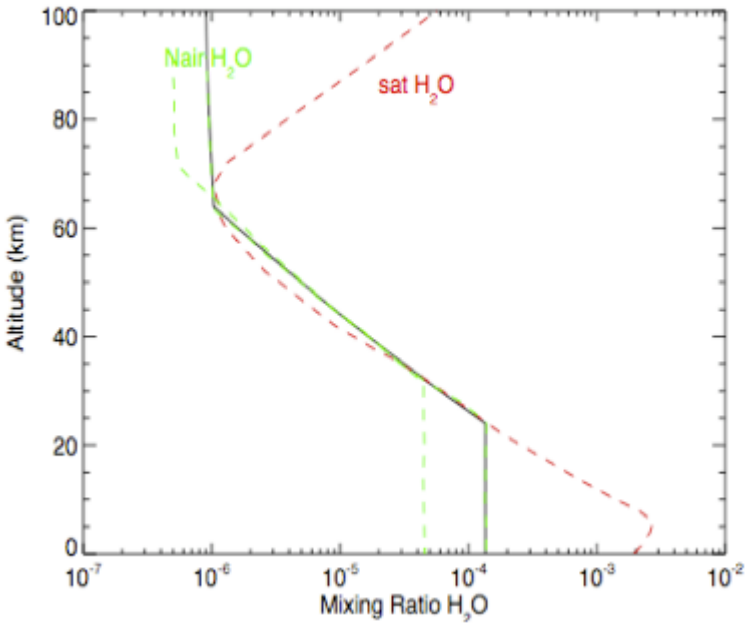

Figure 4.2: Water Vapor profiles from Nair models, with H_2O saturation curve, for current Mars temperature

CH_4, or have not been measured and only upper limits assigned, for example, SO_2.

The water profile, Figure 4.2, shows both Nair models high and low water mixing ratios and the saturation water level for the current temperature range. Water vapor is initially held constant within the model and below saturation under 40km as shown. Although reactions were updated, initial model runs show agreement with Nair *et al.* [6]. Thus, changes can be made to represent early Martian atmosphere from this working current Martian atmospheric model.

Table 4.3: Reactions added to model since Nair *et al.* [6]

No.	**Chemical Reaction**	**Rate Coefficient**[1]	**Reference**
116	$OH + CH_4 \rightarrow CH_3 + H_2O$	2.4	[51]
117	$O\left(^1D\right) + CH_4 \rightarrow CH_3 + OH$	$1.130\text{x}10^{-10}$	[52]
118	$O\left(^1D\right) + CH_4 \rightarrow CH_3O + H$	$3.00\text{x}10^{-11}$	[52]
119	$O\left(^1D\right) + CH_4 \rightarrow H_2CO + H_2$	$7.500\text{x}10^{-12}$	[52]
120	$O + CH_4 \rightarrow CH_3 + OH$	$2.63\text{x}10^{-12}e^{-378./T}$	[53]
125	$CH_3 + O \rightarrow H_2CO + H$	$1.100\text{x}10^{-10}$	[54]
126	$CH_3 + O_2 + M \rightarrow CH_3O_2 + M$	$1.220\text{x}10^{-23}\ \text{T}^{-3.00}$	[51]
127	$CH_3 + O_2 \rightarrow H_2CO + OH$	$3.000\text{x}10^{-16}$	[51]
128	$CH_3 + O_3 \rightarrow CH_3O + O_2$	$5.400\text{x}10^{-12}e^{-220./T}$	[51]
130	$O + H_2S \rightarrow OH + SH$	$9.200\text{x}10^{-12}e^{-1800./T}$	[51]
131	$OH + H_2S \rightarrow SH + H_2O$	$6.000\text{x}10^{-12}e^{-75./T}$	[51]
132	$SH + O \rightarrow H + SO$	1.600x^{-10}	[51]
133	$SH + O_2 \rightarrow OH + SO$	4.000x^{-19}	[51]
134	$SH + O_3 \rightarrow HSO + O_2$	$9.000\text{x}10^{-12}e^{-280./T}$	[51]
135	$SH + NO + M \rightarrow HSNO + M$	$6.480\text{x}10^{-24}T^{-3.00}$	[55]
136	$SH + NO_2 \rightarrow HSO + NO$	$2.900\text{x}10^{-11}e^{240./T}$	[55]

Table 4.3: Reactions added to model since Nair *et al.* [6]

No.	**Chemical Reaction**	**Rate Coefficient**[1]	**Reference**
140	$OH + NH_3 \rightarrow NH_2 + H_2O$	1.700x10$_{-12}e^{-710./T}$	[51]
141	$O\left(^1D\right) + NH_3 \rightarrow NH_2 + OH$	2.500x10^{-10}	[51]
142	$NH_2 + HO_2 \rightarrow NH_3 + O_2$	1.700x10^{-11}	[56]
143	$NH_2 + HO_2 \rightarrow HNO + H_2O$	1.700x10^{-11}	[56]
144	$NH_2 + O_3 \rightarrow HNO + H + O_2$	4.300x10$^{-12}e^{-930./T}$	[56]
145	$NH_2 + NO \rightarrow N_2H + OH$	3.60x10$^{-12}e^{450./T}$	[56]
146	$NH_2 + NO \rightarrow N_2 + H_2O$	0.40x10$^{-12}e^{450./T}$	[56]
147	$NH_2 + NO_2 \rightarrow N_2O + H_2O$	2.100x10$^{-12}e^{650./T}$	[56]
151	$O + HCN \rightarrow CO + NH$	3.300x10$^{-12}e^{-4000./T}$	[56]
152	$O + HCN \rightarrow H + NCO$	6.700x10$^{-12}e^{-4000./T}$	[56]
153	$OH + HCN \rightarrow CN + H_2O$	1.200x10$^{-13}e^{-400./T}$	[56]
154	$CN + O_2 \rightarrow NCO + O$	1.100x10$^{-11}e^{205./T}$	[57]
157	$OH + H_2CO \rightarrow HCO + H_2O$	1.000x10^{-11}	[51]
158	$NO_3 + H_2CO \rightarrow HCO + HO_3$	5.800x10^{-16}	[58]
159	$O + H_2CO \rightarrow OH + HCO$	3.400x10$^{-11}e^{-1600./T}$	[51]
160	$HCO + O_2 \rightarrow CO + HO_2$	3.500x10$^{-12}e^{140./T}$	[51]
162	$OH + CH_3OOH \rightarrow CH_2OOH + H_2O$	1.14x10$^{-12}e^{200./T}$	[51]
163	$OH + CH_3OOH \rightarrow CH_3O_2 + H_2O$	2.66x10$^{-12}e^{200./T}$	[51]
164	$HO_2 + CH_3O_2 \rightarrow CH_3OOH + O_2$	3.800x10$^{-13}e^{800./T}$	[51]
165	$NO + CH_3O \rightarrow HNO + H_2CO$	8.00x10^{-12}	[56]
166	$NO + CH_3O + M \rightarrow CH_3NO_2 + M$	3.62x10$^{-20}T^{-3.80}$	[51]
167	$CH_3O + O_2 \rightarrow H_2CO + HO_2$	3.900x10$^{-14}e^{-900./T}$	[51]
168	$NO_2 + CH_3O_2 + M \rightarrow CH_3O_2NO_2 + M$	1.220x10$^{-20}T^{-4.00}$	[51]
169	$HO_2 + CH_3O_2 \rightarrow CH_3OOH + O_2$	3.81x10^{-13}	[51]

Table 4.3: Reactions added to model since Nair *et al.* [6]

No.	Chemical Reaction	Rate Coefficient[1]	Reference
170	$NO + CH_3O_2 \rightarrow CH_3O + NO_2$	$3.000\text{x}10^{-12}e^{(280./T)}$	[51]
174	$OH + SO_2 + M \rightarrow HOSO_2 + M$	$4.480\text{x}10^{-23}T^{-3.30}$	[55]
175	$O + SO_2 + M \rightarrow SO_3 + M$	$4.000\text{x}10^{-32}e^{(-1000./T)}$	[55]
178	$SO + O_2 \rightarrow SO_2 + O$	$2.600\text{x}10^{-13}e^{(-2400./T)}$	[51]
179	$SO + O_3 \rightarrow SO)2 + O_2$	$3.400\text{x}10^{-12}e^{(-1100./T)}$	[59]
180	$SO + OH \rightarrow SO_2 + H$	$8.600\text{x}10^{-11}$	[51]
181	$SO + NO_2 \rightarrow SO_2 + NO$	$1.400\text{x}10^{-11}$	[51]
182	$HSO_3 + OS \rightarrow HO_2 + SO_3$	$1.300\text{x}10^{-12}e^{(-330./T)}$	[51]
183	$SO_3 + H_2O + M \rightarrow HSO_4 + M$	$1.200\text{x}10^{-15}$	[60]
185	$S + O_2 \rightarrow SO + O$	$2.300\text{x}10^{-12}$	[51]
186	$S + O_3 \rightarrow SO + O_2$	$1.200\text{x}10_{-11}$	[51]
187	$S + OH \rightarrow SO + H$	$6.600\text{x}10^{-11}$	[51]
188	$O_3 + SO_2 \rightarrow SO_3 + O_2$	$3.000\text{x}10^{-12}e^{(-7000./T)}$	[51]
189	$SO + O + M \rightarrow SO_2 + M$	$5.100\text{x}10^{-31}$	[9]
190	$SO + SO \rightarrow SO_2 + S$	$5.800\text{x}10^{-12}e^{(-1760/T)}$	[9]
191	$HS + H \rightarrow S + H_2$	$2.16\text{x}10^{-11}$	10
192	$HS + HO_2 \rightarrow HSO + OH$	$1.00\text{x}10^{-11}$	[9]
193	$HS + HS \rightarrow S + H_2S$	$4.00\text{x}10^{-11}$	[9]
194	$H_2S + H \rightarrow HS + H_2$	$1.96\text{x}10^{-17}T^{2.10}e^{(-352/T)}$	[9]
195	$HSO + O_2 \rightarrow SO_2 + OH$	$1.70\text{x}10^{-15}$	[9]
196	$HSO + O_3 \rightarrow HS + 2O_2$	$2.54\text{x}10^{-13}e^{(-384/T)}$	[9]

[1]Units for rate values vary, for photolysis units are sec^{-1}, for two body reactions units are cm^3sec^{-1}, for three body reactions units are cm^6sec^{-1}.

Chapter 5: Literature Review of Early Martian Atmospheric Modeling

Although a unified consensus of atmospheric constituents does not exist for early Mars, several models presented in literature agree upon increased levels of atmospheric water and CO_2, as well as an increased average surface temperature to allow for fluvial signatures seen on the surface today. Presently more atmospheric constituents are becoming better constrained as orbiters and on-site rovers enhance our understanding of the surface mineralogy and the atmospheric processes that enabled these minerals to exist on early Mars.

Early atmospheric modeling included warm, wet climates to address the fluvial geomorphology seen on the surface of Mars [61, 62]. To increase the atmospheric surface temperature, early climate models used high levels of CO_2 [62,63]. Subsequent analysis of CO_2 cloud formation causing surface cooling has caused inconsistencies in the CO_2 warming wet models approach as well as a lack of carbonates found on the Martian surface [37, 64].

For surface water to flow, temperatures must be above freezing (with surface pressure above 6mbar), at least locally. Kasting [64] suggested that sufficient CO_2 to warm the surface leads to condensation of stratospheric CO_2 into clouds that would in turn cool the surface. Therefore CO_2 alone could not be the only greenhouse gas present to sufficiently warm early Mars. Figure 5.1 shows data from Kasting (1991) [64], here scaling of the saturation CO_2 pressure in figure (b) allows viewing several models with different temperature curves as seen in Figure 5.1(a) against

the saturation vapor pressure of CO_2. Kasting demonstrated that CO_2 atmospheres above 0.35 bar would lead to saturation around 20km above the surface of Mars and thus produced clouds. Therefore this value is the highest concentration of CO_2 that will not produce cloud cover in his model atmosphere unless other constituents can be induce midlevel warming in the stratosphere.

Forget and Pierrehumbert [32], advanced this research with a more robust cloud model allowing CO_2 ice particles to exceed 6-8 micrometers (Kastings model ice particles were under 6 micrometers) and their model allows multiple scattering. Their results indicated that cloud cover could enhance warming by IR scattering partly in contradiction to Kastings results. Although initial results mimic Kastings results, Forget and Pierrehumbert allowed for larger CO_2 ice particles that would have likely existed. These large particles allowed for a larger greenhouse effect that enhanced warming as well as increasing albedo, but the net effect was an increase in the surface temperature except for clouds situated very near the planetary surface.

Mischna *et al.* [65] reexamined this problem with a single computer model combining both the radiative-convective atmospheric model and the cloud formation and scattering model. Previous work by Kasting, and Forget and Pierrehumbert used two separate models, inputting scattering results into a radiative-convective atmospheric model. Mischnas results followed Forget and Pierrehumbert in many aspects but found for high opacity ($\tau > 10$) surface cooling was found and cloud level had a greater impact on surface warming or cooling than reported previously. The limit of the warming of the surface was modeled in a 2-bar CO_2 atmosphere with $\tau = 10$, see Figure 5.2. Two-bar atmospheres with higher opacity no longer had sufficient greenhouse to combat the increasing albedo. Less radiation, due to scattering, was allowed to pass through clouds that led to less IR radiation from the surface to be trapped and surface temperatures decreased.

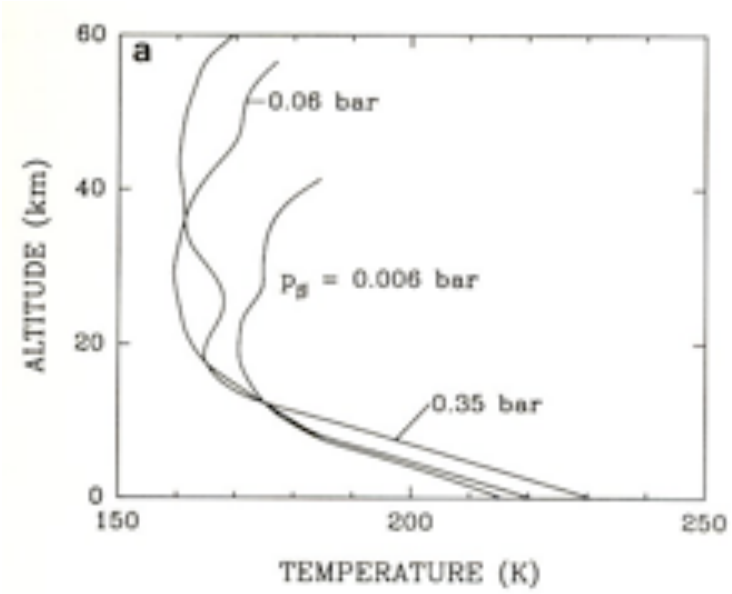

(a) Temperature Curves

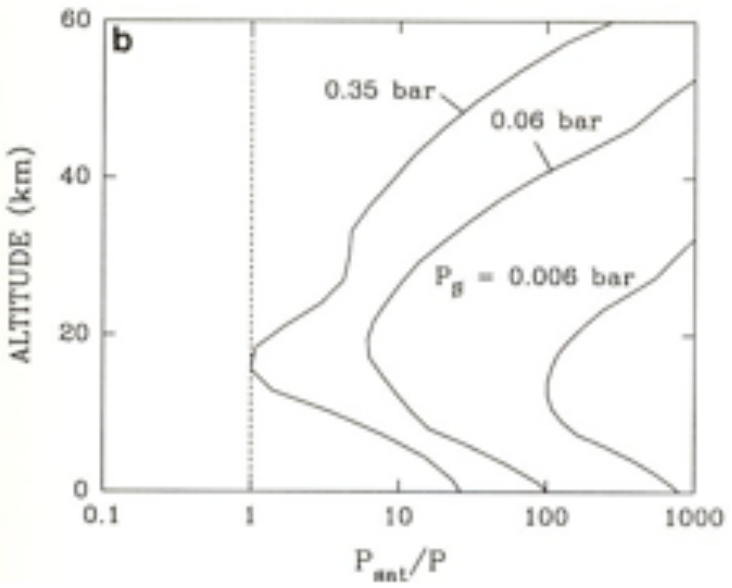

(b) Pressure Curves

Figure 5.1: Temperature and Pressure Curves for varying levels of CO_2, reproduced from Kasting 1991

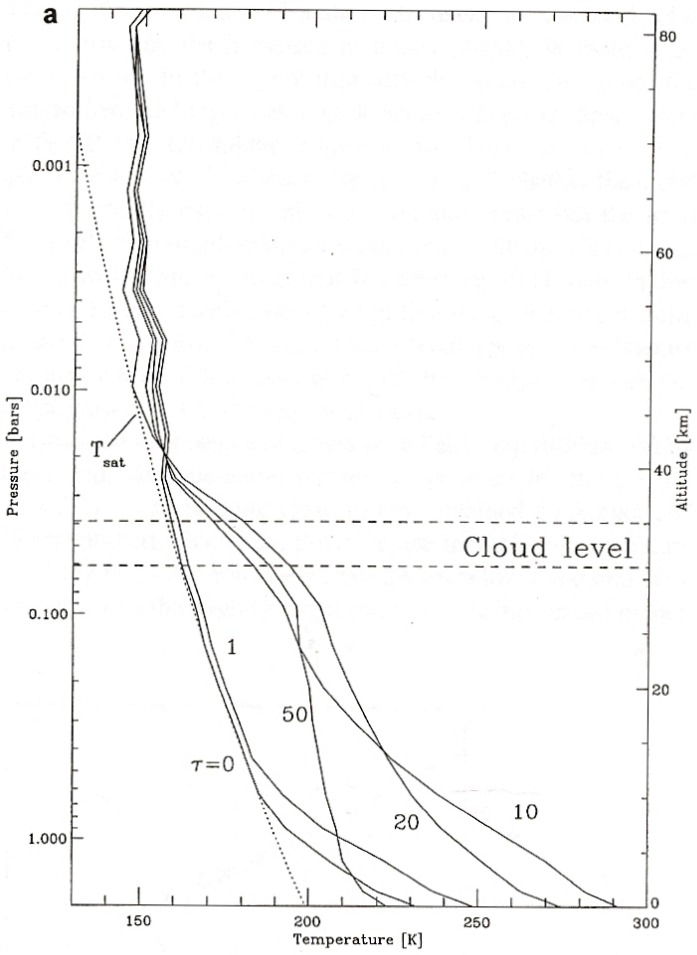

Figure 5.2: Proposed Atmospheric curves for varying τ, reproduced from Mischna et al. 2000

Vertical cloud placement also dictated warming or cooling, high clouds tended to warm the surface while low level clouds tended to cool the surface in general agreement with previous work. With the optical thickness equal to 10, the temperature was found to change from approximately 292K to 247K with clouds placed initially at 35km then reduced to 15km. Thus, an easy view of cloud cover and its influence on surface temperature is not found. What effect clouds played in the warming or cooling of the surface is unknown but data shown in Figure 5.2 required in most cases 100% cloud cover which even when considering a main constituent condensate (CO_2) may be overstated. The high sensitivity of temperature to CO_2 cloud cover makes CO_2 clouds alone an unlikely solution to the warming of Mars for the development of water structures found on the surface which are dated to the earliest epochs of Mars.

Although differing in the chemistry, several scientists, beginning in 1997 with

Yung *et al.* [66], proposed SO_2 as a solution for early Mars atmospheric modeling. Yung demonstrated that with sufficient SO_2 present in the middle atmosphere, CO_2 clouds would be abated and more surface warming could take place with higher CO_2 concentrations that would be obtainable. A recent publication by Tian *et al.* [67] claims that although this warming would take place it would be more than offset by the cooling introduced by the presence of sulfate and sulfur aerosols which were not included in the work previously published by Yung *et al.* [66].

Other theories on the introduction of SO_2 in the atmosphere address the additional question of sequestered carbonates. Acidic water from precipitation of H_2 SO_4 due to volcanic release of SO_2 and H_2S could halt carbonate formation and in turn lead to sulfur species formation as found presently in Martian surface data [20], [8]. Bullock and Moore [37] suggest acidic water from this precipitation would limit carbonate formation and lead to sulfate species precipitation as seen for example at West Candor Chasma [68], Meridiani Planum, and various regions mainly confined to the Southern highlands on Mars. SO_2 would help sustain a thick CO_2 atmosphere as described by Yung *et al.* as limited carbonate formation would not sequester the CO_2 out of the atmosphere [20, 68, 69]. Bullock and Moore [37] suggests this change in the atmospheric constituents but do not model the effects of SO_2 in such an atmosphere for viability of this constituents lifetimes in model atmospheres.

Preliminary modeling with SO_2 set to 1ppmv has shown the lifetime of SO_2 to increase dramatically when CO_2 levels were increased from todays levels to 100 times todays levels, see Figure 5.4. Wongs present day Martian SO_2 lifetime calculation is 40 days. Preliminary data shows an atmosphere of 0.6 bar CO_2 is sufficient to increase the SO_2 lifetime to be on the order of 10 years in agreement with [70] but shorter than the 100 to 1,000 year e-folding values seen in pulsed introduction of sulfur species modeled by Johnson *et al.* [71]. Initially testing with pulsed type input shows

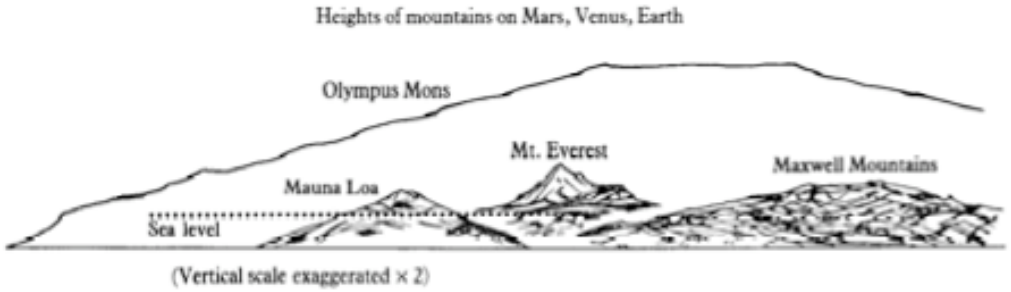

Figure 5.3: Comparison of Terrestrial Planet Mountains (Morrison and Owen, 1996)

e-folding times of approximately 200 years using current model parameters; shorter but of the same order of Johnson's results. Throughout the Noachian and Hesperian Epochs, see Table 2.1, Mars likely had at least an episodic supply of SO_2 from volcanic eruptions. Looking at the height of Olympus Mons one can infer the length of time necessary through eruptions to construct this volcanic mountain. The estimated amount of eruption time for the Mauna Loa volcano on Earth is approximately 1 million years [3]. MacDonald *et al.* [3] state that even though this is the length of time for the eruptions to grow the volcano to the appropriate height, periods may have been less active than others implying Mauna Loa may be older than its size implies. A size comparison of Mauna Loa to Olympus Mons shown in the cartoon drawing of 5.3 implies a much larger period of time of volcanic eruption if this Martian shield volcano erupted in the same fashion as the Hawaiian island volcanoes. The height of Mauna Loa above sea level is approximately 4.1km (9km above the ocean floor) having a total volume of 80,000km^3.

Olympus Mons towers over 21km above the average ground level of Mars and its volume is approximately 100 times that of Mauna Loa. Olympus Mons growth was not mitigated by tectonics and the higher surface gravity of the Earth and therefore

was been able to attain its great height. But, these differences alone cannot account for the size differential. Olympus Mons must have been active for a longer period of time than Mauna Loa if the construction of these two shield volcanoes were similar. If one takes the approximate time multiplied by 100 for the construction of Olympus Mons this would imply the volcano eruptions would have had to take place over at least 100 million years of steady eruptions. This value ignores other volcanoes on Mars and therefore a steady stream of eruptions gases over a large time periods appears likely.

Halevy *et al.* [72] published preliminary work suggesting a SO_2 feedback cycle which would allow clays to be formed in the early Noachian epoch. This approach would allow for neutral or lightly acidic water rather than highly acidic water seen in Bullocks approach. Neutral water is needed for clay formations found during the Noachian, namely during the geomorphologic Phyllocian epoch. With this present influx of potential early atmospheres being considered as plausible, sulfur species emitted by volcanic activity appears to have likely influenced the atmosphere in the early Martian climate.

While sulfur dioxide appears to be a viable greenhouse gas, the recent measurement of methane on the surface of Mars has launched this gas to notoriety. Although methane is not made in the present atmosphere of Mars, it could have entered the planetary atmosphere through venting of primordial methane or an influx with meteor/asteroid deposition. The continuing presence of methane on Mars in even the present day low quantity of approximately 10ppb [5] invokes the question of where this methane originated. With a lifetime in the present atmosphere of approximately 400 years, replenishment is essential, but if CO_2 levels were higher in Martian history, CH_4 lifetimes are seen to increase to 10^5 years with CO_2 levels 600 mbar (100x), see Figure 5.4. Recently the likelihood of methane as an early Martian greenhouse gas was

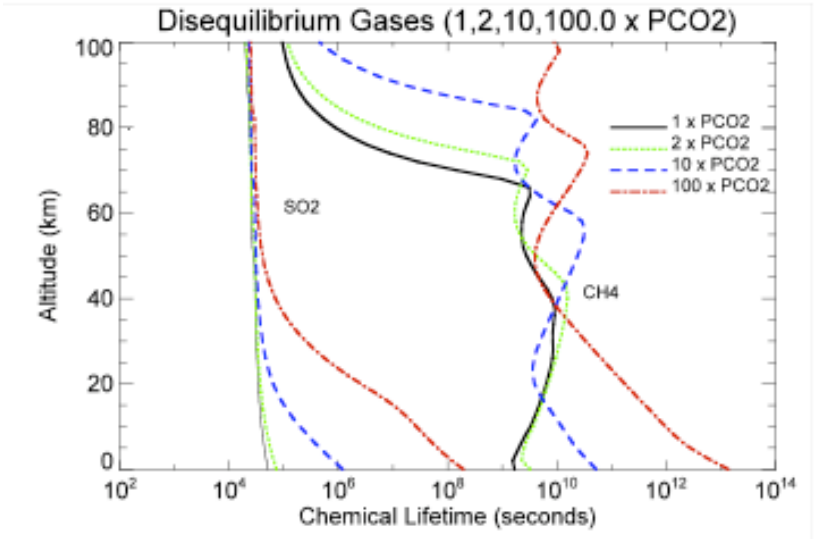

Figure 5.4: Lifetimes of CH_4 and SO_2 in varying atmospheres CO_2, courtesy of M. Summers

explored with a primitive 1-d modeling by [73]. More promising results were found in the high temperature, high surface pressure regime than in the high pressure, lower temperature. More work is needed but methane may solve some warming problems found in an atmosphere with only CO_2 or in combination of other greenhouse gases such as SO_2.

The amount of each gases contribution to the warming of the surface or the geomorphology is yet to be discovered but whatever the final atmospheric make up it must allow for clay formation in the Noachian epoch, a lack of observable carbonate formation, and water, at least episodically, to create the fluvial features seen on Mars.

Chapter 6: Review of Martian Model Bacteria/Archaea

Life on Mars has long been a tantalizing scientific question that presently does not have an answer. Navarro-Gonzalez *et al.* [74] tested Martian-like soils on Earth and suggest that the Viking testing instrumentation may have been blind to low level organics on Mars. Navarro-Gonzalez *et al.* [74] go on to suggest that organics may exist in higher levels even at the landing site of the Viking spacecraft (not considered a likely place to look for Martian life) that the detection equipment available would not see due to not only sensitivity limitations but to the technique used in the testing of the sample. Thus, although no organics were found during the Viking experiments, life still could have formed and even flourished during past epochs of Martian history and could possibly survive today in subsurface reservoirs or possibly caves recently discovered [75]. Although extremophiles were first discovered in 1957, researchers have in only the past decade begun to test the viability of these life forms in Martian-like conditions [15, 76]. Bacterial cyanobacteria, and radiophiles as well as Archaean halophiles have been proposed as analogous to potential Martian life [12, 15, 76, 77]. Researchers, such as Houtkooper and Schulze-Makuch, have suggested new life forms that produce H_2O_2 as an answer to the lack of organics found in the Viking results [78].

Cyanobacteria and radiophiles of interest in this paper belong to the phylogenic kingdom Bacteria. The halophiles studied belong to the kingdom Archaea. Examining the Tree of Life in 6.1 it is seen that both of these branches or kingdoms originate

from the Prokaryotes or the trunk of the tree. This classification system has been updated in recent years with the aid of RNA and DNA analysis and the tree is in a state of flux as many organisms have been reclassified. The organization of the kingdoms into branches is presently being debated as lateral gene transfer likely creates overlapped branches. It is not the purpose of this paper to make any determination of the present tree of life controversy but to use accepted branching with the caveat that lateral gene transfer likely causes the branches to overlap rather then exist in the separated state shown in Figure 6.1. For the sake of brevity, in this paper when writing about these organisms as a group, the reference will be to microorganisms and not separately as bacteria and archaea. Even though the writer is aware that microorganisms typically cross kingdoms and therefore includes a wide range of life in both the kingdoms Bacteria and Archaea as well as Eucaryota in the context of the paper the term will simply refer to the species of interest outlined in the paper and not other life forms.

Surface UV shielding may have occurred in Martian history but likely not to the extent of the ozone shielding on the surface of present day Earth. Therefore, organisms that can sustain UV radiation would be likely candidates for Martian life modeling. Thus, a modeling constraint to potential Martian life is the UV flux that penetrates to the surface with special attention to the UV wavelengths that lesions on DNA and inniciate cell death.

Wierzchos *et al.* [76] found a *Chroococcidiopsis* morphospecies of cyanobacteria in halite rock formations in the arid region of Atacama Desert. This photosynthetic bacterium subsists in the pores of rocks. This species is able to withstand the hyper-dry conditions in the Atacama Desert that have existed on the Earth in that region for 10-15 million years. Other life typically found in arid desert regions were absent in this hyper-arid region indicating the harsh living conditions. The soil also shows

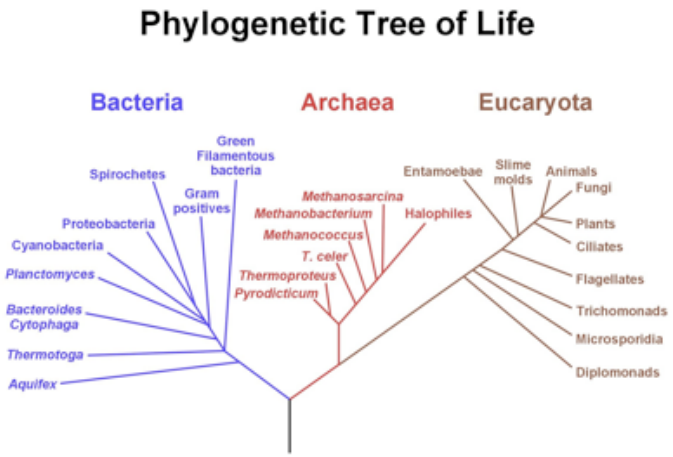

Figure 6.1: Tree of Life (originally published in article by David Morrison, 2003, NASA Astrobiological Institute

similarities to Martian soil, for example the lack of organics except refractory organics that do not break down under GCMS, and halite rock also found in the SNC meterorites and on the surface of Mars in salt evaporates linked to previous surface waters [76] and within. Although this species has not been reproduced in a laboratory setting for further study Cockell *et al.* [15] has tested *Chroococcidiopsis sp. 029* in Martian-like UV conditions. Viability at the surface of present day Mars was not found but increased dramatically if the organism lived 1mm below the surface in its native sandstone. These bacteria not only survived but also grew after 8 hours of exposure to Martian-like UV radiation in its native setting but not when model Martian soil was used. The bacteria was able to withstand cold temperatures, -10°C, and lower pressure, 8.5 0.2 mbar CO_2 used in the experiments. These bacteria can also survive extreme desiccation and with re-hydration return to a viable state with desiccation lasting up to 5 years before re-hydration [15]. Although high viability was only seen in the bacteria‘s natural soil, this may be expected for such a specialized

bacteria well adapted for its particular environment. Sandstone differs greatly from halite or its more common name, rock salt, being predominantly composed of quartz with the addition of such minerals as hematite (an iron oxide).

D. radiodurans, another class of bacteria, are able to withstand even higher levels of radiation (see Figure 6.2) and extreme desiccation. Thus, these bacteria have been a favorite of researchers looking for life on the Earth that would be plausible survivors on the harsh Martian surface. *D. radiodurans* are gram-positive mesophilic bacteria first discovered in irradiated meat in the late 1950s. With the advent of DNA analysis much study has centered around the biochemical makeup that allows these bacteria to withstand high levels of radiation lethal to other life on Earth and its ability to survive desiccation for long periods much like spore forming bacteria. Examinations of the cell walls of these bacteria indicate a closer link to gram-negative bacteria, thus a possible sign of engulfment and symbiosis in the bacterias past. The coiling and repetition of the DNA strands as well as the microorganisms repair mechanism are believed to be factors addressing radiodurans UV survivability. Repetitive DNA sequences (4-10 identical copies of its genome per cell) within the strands exist so if damaged, the bacterium has multiple copies available, thus preserving the DNA structure even in the presence of UV radiation. On going research into the mechanisms used by radiodurans to achieve high survivability include investigations into repair genes seen in the species. These microorganisms are mostly highly aerobic and grow in specific mineral make-ups.

Shapiro *et al.* studied *D. radiodurans* to determine the limiting factors for the growth in agar [79]. These bacteria within this genus *Dienococcus* needed magnesium and for the *D. radiophilus* species, Fe^{3+} for growth. The optimal growth temperature is 30°C but the bacteria will grow at temperature between 4°C and 45°C [80]. Although radiodurans have adapted to a warmer climate here on the Earth, the mineral

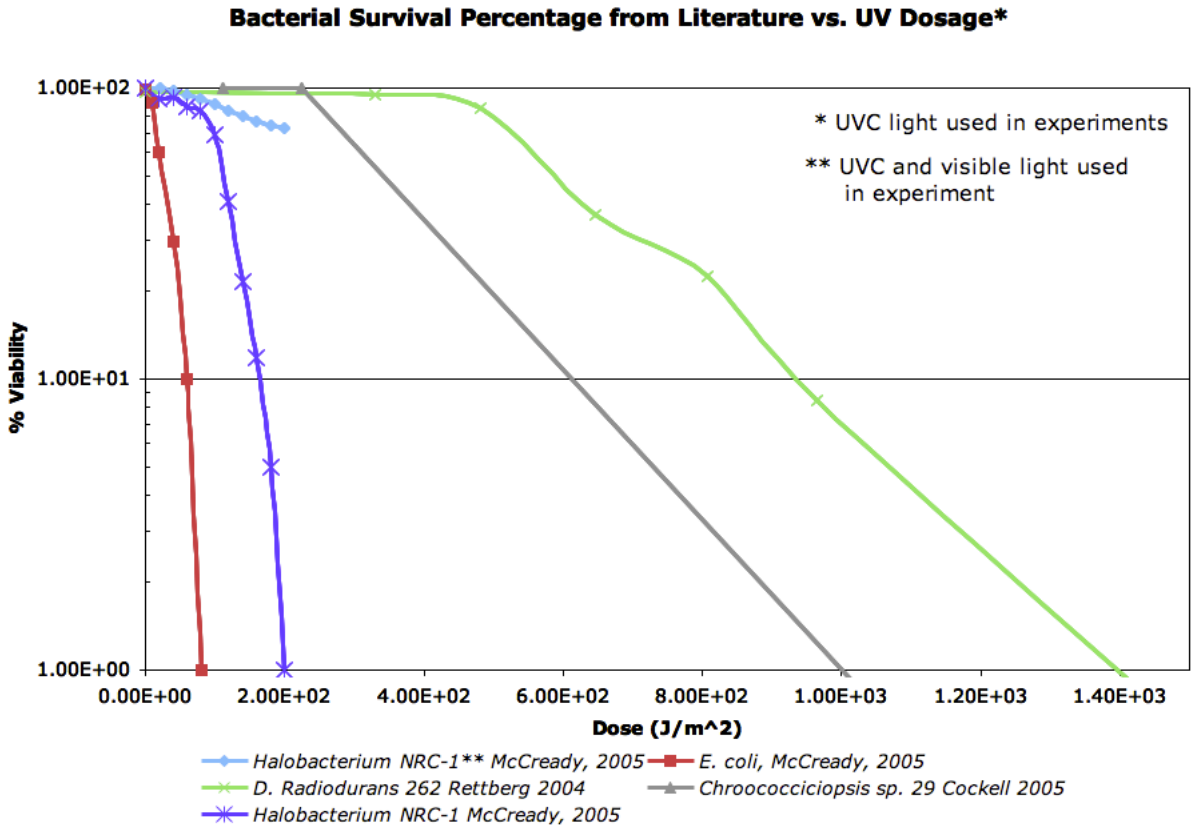

Figure 6.2: Bacterial Survival after exposure to UVC lamps for varying dosages. Compiled from published work by Shahmohammadi *et al.* [11] and McCready *et al.* [13]

requirements of Fe^{3+} and magnesium are met by the Martian regolith. If a warmer climate did exist on Mars, these bacteria could be analogous to potential surface survivors as Fe^{3+} is the ferric form of iron found in oxidizing condition which likely existed at least episodically when water was present on Mars.

Halobacterium sp. NRC-1 is also UV resistance as shown in Figure 6.2 [13, 16] and possible viable halophilic life has been found in over a hundred million year old halite pores [81]. These halophiles exhibit increased UV resistance but need salt water solutions ranging from 1.2-5.5 M NaCl [16, 82]. *Halobacterium salinarum sp. NRC-1* as well as being resistant to UV-C is very resistant to UV-A and UV-B with colony forming units before and after UV exposure of up to 39 KJm^2 of approximately 100% [16]. In fact the UV resistance increases with increased salinity, a trait likely to provide an evolutionary edge in evaporative waters. *Halobacterium salinarium NRC-1* and a *Haloarcula-G* were found viable after exposure to desiccation and 10 freeze and thaw cycles with temperatures of -20°C (253K) and -80°C (193K) for at least 144 days, even *D. radiodurans* did not survive this exposure at -20°C but did at -80°C [19]. Recently, growth of *Halobacterium salinarium sp. NRC-1* was seen after exposure to -15°C temperature for several weeks, the growth chart reproduced from Weidler [14] is shown in Figure 6.3. Halophiles have thus been viewed as possible homologues to Martian life, not only because of the traits listed above, but also because of the salt layering seen on the Martian surface in areas where liquid water is suggested to have existed such as Meridiani Planum [83]. Since water likely appeared episodically on the Martian surface bacteria with the these traits could have likely survived in the increasing saline and UV environment.

More recently sulfate-reducing bacteria (SRB) have captured the attention of researchers because of the large sulfur mineral content found in possible previous salt lake areas on the surface of Mars. These areas suggest a drying of water by the

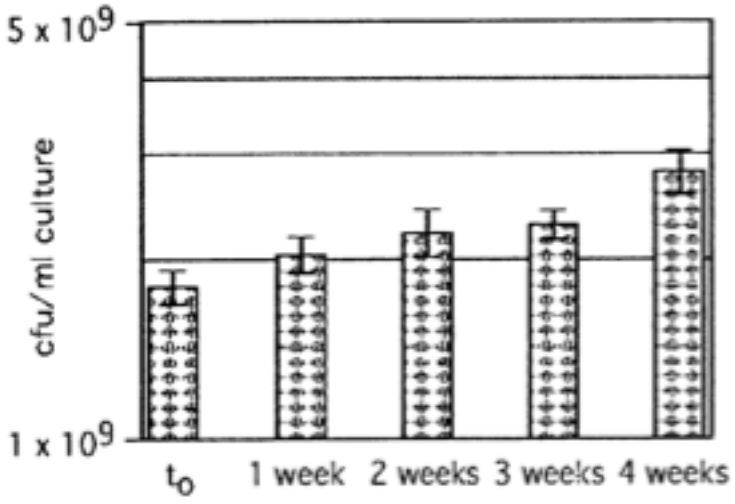

Figure 6.3: "Growth of *Halobacterium sp. NRC-1* in liquid medium at -15 °C." [14]

layering of the salts seen [21]. Since the sulfate salts would provide a hospitable environment for this bacteria, these microorganisms are starting to be more deeply studied for potential for possible life on Mars [84]. Although UV susceptibility is only presently being tested in Martian like conditions, here on Earth in experimentation to destroy SRBs in groundwater show promising results for 254nm wavelength and the possibly of survival in ancient Martian UV environment [85]. The energy source for these organisms is hydrogen, thus, if hypersaline water was present, the prospect for life on Mars greatly improves as a viable energy source and environment is found. Recently research by Marnocha *et al.* [84] is examining the deposits of such bacteria in Martian type soils to address possible biotic signatures for this microorganism.

Escherichia coli (E. coli) bacteria have been much studied. *E. coli* bacteria are gram-negative non-sporing bacteria commonly found warm-blooded mammalian intestinal tract. There are hundreds of different strains of *E. coli*, a few strains are toxic to man [86]. Bacterial growth is seen at temperatures between 15°C to 37°C. Resistance to radiation is not high, as for much life on Earth. From Figure 6.2 one

can see the difference in radiation tolerance between *D. radiodurans* and *E. coli*. *E. coli* bacteria for this paper will be used as a standard bacterial model with which to compare standard bacterial life on Earth to early Martian UV conditions.

Chapter 7: Approach to Early Mars Atmospheric Modeling

To model the early atmosphere of Mars various constraints must be placed on its reactive constituents. Although the specific amounts of these constituents, or even which constituents are present, cannot be known with certainty, inferences can be made by examining Noachian/Hesperian dated surfaces on Mars. Of interest is the amount of UV protection afforded the Martian surface because of UV absorbing molecules in the atmosphere such as water, oxygen, ozone, and sulfur species. As shown in Figure 7.1 the sulfur species and ozone absorb in the most DNA sensitive wavelength region between 200 – 300 nm. Other proposed constituents absorb heavily in the low UVC region, e.g. carbon dioxide and water. Therefore, the proposed early Martian atmosphere should not only be plausible, but results suggest specific UV regions were likely absent during periods on the surface of Mars. A review of model runs is shown in Table 7.1.

Carbon dioxide, the main Martian atmospheric constituent today, has long been theorized as the ancient greenhouse gas that warmed the early surface of Mars [32, 65,87]. As outlined in the Chapter 6 questions arise to the amount of cloud cover and cloud location above the surface because of the variable effects on surface warming in an atmosphere comprised of CO_2 and water vapor but not other greenhouse gases [32,64,65]. Kastings reported CO_2 model results were limited to the first 60km above the Martian surface see Figure 5.1. The Nair model used in this investigation has a temperature profile to 240km above the Martian surface.

Table 7.1: Model Parameter Change for Atmospheric Simulations

Parameter Change	**Description of Change**	**Reference**
	CO_2	
1. a. $SP = 6mbar$	Similar to current surface pressure Ps = 0.006 bar	Kasting 1991 [64]
1. b. $SP = 60mbar$	10x a. ($SP = 6mbar$)	Kasting 1991[64]
1. c. $SP = 350mbar$	Maximum pressure before CO_2 cloud formation in stratosphere $P_s = 0.35$ bar	Kasting 1991[64]
	Temperature	
2. a. Nair high temp. curve	Model present day temp.	Nair *et al.* 1994 [6]
2. b. Kasting 1.a. temp. curve	Model curve augmented with appropriately fitted Nair curve above 60km	Kasting 1991[64]
2. c. Kasting 1.b. temp. curve	Model curve augmented with appropriately fitted Nair curve above 60km	Kasting 1991 [64]

Table 7.1: Model Parameter Change for Atmospheric Simulations

Parameter Change	**Description of Change**	**Reference**
2. d. Kasting 1.c. temp. curve	Model curve showing warmest temperature with only CO_2 in atmosphere and without cloud formation augmented with appropriately fitted Nair curve above 40km	Kasting 1991[64]
H_2O		
3. a. Nair/saturation curve	Nair water curve limited in values by H_2O saturation curve for temperature curves above and remaining constant above 20km	Nair *et al.* 1994 [6]
Boundary Conditions SO_2		
4. a. BC=1.06x10^{10} $cm^{-2}s^{-1}$ surface flux	Estimated flux value from comparison to Earth shield volcano output	Lenine (personal communication)

Table 7.1: Model Parameter Change for Atmospheric Simulations

Parameter Change	**Description of Change**	**Reference**
4. b. BC =1.06x10^{11} $cm^{-2}s^{-1}$ surface flux	10x estimated amount	Lenine (personal communication)
4. c. BC=1.06x10^{09} $cm^{-2}s^{-1}$ surface flux	1/10th estimated flux	Lenine (personal communication)
H_2SO_4 condensation rate		
5. a. pseudo reaction rate to model condensation of H_2SO_4 = 5x$10^{-20}cm^{-3}s^{-1}$	Estimated using theory from Summers Uranus paper	Summers and Strobel 1989
5. b. pseudo reaction rate = 5x$10^{-22}cm^{-3}s^{-1}$	10x estimated value	Summers and Strobel 1989 [88]
5. c. pseudo reaction rate = 5x$10^{-19}cm^{-3}s^{-1}$	1/10x estimated value	Summers and Strobel 1989 [88]

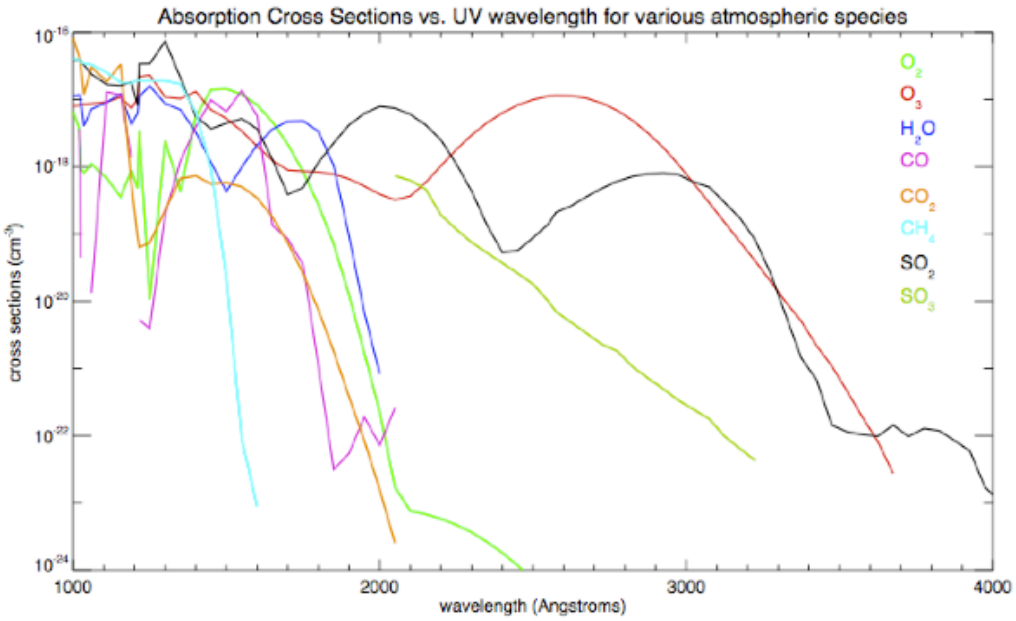

Figure 7.1: Absorption cross sections for UV absorbing species in the Martian atmosphere

For this reason the temperature profiles used by Kasting [64] will be modified with the present temperature model scaled appropriately above 60–80km. Smoothing between the models will be accomplished by using Microsoft Excels solver for a parabolic equation. Although present temperature models for Mars differ from the reported results in Kasting, this paper stands as the model for no CO_2 cloud formation on early Mars and will therefore be used in addition to the present day temperature profile for temperature sensitivity runs. All CO_2 levels are modeled and results compared to previous results before trace constituents are added to see the effects on the enhancement of the UV shielding at the surface.

Sulfur species proposed to have been present in the atmosphere of early Mars are related to surface volcanic activity [66,89]. Yung *et al.* [66] examined the introduction of sulfur dioxide in the atmosphere to deter CO_2 cloud formation. With an addition

of 0.1ppmv of SO_2, initial model results demonstrated midlevel warming in the atmosphere that could inhibit cloud formation by allowing more CO_2 to be present before condensation. Although Mischna *et al.* [65] concluded that clouds could have both a warming and a cooling effect on surface temperature. The introduction of SO_2 could enhance such possible warming effects. SO_2 could also enhance UV absorption in the atmosphere. Referencing Figure 7.1, one notices that along with ozone, SO_2 absorbs in the high UVC range specifically harmful to Earth type life. Thus, not only could SO_2 enhance warming effects on the surface of early Mars, it may have offered UV protection as well. Examining Noachian age volcanic features and referencing the volcanic emissions to similar Earth volcanoes estimates can be made of total volcanic output during the epoch.

Care must be taken to examine the potential magma content of Mars contrasted against the Earths volcanic output with appropriate adjustments made to the estimates where differences exist. Levine estimates SO_2 emissions for Mars to be between 4-8 x 10^{11} moles S/year (Levine, personal communication). This implies that flux rates from the surface would be approximately 1x10^{10} $cm^{-2}s^{-1}$. This value was used as the upward flux boundary condition on the surface of Mars for all early atmospheric simulations except for sensitivity runs which examine the atmospheres sensitivity to variable SO_2 output. These runs will address two issues: the likelihood of variable volcanic output on Mars rather than steady state output estimated above and the sensitivity of the model to the approximation to the upward flux of SO_2. Since this boundary condition is an estimate based upon the make up of volcanic output on the Earth, the value is not tightly constrained. Therefore, simulations are run with SO_2 varying above and below this value to examine significant atmospheric impact, if any, to this boundary condition.

Other gases, including H_2O, H_2, and S_2, also are released into the atmosphere

Table 7.2: Percentage of Volcanic Gases comparison from Table 2.2, recreated from USGS website [3] and Holland [7]

Gas	Erta‘ Ale Divergent Plate, 1130°C	Holland, 1978
Water Vapor H_2O	77.2	79.31
Carbon dioxide CO_2	11.3	11.61
Sulfur Dioxide SO_2	8.34	6.48
Sulfur S_2		0.24
Hydrogen H_2	1.39	0.58
Carbon Monoxide CO	0.44	0.37

with volcanic eruptions see Table 2.2 for a list of volcanic gases. Although varying from the percentages used by Levine to approximate the SO_2 output of an average Martian volcano, the differences are small as seen in the comparison of values shown in Table 7.2. It can be seen though that most of the eruption gases are made up of water vapor, CO_2, and SO_2. Therefore, concentrations of these gases are explored and the impact of the influx of these gases on the atmosphere.

Finally, oxygen, ozone, and other atmospheric constituents dependent upon the presence of CO_2, SO_2, and water were examined. As adjustments are made to the levels of CO_2, SO_2, and water, the model will appropriately adjust levels for these dependent gases by modeling chemical reactions involving these gases. Some of these gases, such as oxygen and ozone offer UV surface shielding, see Figure 7.1. During sensitivity runs for these primary constituents, dependent gases were also be examined. How does the variability of these primary volcanic gases influence dependent constituents? This question is addresed in each sensitivity run to explore the impact of the primary gas not only on the atmospheric balance of constituents but also the role of UV shielding gases in the atmosphere. UV surface fluxes are examined with special attention to the specific UVC range sensitive to Earth's life DNA around 254nm.

A microorganisms ability to withstand UV radiation is dependent upon the amount

of UV radiation present at specific wavelengths on the surface of the planet. Survivability can also depend upon the amount of darkness during a Martian day. Many studies compare repair to subsequent UV radiations to determine long-term viability, not just the survival of the organism but its ability to reproduce. The viability can change over time if repair time is inadequate and damage accumulates over days. UV fluxes are calculated for days and months to see the effect on the viability of the microorganism in question. Finally, requirements for survivability of microorganisms are matched to epochs in Martian history and possible locations on the surface which could have supported life.

Chapter 8: Bacterial Survivability: Analysis Method

UV survivability of microorganisms has been an interest to microbiologists since *D. radiodurans* were first discovered in the late 1950s. With the onset of more advanced laboratory techniques, the biological mechanisms related to such survival have been an area of active research. The data presented on the UV survivability of the specific microorganisms outlined in this paper were collected from several papers over a span of approximately 40 years. It is therefore relevant to ensure data reliability. Wherever possible multiple data sets were used to demonstrate values obtained were largely independent of specific methodology. Data sets are limited to a narrow range of UV-wavelengths most lethal to DNA, and thus the bacteria‘s viability. Where possible data sets were expanded when sufficient data were found. If data is limited to a single experiment it will be noted. The data collected on the cyanobacteria are recent and multiple data sets for a specific cyanobacterium were not found in the literature.

Initially to test feasibility of methodology survivability data for *D. radiodurans* from Rettberg *et al.*, Cockell *et al.*, Moseley, Setlow, and Mancinelli *et al.* [12, 15, 19, 90, 91] were fitted using the method outlined in John Sutherland‘s paper on fitting organisms survival curves when exposed to radiation [92]. Several types of curves are examined in his paper presenting a stochastic model solution. *D. Radiodurans* survivability curve is presented in Figure 8.1 as an example of flat-shouldered curves. This implies that the drop off rate is small to none until a threshold dose is found. After this threshold, the survivability curve drops more rapidly. This type of curve is

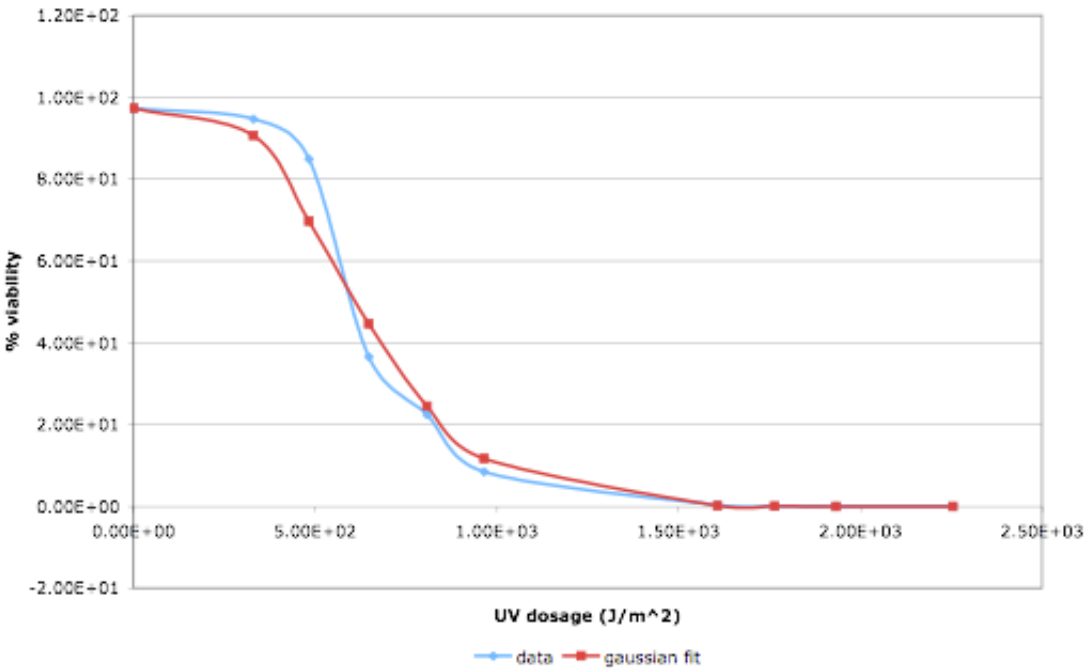

Figure 8.1: D. Radiodurans viability vs. UV Dosage

seen not only for UV dosing for *D. radiodurans* but for each microorganism discussed in this proposal to some extent except for the test bacteria *E. coli* which readily reacts to smaller doses of UV radiation. This curve fit will be used where appropriate and adjusted for *E. coli* to represent proper curve fitted as outlined in Sutherland. The flat-shouldered curve fitting employs an incomplete gamma function to fit survivability vs. UV dose curves. The functional form is as follows (for equation development see Sutherland, 2006 [92]):

$$S\left(\bar{\mu},n\right)\equiv e^{-\mu}\sum_{i=0}^{n-1}\frac{u^{-i}}{i!}=Q\left(n,\bar{\mu}\right)\rightarrow Q\left(n,\frac{D}{D_1}\right) \tag{8.1}$$

Here $Q\left(\bar{n},\frac{D}{D_1}\right)$ represents the regularized gamma function $Q\left(\bar{n},\frac{D}{D_1}\right)\equiv\frac{\Gamma\left(\bar{n},\frac{D}{D_1}\right)}{\Gamma(\bar{n})}$. The numerator of the regularized gamma function represents the upper incomplete gamma

function $\Gamma\left(\bar{n}, \frac{D}{D_1}\right) \equiv \int_{\frac{D}{D_1}}^{\infty} t^{\bar{n}-1} e^{-t} dt$ and the denominator a complete gamma function, $\Gamma(\bar{n}) = (\bar{n}-1)!$. The variables are defined as follows: $\bar{\mu} = \frac{D}{D_1}$ where $\bar{mu}$ is the average damage frequency, D corresponds to the average frequency of lethal damages with the assumption that damage levels are a linear function of the UV dosage[1]. D_1 represents the dose at which there exists an average of one lethal-damage per member of the population exposed to radiation. Here the average damage frequency, $\bar{\mu}$, is replaced by a dosage ratio which is easier to measure experimentally. In this scenario we assume perfect bounded repair by this it is meant that all microorganisms survive if they have incurred less than n damages, thus allowing the flat-shoulder to exist for low dosages [92]. Once each survival curve was fitted, estimates for various dosages could be made from the functional form of the graph where data might not have been available, see 8.2 for a fitted survival curve.

Using this fitted function new graphs could be made for each UV wavelength vs. survival at a particular dosage level within the data set. Finally, function fitting could be made to these curves. The curves were fitted and initial results using Excels trendline fitting routine found to match polynomial functions of 4^{th} order. The trendline equations gave reasonable results for all dosages graphed see Figure 8.4. What this functional form for survivability could mean for these *D. radiodurans* is unknown at this time.

Many UV data published in literature use present day model Martian UV flux incident on the microorganisms. These experimental dosages attempt to mimic present Martian atmospheric models. Since the UV dosage incident on the microorganisms represents UVC, UVB, and UVA wavelengths together, it is important to distinguish

[1]Double strand breaks and other clustered damages might result from either single or double radiation events, hence giving rise to the linear and quadratic terms, respectively. However, experimental measurements of the dose response functions for double strand breaks and other clustered damages reveal that their induction is a linear function of dose over a range of doses that span the limits of biological relevance [92] and sources within.

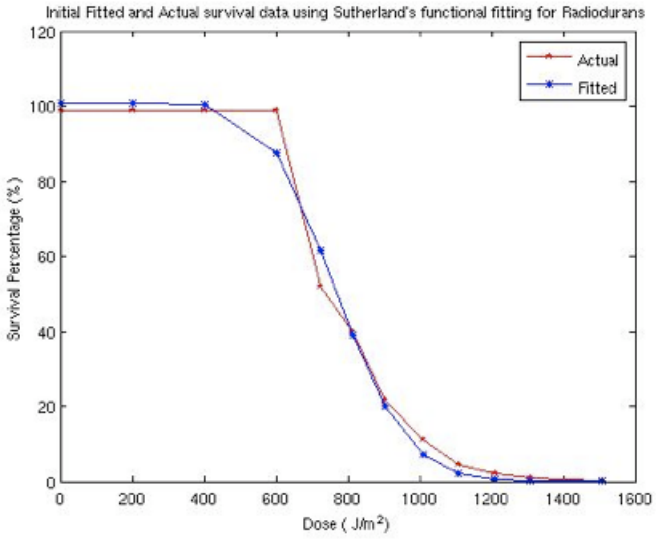

Figure 8.2: Fitted Survival Data using Sutherland's functional fitting for *D. Radiodurans*

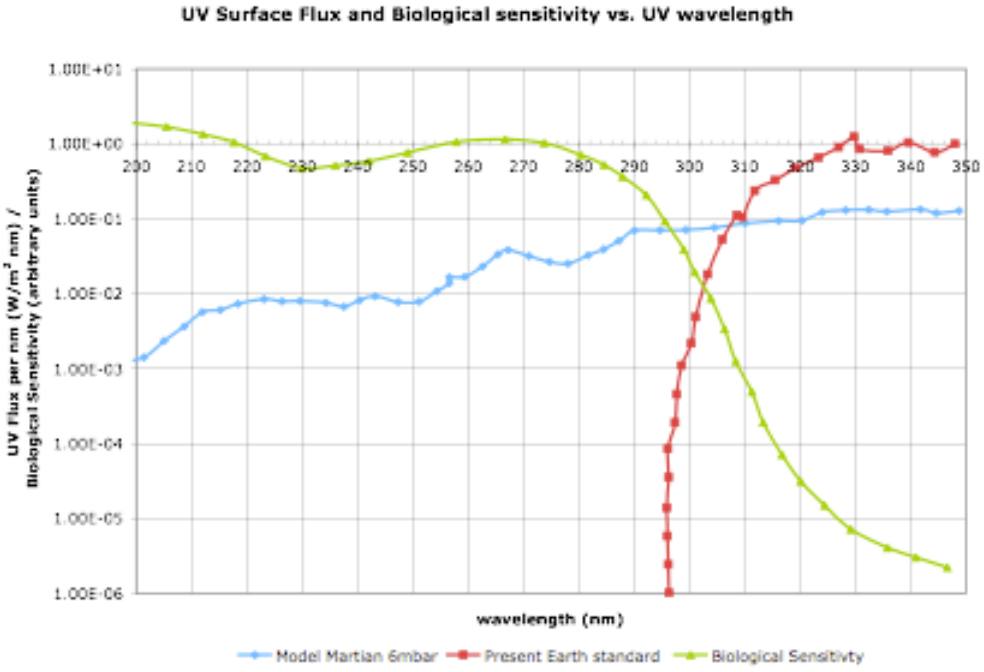

Figure 8.3: Theoretical UV Biological Sensitivity Curve compared with Earth and modeled Mars UV surface spectra

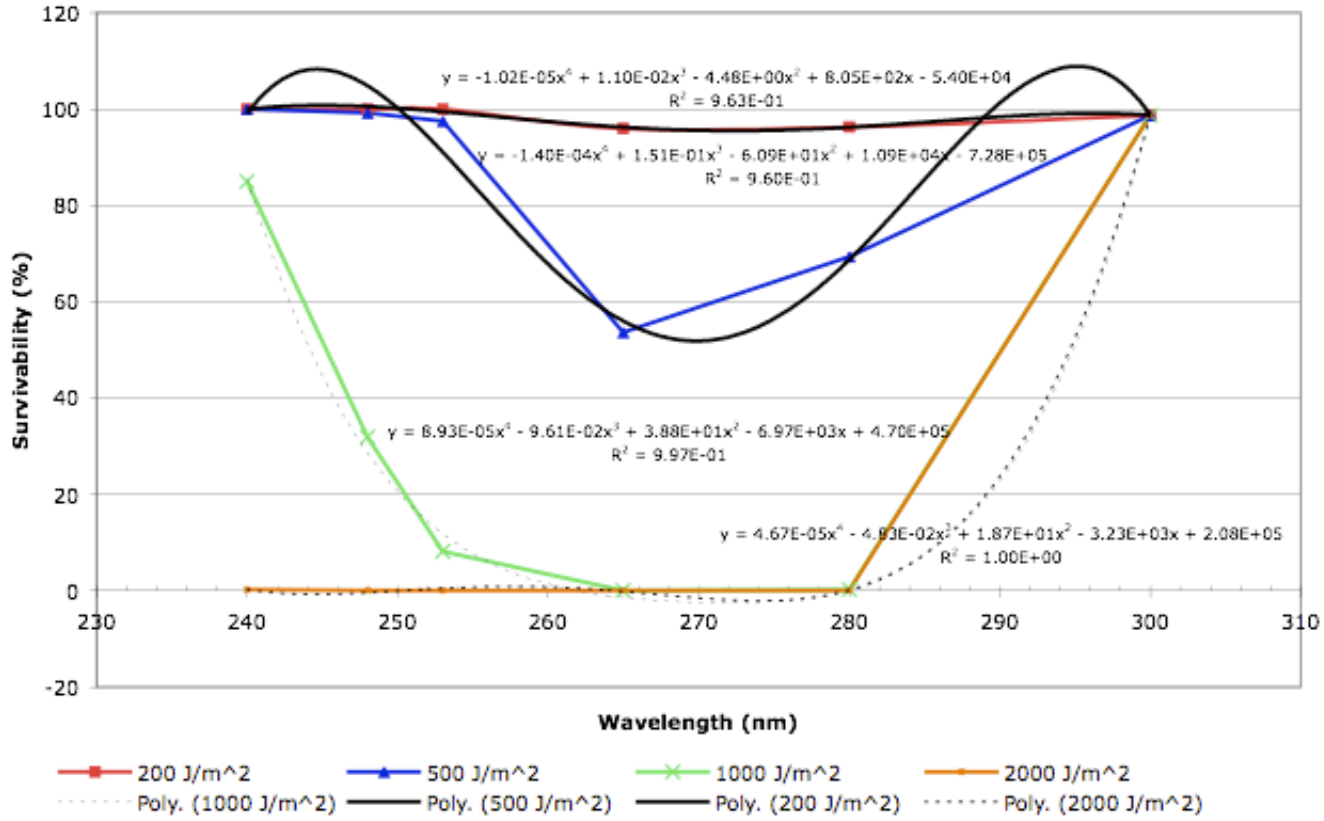

Figure 8.4: Fitted UV Survival Data for *D. Radiodurans* at varying UV dosages

between the sensitivity of the microorganism to each UV wavelength range. Action spectra are graphs which display a sensitivity of an organism to specific wavelengths of light, thus $\phi(\lambda) = \frac{number of events}{number of photons absorbed}$. Setlow in 1965 [91] measured DNA sensitivity curve of radiodurans to UV flux. The graph, Figure 8.3, is recreated by Horneck *et al.* [93] is extended from Setlow's data, following theory to cover part of the UVA spectrum. Here one finds standard present day measured data for the Martian and Earths atmospheric UV flux as well as biological sensitivity normalized to the lethal UV wavelength, $254nm$ [91]. The data taken to produce the biosensitivity curve is a dosage of a specific wavelength to induce cell death. Data is then taken for a sufficient number of wavelengths and fitted. This DNA biological sensitivity curve will be used in conjunction with experimental UV dosages which induced cell death to scale the UV incident flux for comparisons with data which does not separate UVC, UVB, and UVA flux incident on test microorganisms. Although the UVB sensitivity can range from organism to organism it is assumed that the response for UV resistant microorganisms would be sufficiently similar to allow sensitivity comparisons since action spectra for the chosen halophile and cyanobacterium are not available.

Nair modeled parameters provide solar flux dosages at incremental wavelengths and specific line spectra of interest for each model atmosphere. Using the UV flux over specific wavelengths comparisons can be made to the surface dosages for ancient Mars. The effect on the microorganisms can then be correlated to specific model results and survivability of the microorganisms to the solar flux is examined. Since survivability is not only due to UV surface fluxes, these results can be added to a list of survival parameters for the test microorganisms to thrive on the planet surface or within the regolith. After such analysis is completed the impact of future missions to Mars can be discussed and its relevance to the proposed research. Although some questions to the past history of Mars may always exist, with additional information

gathered by future probes and changing or improved measurement techniques, new information may elucidate unanswered questions within the proposed research.

Chapter 9: Atmospheric Model Results

After verifying the current working Martian model parameters, changes are made to mimic Kastings proposed ancient Mars models parameters [64]. These initial model runs without SO_2 were completed to ensure results were comparable to results published by Kasting without additional sulfur chemistry; verifying the Nair model's equivalence. The results of the normalized partial pressure of CO_2 are shown in Figure 9.1. As expected the results, although similar, were not identical due to the additional chemistry in the present Nair model when compared to the simplified model used by Kasting. These three temperature and CO_2 profiles were used as the basis for the study of the early Martian atmosphere. Additional model were run with changes in the water profile, sulfur species boundary conditions and H_2SO_4 condensation rate.

Once comparable results were demonstrated for the initial model, changes to the model parameters were made for SO_2 and H_2SO_4. SO_2 entered the early atmosphere through volcanic emission while H_2SO_4 condenses out of the atmosphere once the sulfur dioxide has cycled through chemical reactions in a proposed sulfur cycle shown in Figure 9.2 (augmented from the sulfur cycle in Wong *et al.* [50]). Rates for influx and deposition of these chemicals were estimated through two distinct methods. SO_2 influx, as a constituent of volcanic emission of similar Earth volcanoes, is dependent upon the amount of volcanic activity and the constituent make up of the expelled gases. Estimates have been made of the amount of SO_2 that entered the ancient Martian atmosphere through analysis of surface geology, chemical make up

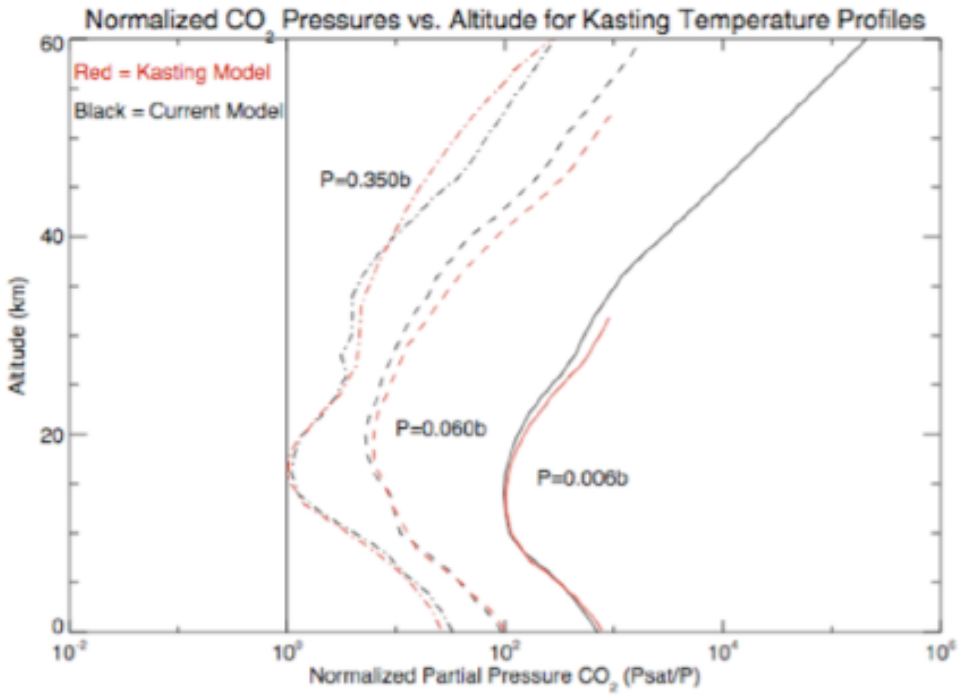

Figure 9.1: Comparison of Kasting 1991 models and current Model CO_2 partial pressures

of gasses expelled from Earth volcanoes compariable Martian volcanoes, and chemical analysis of surface rock. Levine estimates SO_2 emissions for Mars to be between $4-8x10^{11} moles \frac{S}{year}$ (Levine, personal communication). This implies that an averaged upward flux rates would be approximately $0.5 - 1.1x10^{10} cm^{-2} s^{-1}$ during the early volcanic period on Mars. This boundary condition was added to the current model in the form of SO_2 only. Although other sulfur species may be expelled from volcanoes, because of the uncertainty of the composition of the volcanic emissions, the dominant sulfur species from similar Earth type volcanoes was used.

With the introduction of SO_2 into the atmosphere it is crucial to set a condensation rate for H_2SO_4. The H_2SO_4 must have an exit path in the atmosphere as well as a deposition rate on the surface of Mars. A pseudo reaction rate is found for H_2SO_4 condensation and the surface boundary condition of H_2SO_4 is set to $-1.0x10^{-1} \frac{cm}{s}$, in

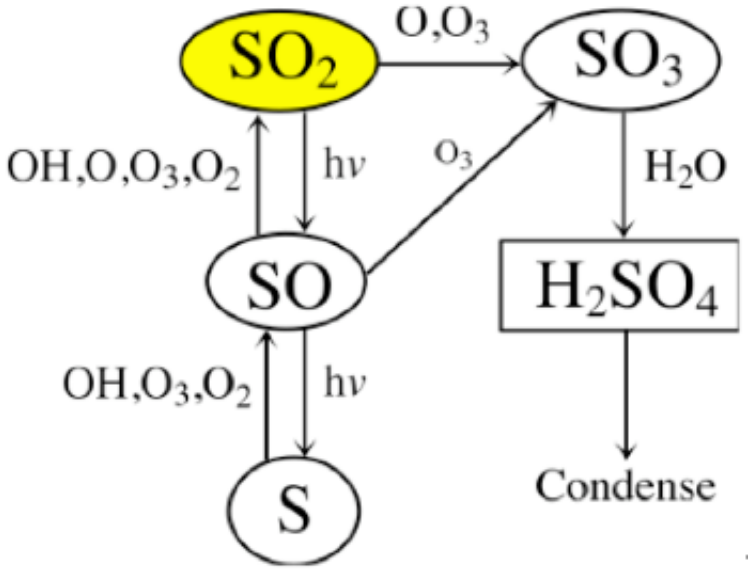

Figure 9.2: Martian Sulfur Cycle used in Simulation surface boundary condition provides influx of SO_2 into the atmosphere from estimated Early Martian volcanic emission

line with the standard downward transport and precipitation out of the atmosphere and onto the surface of molecules. The pseudo reaction rate is set by analysis of condensation time constants following Summers and Stoebel [88] for condensation of minor constituents on Uranus. This calculation was repeated using Martian values and the condensation time constant was then used to produce a reaction rate coefficient for entry into the atmospheric model. Models were then rerun to see affects of the introduction of sulfur species on the model.

With the introduction of sulfur into the model, changes in atmospheric water were examined. Three water scenarios were initially used. Starting with the temperature profile created by Kasting [64], water profiles were generated from saturation vapor pressure for water for the altitudes shown in Kasting data. This constraint is initially necessary so that no water clouds would be formed and therefore requiring additional changes within the atmospheric model. The Nair model requires mixing ratios up to

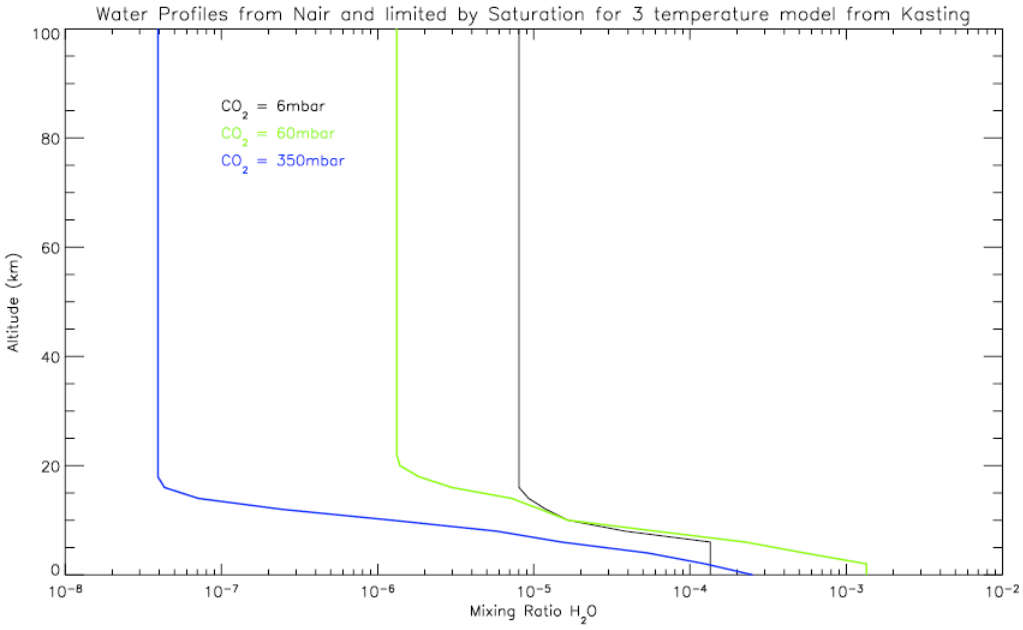

Figure 9.3: H_2O saturation limited curves for 3 model atmospheres

240km. Thus, these water curves were augmented with the minimum mixing ratio seen in the saturation curves obtained from the Kasting models. This is sufficient since above the minimal temperature seen in the models, water vapor is cold trapped and no additional sources of water through atmospheric chemistry exist at higher altitudes. Figure 9.3 shows the three water profiles created using the 6mbar initial Kasting temperature model and limited by water vapor saturation and maintains the lowest mixing ratio above the minimum point. Notice that the water profiles all have the same shape except for the first 10km.

Sensitivity to changes in the water profile were examined. The profiles were increased by 10x and 100x the initial water profiles but saturation limited. This changed only the initial 10–60km of the curves. Sulfur species are not highly sensitive to the changes made to these water profiles. Although the sulfur species themselves change as the water and CO_2 values change in the models below saturation levels, significant change is not seen with additional water limited by saturation. Therefore, water

profiles, limited by saturation and thus not cloud producing, would not influence the presence of sulfur species for these concentrations of CO_2.

Now that saturation limited water has been seen not to influence sulfur species the focus is changed to examine how the differing CO_2 levels affect the levels of sulfur species in the model scenarios. For these scenarios the water profiles will be reset to the standard water saturation curves outlined above. Initial results demonstrate that the surface lifetime of SO_2 increases with increasing CO_2. As shown in Figure 5.4, SO_2 lifetime increases by three orders of magnitude from approximately half a day to a bit over 1.5 years while CO_2 increases by less than 2 orders of magnitude showing sensitivity to the major atmospheric constituent of present day Mars. The sensitivity of the SO_2 lifetime is caused by the increase in O_3, an efficient UV absorber which not only increases in mixing ratio as CO_2 is increased but also increases at higher altitudes removing energetic UV photons that could otherwise reaction with SO_2, see Figure 9.4. In the thinner 6 mbar atmosphere, it is seen in Figure 9.5 that R171 is the dominant loss reaction, R171 is the photolysis of SO_2. But, when viewing the same graph for the 350 mbar atmosphere, see Figure 9.6, one finds not only a reduction in the mixing ratio of SO_2 but also that R171 is not longer the dominant reaction near the surface. It has been replaces by reactions R174 $OH + SO_2 + M \rightarrow SO_3 + M$ and R175 $O + SO_2 + M \rightarrow SO_3 + M$. Thus, in a denser CO_2 atmospheres sulfur photolysis is reduced a the surface and this enables longer lifetimes for SO_2.

The surface influx value estimated for sulfur dioxide is dependent upon volcanic activity that is not tightly bounded, both because of the variability of volcanic activity and the basis of Earths volcanic output for the SO_2 estimates. Therefore additional models were run to examine the sensitivity of the results to changes in the sulfur species themselves. Since the surface influx is estimated from volcanic emissions of sulfur dioxide, SO_2 influx values will be changed to mimic the variability of volcanic

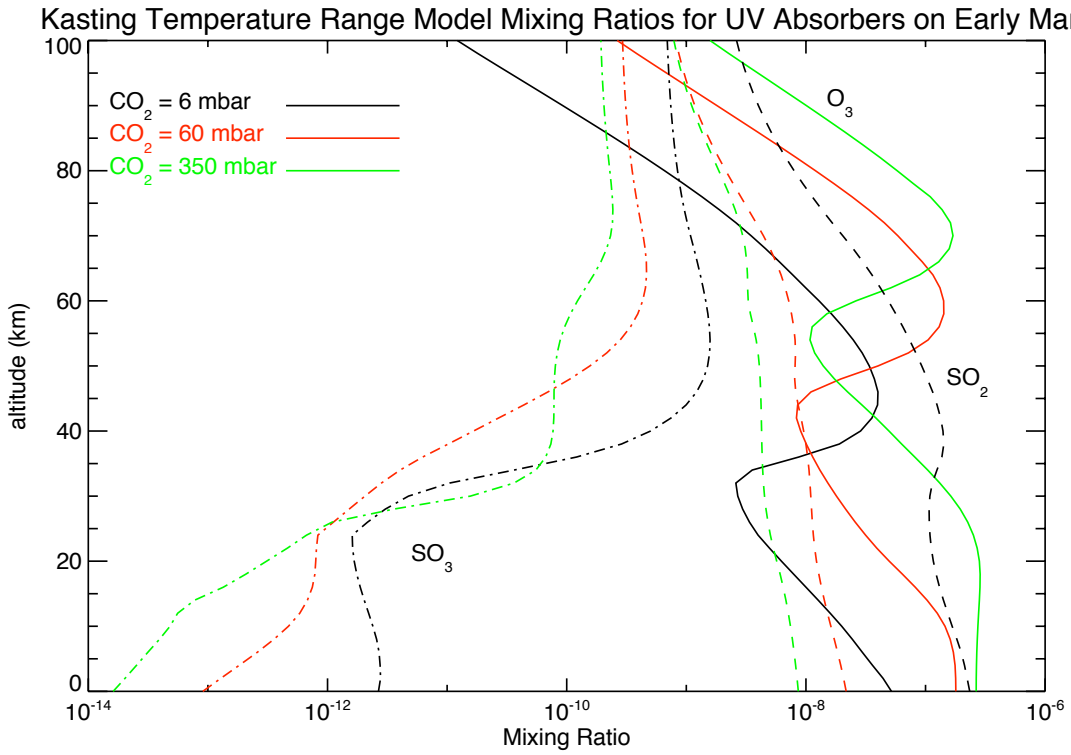

Figure 9.4: UV Absorbers in modeled ancient Martian Atmospheres

activity during active periods. Holding the standard water profiles to saturation for each model, changes were made in the SO_2 upward flux boundary condition to examine how the sulfur cycle would be affected by changes to the upward flux of SO_2. The upward flux values were changed by an order of magnitude larger and smaller than the estimated flux value used to this point in the model. Results are shown in Figures 9.8, 9.9, and 9.10. By inspection it can be seen that changes by an order magnitude in the surface flux of SO_2 leads to similar flux mappings when graphed. Therefore, the SO_2 flux profile appears virtually unaffected by the change in the amount of SO_2 emission except for the now predictable horizontal shifts. Finally, inspection of the H_2SO_4 flux profiles also show similar flux profiles except for changes between 10–20 km that can be linked to the downward transport of the H_2SO_4.

With SO_2 in the atmosphere from approximately one day to one year, the sulfur

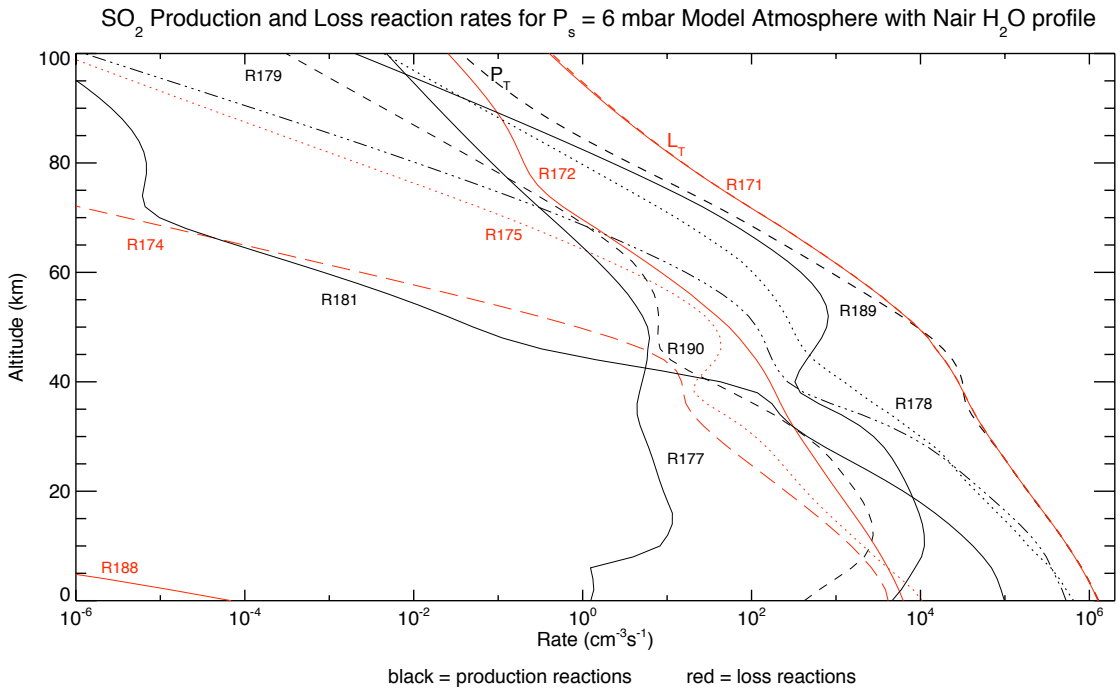

Figure 9.5: Production and Loss of SO_2 in 6 mbar modeled ancient Martian Atmosphere

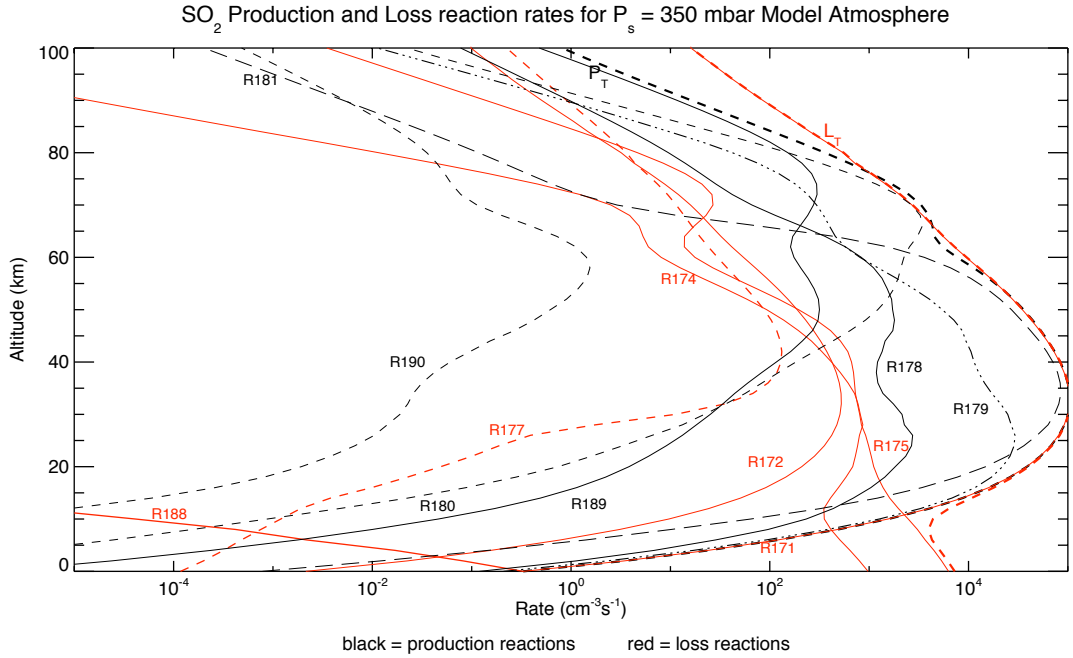

Figure 9.6: Production and Loss of SO_2 in 350 mbar modeled ancient Martian Atmosphere

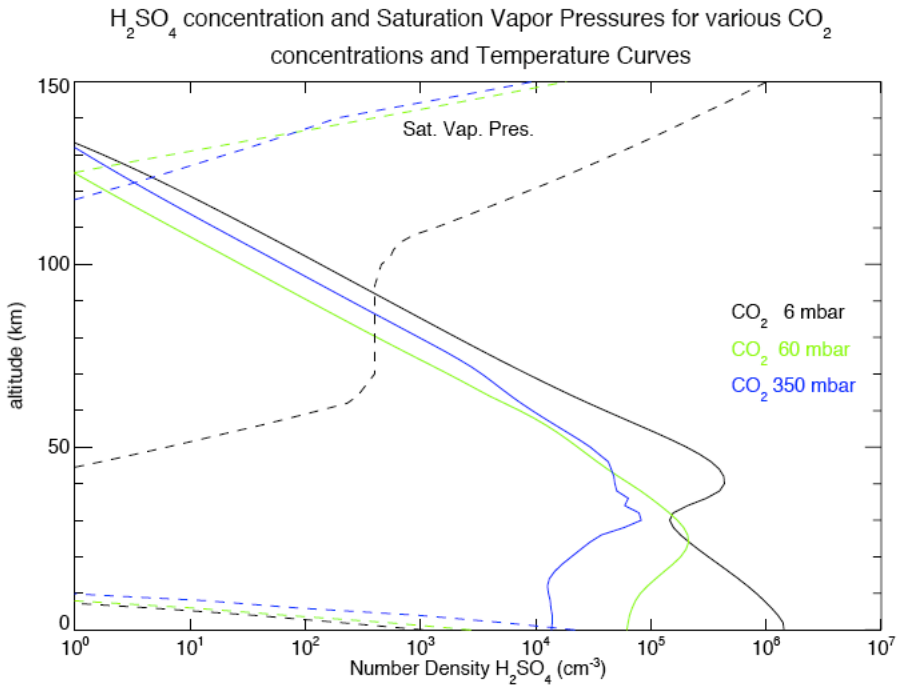

Figure 9.7: H_2SO_4 concentration and Saturation Vapor Pressure for 3 model CO_2 Atmospheres

dioxide reacts with oxygen species or breaks up due to photolysis creating new sulfur species such as SO and SO_3 shown in Figure 9.20, 9.21, and 9.22. These species are short-lived and relatively insensitive to the increase in CO_2. H_2SO_4 will be produced after SO_2 react with photons and oxygen species. It then accumulates in the atmosphere and precipitates out onto the planetary surface. This is seen by examining the saturation vapor pressure curve relative to the accumulated amounts of H_2SO_4 for the three CO_2 scenarios shown in Figure 9.7.

Since H_2SO_4 accumulates in the atmosphere, a pseudo-reaction rate is introduced into the model to mimic the precipitation of sulfuric acid out of the atmosphere and on to the surface. This reaction is entered into the model reactions as: $H_2SO_4 + M \rightarrow PROD$ where M is a non-specific molecule and $PROD$ is an end product removed from further atmospheric analysis. Thus, H_2SO_4 molecules are effectively removed

from the atmosphere as desired but dependent upon the total atmospheric content rather than condensation on aerosols. In setting a value for the reaction rate one must mimic the rate of condensation of H_2SO_4 out of the atmosphere. To estimate this value we start by estimating the condensation time constant for H_2SO_4, τ, following Summers and Strobel, Appendix A [88]. This condensation time constant is translated into a reaction rate for entry into the model by solving $\dot{n} = kn_{H_2SO_4}n_M$ for the k where $\tau = \frac{n}{\dot{n}}$. The initial value used as the initial reaction rate for H_2SO_4 is $5x10^{-23}cm^3s^{-1}$. Condensation rate sensitivities were also run for this pseudo-reaction rate, changing the rate by two orders of magnitude larger and one order of magnitude smaller. The results are shown in Figures 9.8, 9.9, and 9.10. Since the condensation rate was approximated by a pseudo-reaction rate one must be sure that H_2SO_4 is not sensitive to the changes made to this parameter. Looking at the total production and loss results from the model in Figures 9.11, 9.12, and 9.13 one sees that near-surface level (approx. 20km) values for H_2SO_4 production and loss are not impacted by changes in the condensation time constant. Thus, the pseudo-reaction rate estimation is sufficient for modeling the condensation of H_2SO_4.

The increase of SO_2 in the atmosphere decreases the UV solar flux incident on the surface according to model results; this is to be expected as SO_2 is a known greenhouse gas. This decrease in solar flux could have influenced the habitability of the surface of Mars during the outgassing of volcanoes, when SO_2 was injected into the atmosphere. Figures 9.14, 9.15, and 9.16 show the impact of the changes of the modeled upward flux of SO_2 on the solar incident flux at the surface. Here we find the greatest decrease in solar flux in the most sensitive wavelength range for DNA in Earth-type life. The initial decrease in surface solar flux due to the increase in CO_2 is seen mainly because of the increase in O_3 as shown in Figure 9.26. Although the surface O_3 is depleted in the 350mbar CO_2 atmosphere, at higher elevations an

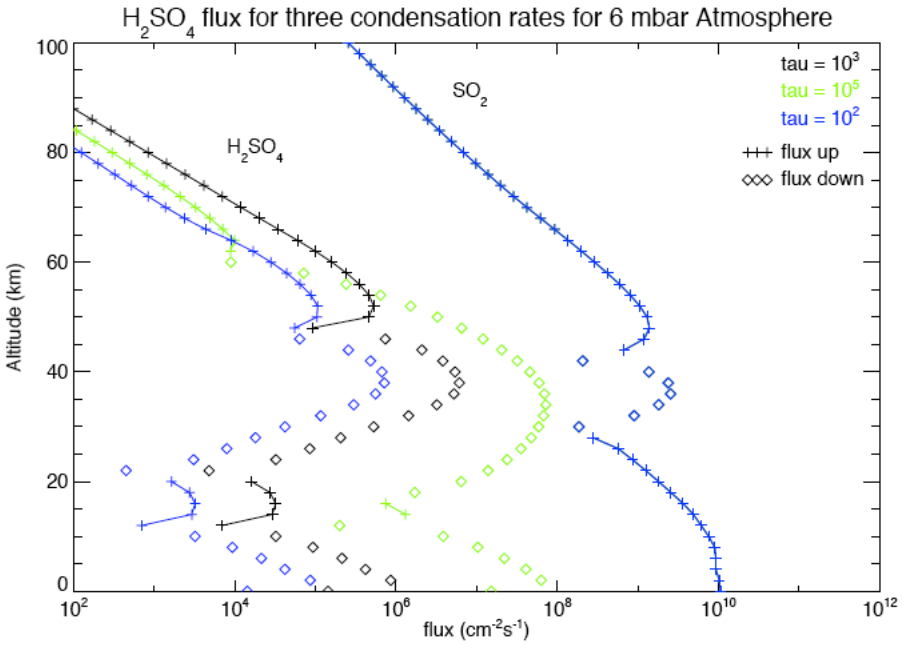

Figure 9.8: H_2SO_4 flux sensitivity for 6mbar CO_2 Atmosphere

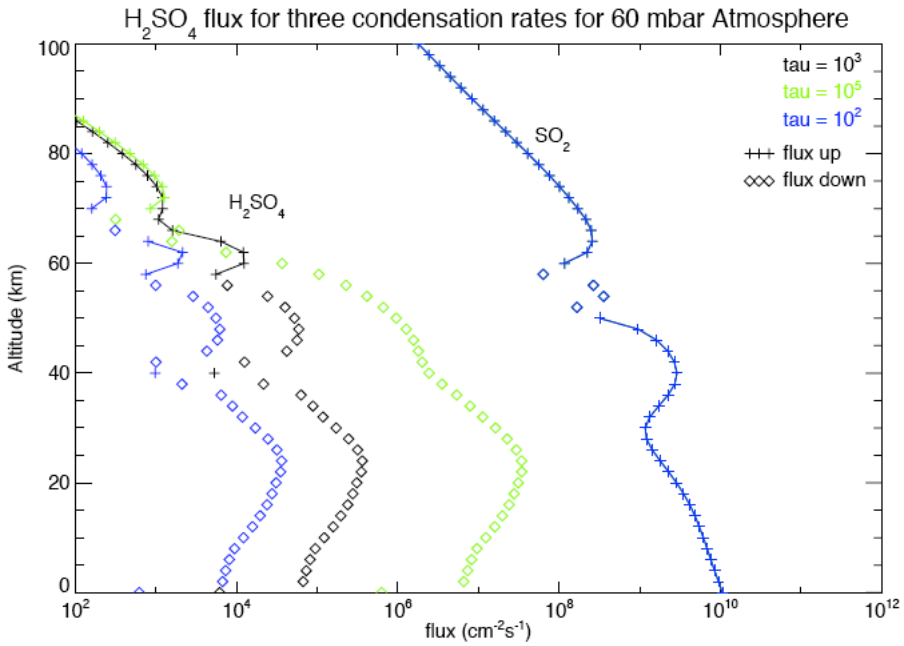

Figure 9.9: H_2SO_4 flux sensitivity for 60mbar CO_2 Atmosphere

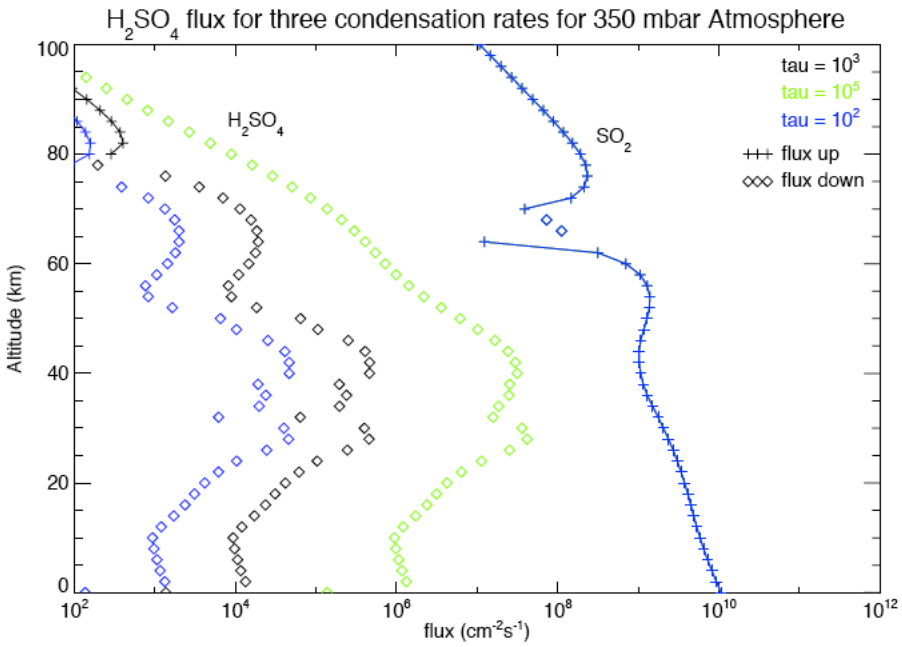

Figure 9.10: H_2SO_4 flux sensitivity for 350mbar CO_2 Atmosphere

increase in O_3 is seen. By looking back at Figure 7.1 it is seen that SO_2, SO_3, and O_3 are the molecules which efficiently absorb in the UVC range and thus impact the UV surface flux. SO_3 is negligible as shown in Figure 9.20, 9.21, and 9.22. Thus SO_3 is only a transient molecule with absorption in the UV in the modeled atmosphere and a minor UV surface flux constituent.

The solar flux used in the Nair model is the present day flux incident on Mars. The solar flux incident on ancient Mars is thought to be approximately 75% of the present day solar flux due to a higher ratio of hydrogen to helium. Since less incident flux obviously could impact the UV flux incident on the surface model runs were performed lowering the incident flux to 75% of today's values. The result are shown for 6mbar and 60mbar, and 350mbar atmospheres in Figures 9.17, 9.18, and 9.19. The 6mbar and 60mbar models show a modest and a larger impact to the reduced flux. Therefore, these UV flux parameters will be used when comparing results for microorganisms survivability on the surface of Mars. It is noted that the 350mbar

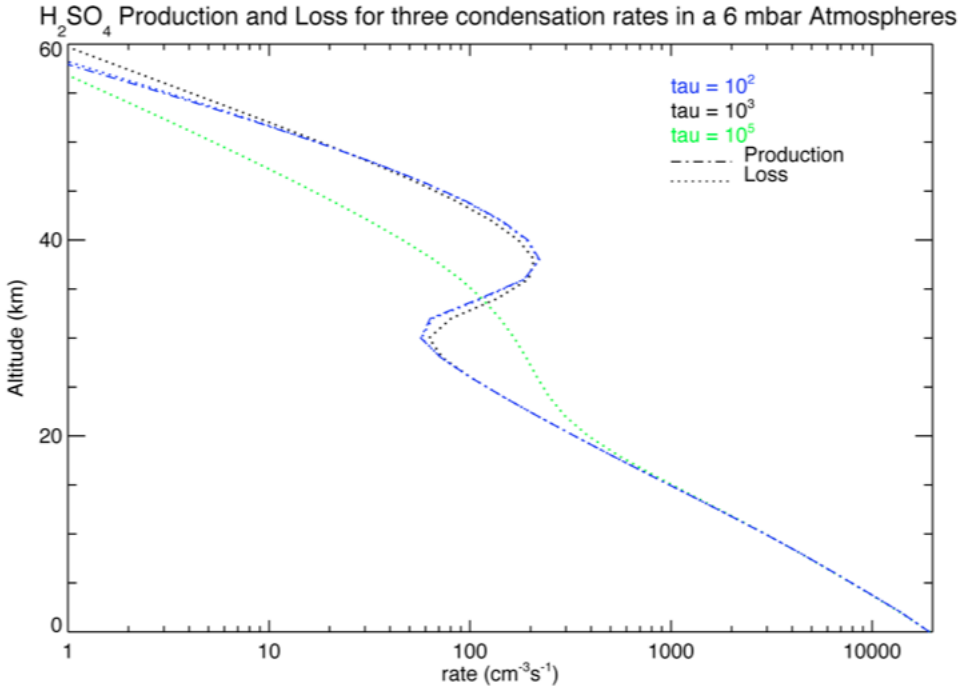

Figure 9.11: H_2SO_4 total Production and Loss rates in a 6 mbar CO_2 Atmosphere]

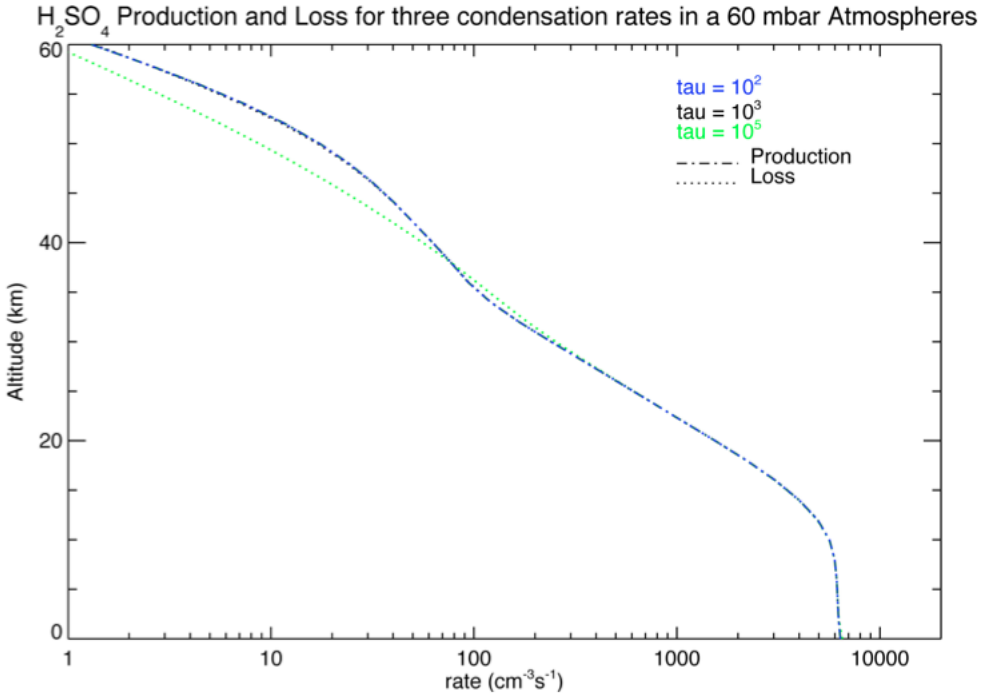

Figure 9.12: H_2SO_4 total Production and Loss rates in a 60 mbar CO_2 Atmosphere

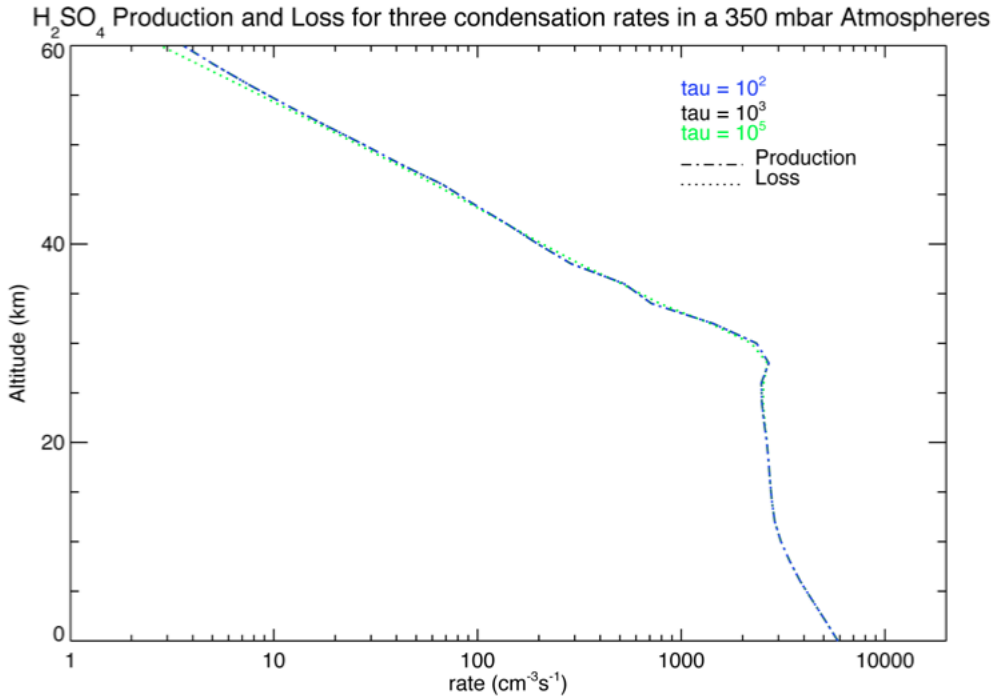

Figure 9.13: H_2SO_4 total Production and Loss rates in a 350 mbar CO_2 Atmosphere

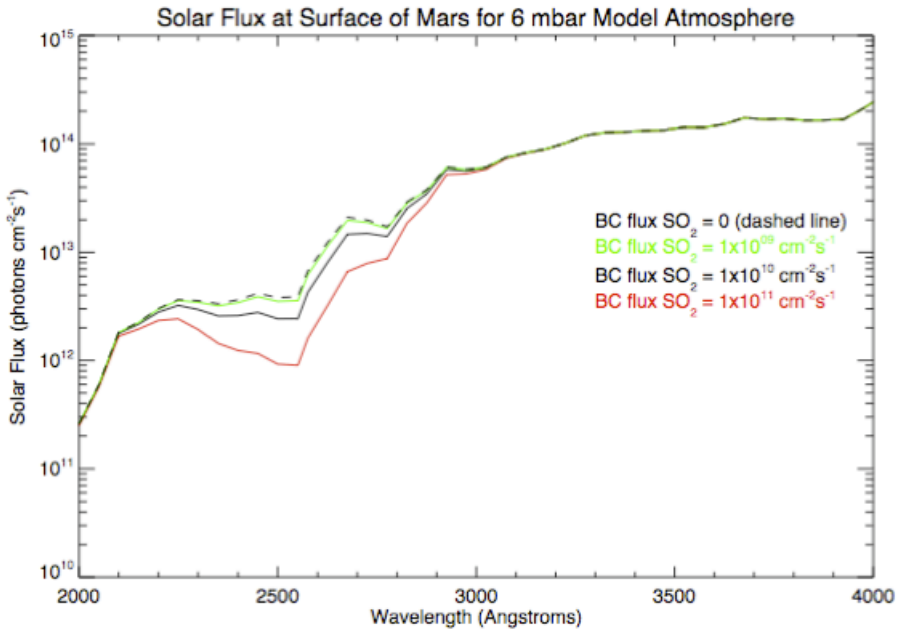

Figure 9.14: Solar Flux data for varying 6mbar model Martian atmospheres

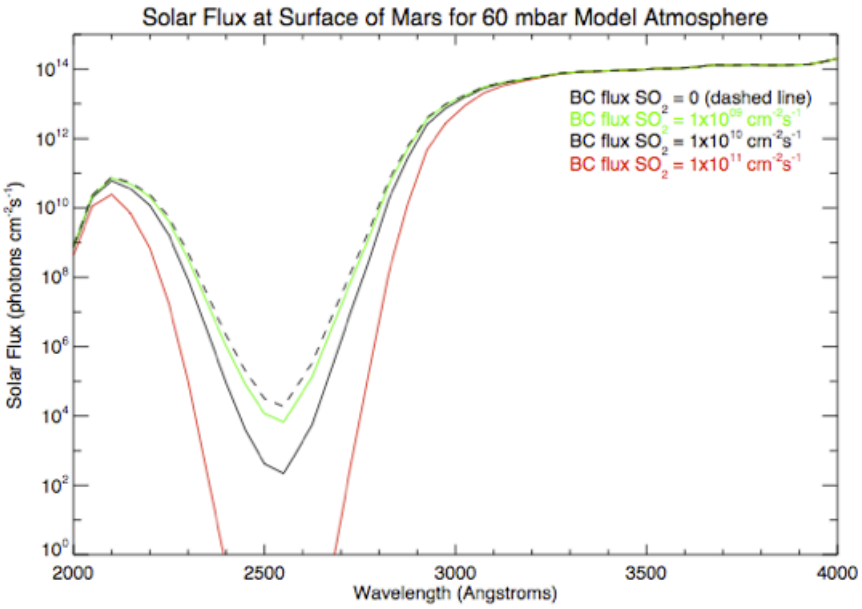

Figure 9.15: Solar Flux data for varying 60mbar model Martian atmospheres

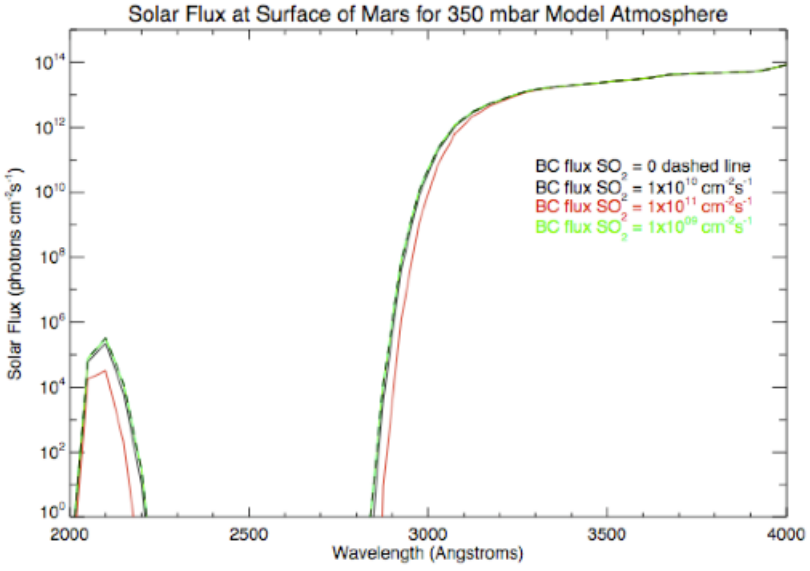

Figure 9.16: Solar Flux data for varying 350mbar model Martian atmospheres

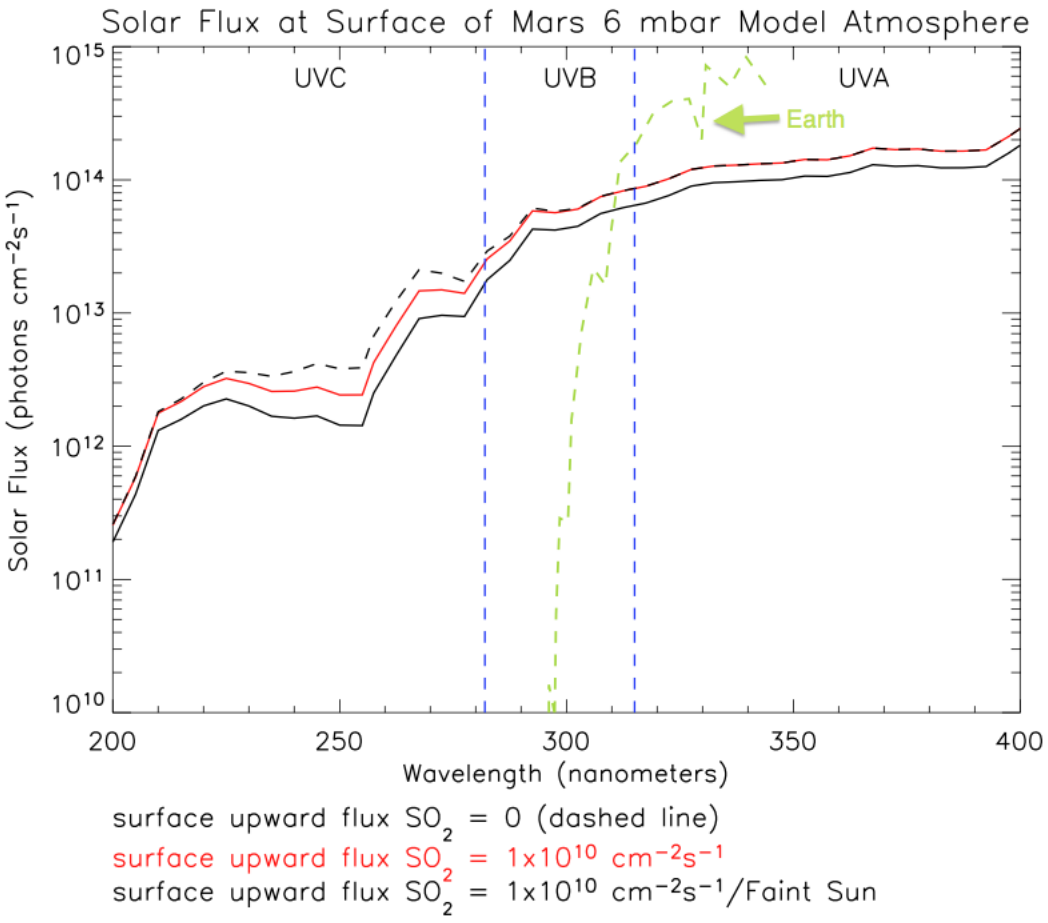

Figure 9.17: Solar Flux data for faint sun comparison in a 6mbar model Martian atmospheres

atmosphere shows little change in the UV flux as most of the UVC has been removed already. Thus, the faint sun's reduced UV flux is not an important factor in the modeling scenario as long as CO_2 is of sufficient concentration in the atmosphere of Mars.

Following Kasting CO_2 concentrations and temperature curves as input into the Nair model the following conclusions are drawn from data output. Sulfur dioxide lifetimes found in this model agree with earlier values estimated or modeled values previously published except for Johnson *et al.* [71]. Johnson *et al.* used a pulsed sulfur input model to mimic volcanic eruptions found lifetimes 10 to 100 times longer

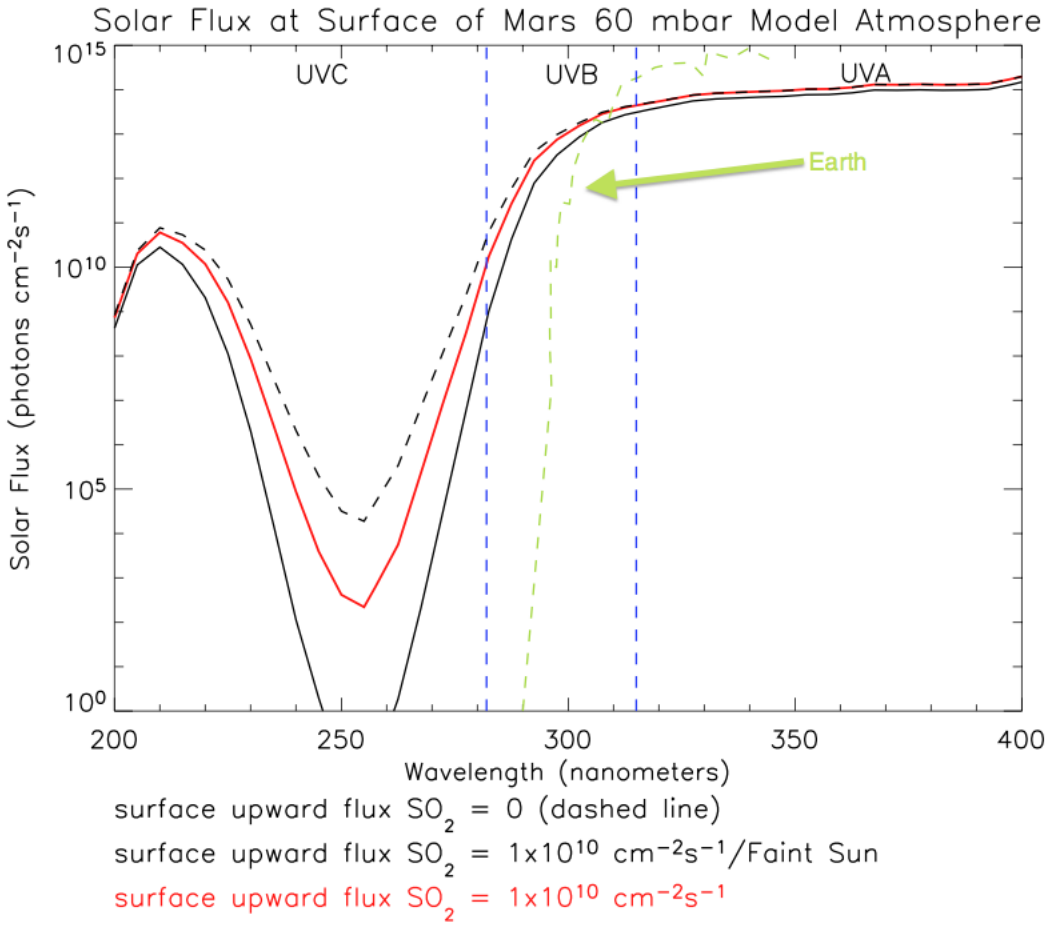

Figure 9.18: Solar Flux data for faint sun comparison in a 60mbar model Martian atmospheres

in some 600mbar atmosphere models. This result likely differs because of high SO_2 influx into Johnson's model rather than a constant averaged influx as used in the Nair model in this paper as well as the increased surface pressure, almost double the amount of CO_2. When changes were made to the amount of SO_2 in the Nair model, results were found to increase e-folding lifetimes of SO_2 by 10, although still indicating differences in model results. More testing with higher concentrations of CO_2 are needed to verify the equivalency of results.

If CO_2 levels were higher than these Nair model saturation values (implying a higher temperature profile), even more sulfur dioxide would likely have existed and

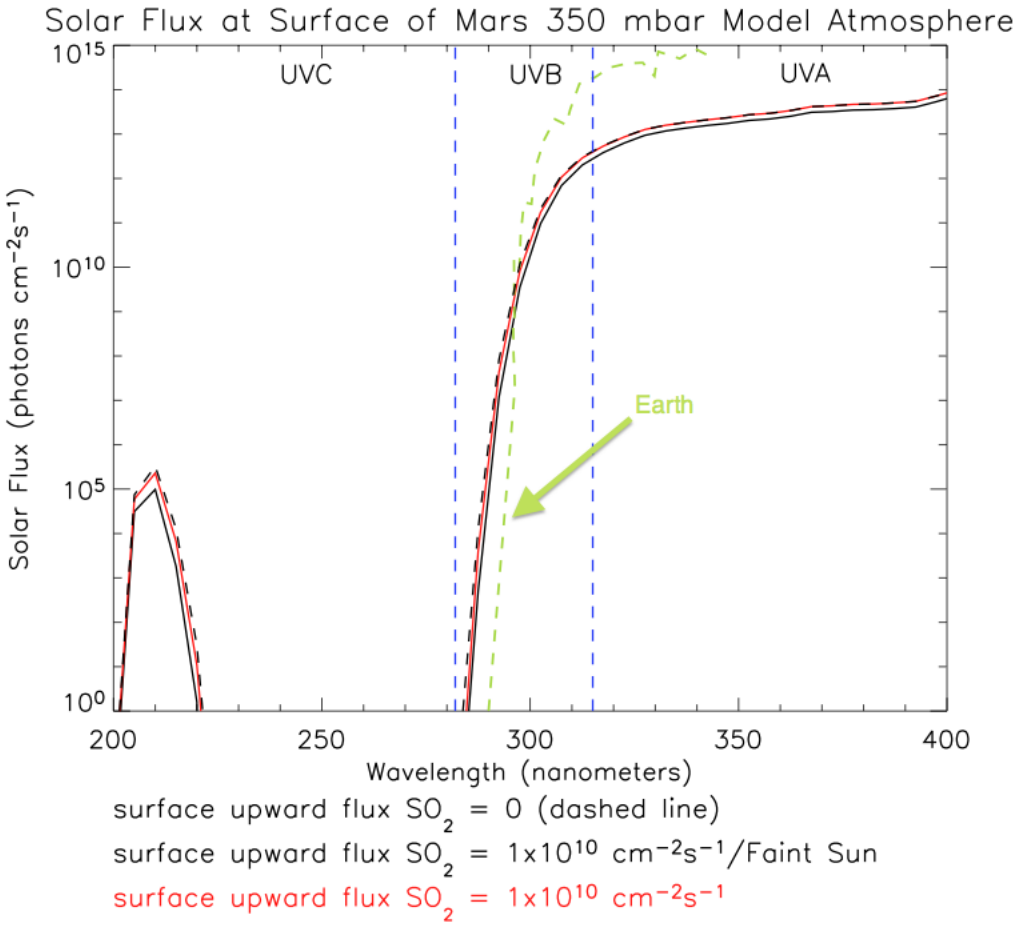

Figure 9.19: Solar Flux data for faint sun comparison in a 350mbar model Martian atmospheres

longer lifetimes would be seen. The water profiles limited at saturation do not change the sulfur dioxide profile but the addition of super-saturated H_2O at specific CO_2 atmospheric concentrations shorten the SO_2 lifetimes and therefore the life cycle of end product H_2SO_4. The insensitivity to the saturation limited water profiles is not surprising as water saturation limited curves change only in the bottom layer for 1x-100x H_2O model levels. The additional runs at super-saturation water levels were run, even though the concentrations are not physically obtainable in a real atmosphere, as limits to changes in the atmosphere due to the presence of water. Sulfur species in these runs were found to have similar lifetimes with only the short-lived SO_3 species

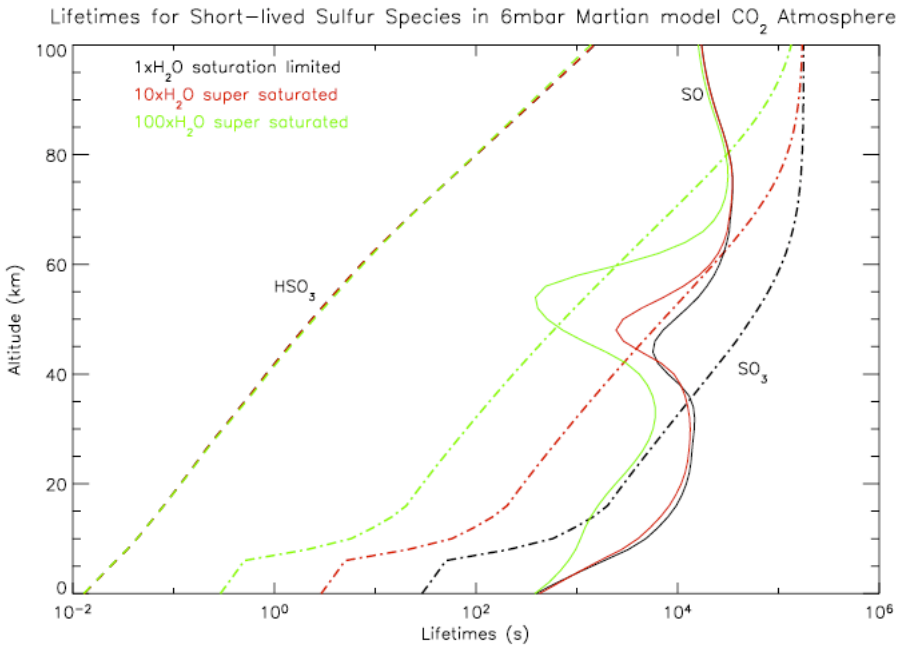

Figure 9.20: Short-lived Sulfur Species in 6mbar CO_2 Atmosphere

with the only discernible difference that could have been predicted from Reaction 183 ($SO_3 + H_2O \rightarrow H_2SO_4 + M$), see Figures 9.20 – 9.25. With water a likely volcanic emission as well as sulfur, model exploration of saturated water levels including cloud formation need to be generated.

The SO_2 surface flux boundary conditions do not show great sensitivity to order of magnitude changes to the upward flux. This is important as upward flux of SO_2 would likely change by orders of magnitude during early Martian history as volcanic activity is not constant. H_2SO_4 formed in the atmosphere (the dominant end product of SO_2) would condense onto the surface with the introduction of SO_2 into a predominately CO_2 atmosphere – this could address the lack of carbonates on the surface of Mars and explain the sulfur minerals found on Mars. With super-saturation of water in the atmosphere one notices that the lifetimes for H_2SO_4 decrease with increasing CO_2 but are not affected by the increase of water to 100x saturation. Although this

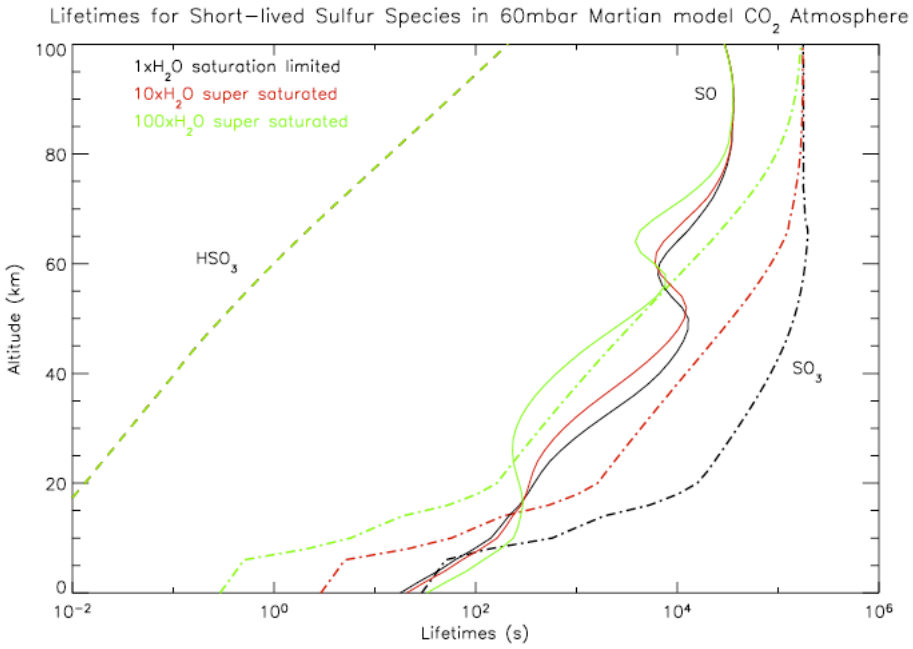

Figure 9.21: Short-lived Sulfur Species in 60mbar CO_2 Atmosphere

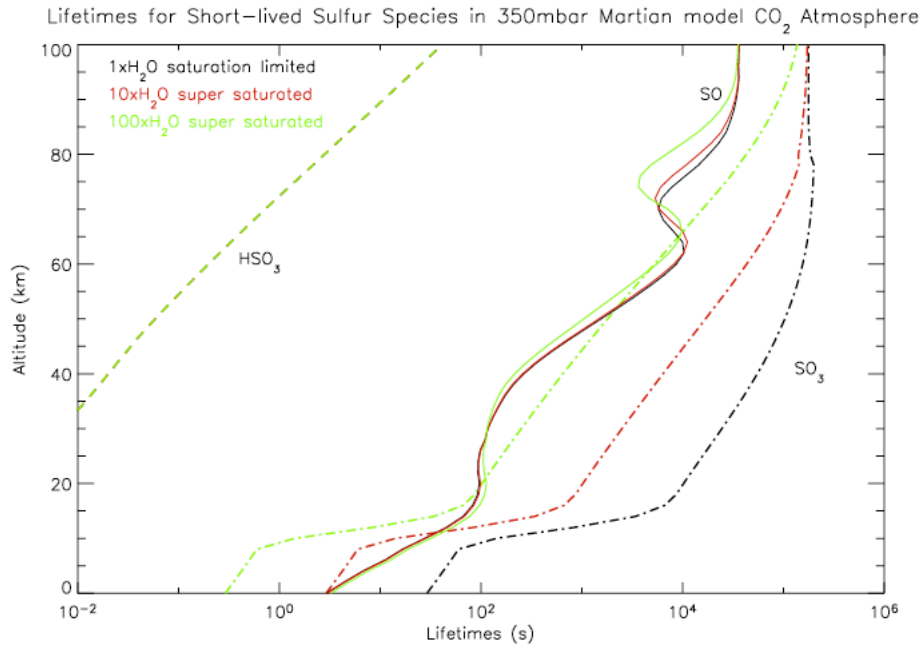

Figure 9.22: Short-lived Sulfur Species in 350mbar CO_2 Atmosphere

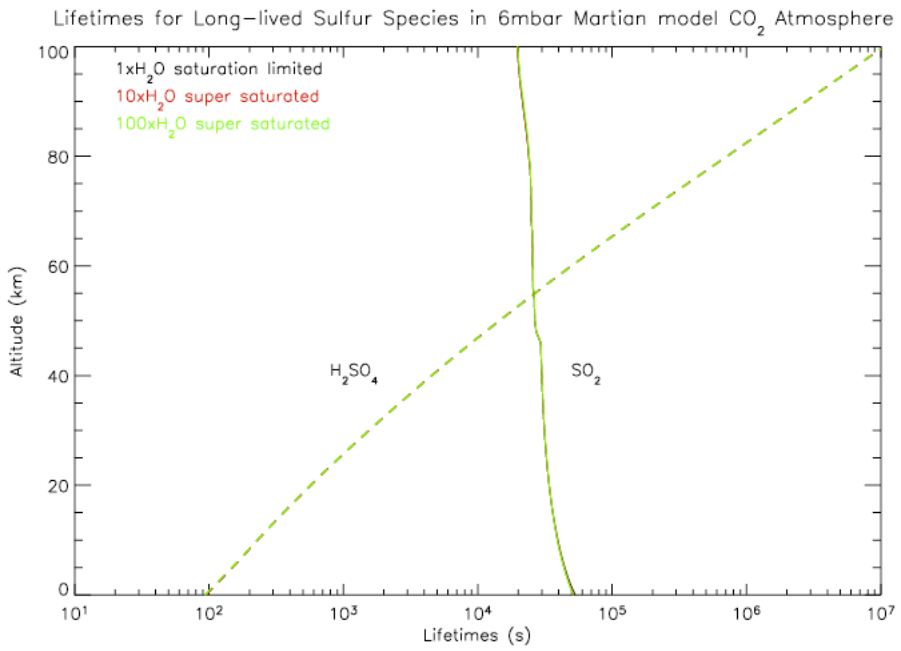

Figure 9.23: Long-lived Sulfur Species in 6mbar CO_2 Atmosphere

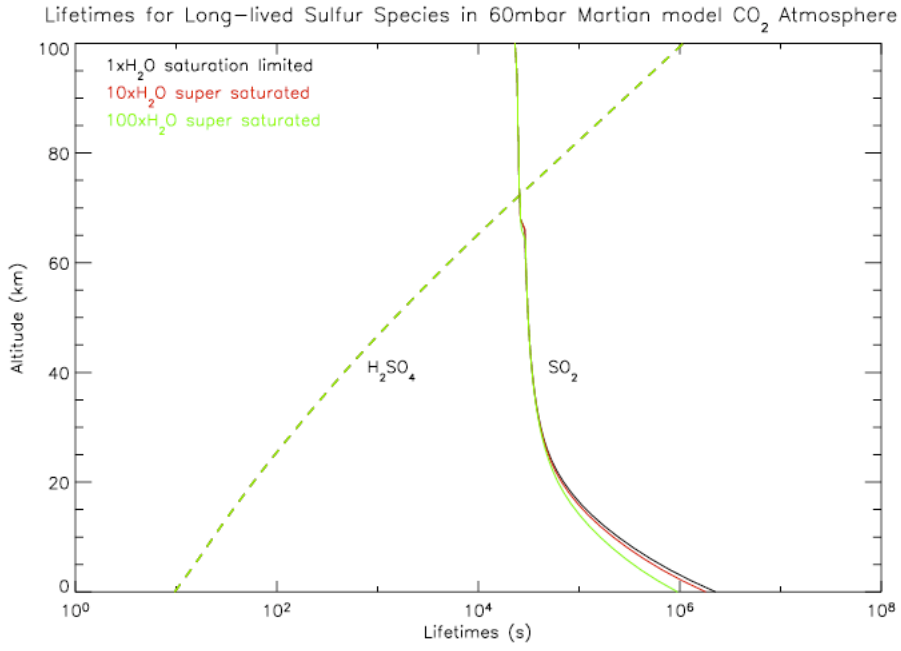

Figure 9.24: Long-lived Sulfur Species in 60mbar CO_2 Atmosphere

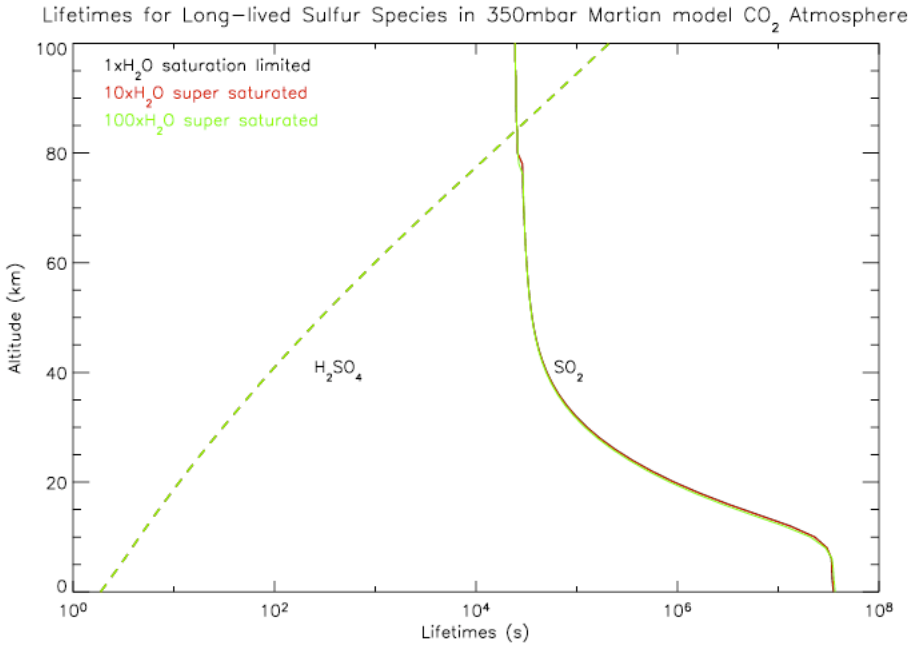

Figure 9.25: Short-lived Sulfur Species in 350mbar CO_2 Atmosphere

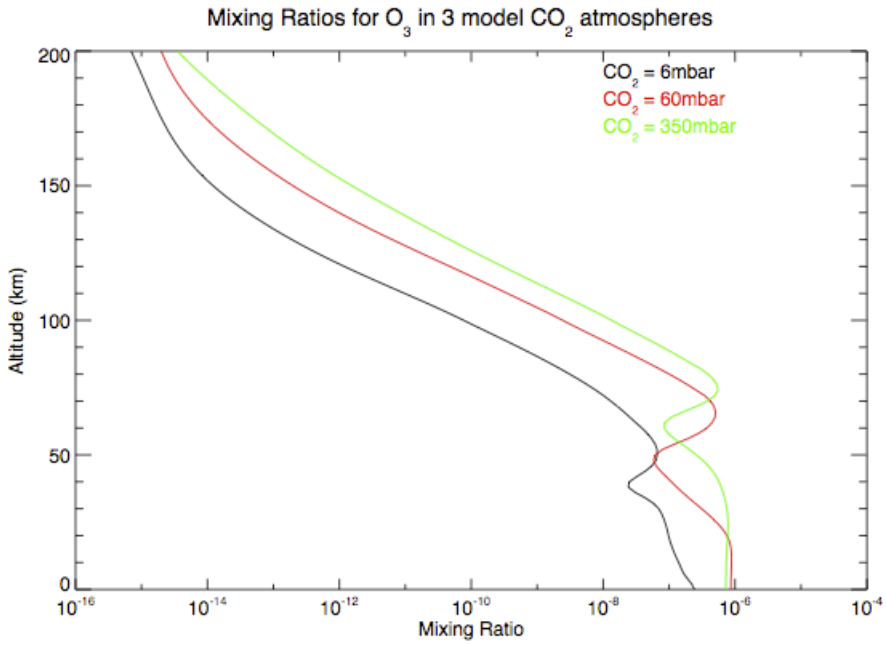

Figure 9.26: Ozone mixing ratios for varying modeled Martian atmospheres

super-saturation level is not physically realizable these model results demonstrate sensitivity to CO_2 levels and not H_2O levels to the ultimate lifetime of sulfur species in the atmosphere, since the end atmospheric product of H_2SO_4 is deposited onto the Martian surface. The atmospheric loss rate due to the condensation of H_2SO_4 is not affected by the use of an approximation rather than the calculated aerosol condensation rates. The sensitivity runs to this simplification demonstrated that this reaction rate is robust with similar model results for 5 orders of magnitude and thus it is likely this approximation is sufficient.

Chapter 10: Survivability to modeled UV flux results for chosen microorganisms

Nair model surface UV solar flux data were gathered by wavelength and binned into specific UV ranges using nominal values of UVC, 200-282nm, UVB, 283-315nm, and UVA 316-400nm respectively for microorganism sensitivity analysis. These results are shown for UVC, UVB, and UVA in Tables 10.1, 10.2, and 10.3 respectively. The results show the expected decreases in UVC and UVB when additional CO_2 and SO_2 are added to the atmosphere. When using the Nair solar flux results to analyze survivability due to UV exposure, adjustments may be required due to sensitivity of DNA to specific UV wavelength exposure and the lack of UVB only fluence experiments in literature. A graph of the calculated results of such theoretical analysis for *D. radiodurans*, performed by Setlow [91], is shown in Figure 10.1. No theoretical data are available for some of the chosen UV radiation resistant microorganisms and therefore DNA bio-sensitivity data obtained from experimentation on *D. radiodurans* will be used. This biological sensitivity will likely be similar for all UV resistant microorganisms even if the fluence withstood by the microorganisms change. Since this biological sensitivity curve is normalized it can be scaled properly by the UVC data obtained for each microorganism studied. The graph also shows model Martian atmospheres (both present day and Nair model results) as well as a standard Earth surface flux from Horneck *et al.* [93]. The additional Nair model results in Figure 10.1 are for the standard SO_2 upward surface flux ($1.06x10^{10}cm^{-2}$). Here one sees that the standard Martian model curve from Horneck *et al.* is very similar to the Nair

model results of 6mbar atmosphere, as expected, since present day concentration of CO_2 is similar. Also, as seen in model results previously, large changes are seen in the UV surface flux for the 60mbar and 350mbar Nair model results. Finally, UVA data curve for Earth is above (higher flux rate) the Martian UVA curve. This is caused by the smaller distance from the Earth to the Sun.

With the UV model flux data properly binned comparisons can be made with literature results from published experiments of UV survivability for chosen microorganisms. The UV survivability for microorganisms is typically provided in the UVC wavelength range, the range that includes the most lethal wavelengths to Earths life DNA structure, approximately 250-260nm. By inspection of the UVC flux rate one finds the most absorption by SO_2 in the model results (see tables 10, 11, and 12) as expected from its absorption cross-section. A full UV survivability spectrum is available for two of the chosen microorganisms, *D. radiodurans* and *Chroococcidiopsis sp. 29* [15, 94]; experimenters used a modeled present day Martian atmosphere exposing the microorganisms to UV ranges >200nm. The remaining microorganisms are exposed to limited UV ranges and visible light during experimentation. Figure 10.2 shows the chosen microorganisms selected because of UV survivability vs. UV dosage (or fluence). In comparing results from literature to the UV flux found through the Nair model care must be taken. Fluences provided in literature express various exposure times to UV radiation for survivability curves.

Table 10.1: Model results for UVC (100-282nm) range on surface of Ancient Mars

Flux SO_2	**6 mbar** $\frac{J}{m^2 s}$	**60 mbar** $\frac{J}{m^2 s}$	**350 mbar** $\frac{J}{m^2 s}$
No SO_2	1.07	0.00220	$3.94x10^{-9}$
$1.06x10^{09}\frac{1}{cm^2 s}$	1.02	0.00194	$3.94x10^{-9}$
$1.06x10^{10}\frac{1}{cm^2 s}$	0.82	0.00135	$2.81x10^{-9}$
$1.06x10^{11}\frac{1}{cm^2 s}$	0.49	0.00041	$4.83x10^{-11}$

Table 10.2: Model results for UVB (283-315nm) range on surface of Ancient Mars

Flux SO_2	**6 mbar** $\frac{J}{m^2 s}$	**60 mbar** $\frac{J}{m^2 s}$	**350 mbar** $\frac{J}{m^2 s}$
No SO_2	17.79	0.994	0.0629
$1.06x10^{09}\frac{1}{cm^2 s}$	17.78	0.974	0.0629
$1.06x10^{10}\frac{1}{cm^2 s}$	17.70	0.915	0.0629
$1.06x10^{11}\frac{1}{cm^2 s}$	17.52	0.710	0.0629

Table 10.3: Model results for UVA (316-400nm) range on surface of Ancient Mars

Flux SO_2	**6 mbar** $\frac{J}{m^2 s}$	**60 mbar** $\frac{J}{m^2 s}$	**350 mbar** $\frac{J}{m^2 s}$
No SO_2	15.10	11.12	3.46
$1.06x10^{09}\frac{1}{cm^2 s}$	15.10	11.12	3.46
$1.06x10^{10}\frac{1}{cm^2 s}$	15,10	11.11	3.46
$1.06x10^{11}\frac{1}{cm^2 s}$	15.09	11.05	3.46

The first selected microorganism from literature, a cyanobacterium *Chroococcidiopsis sp. 029*, was exposed to a modeled standard flux similar to a Martian day at the equator, taken to be exposed to daylight for approximately an eight-hour period [15]. The bar chart of the survival of the microorganism is shown in Figure 10.3. Although data in the graph were for experiments conducted in ambient Earth atmosphere, repeated experiments showed similar order of magnitude reductions and results for simulated present day Martian atmosphere, thus similar to the Nair model atmosphere of 6mbar without SO_2. From Figure 10.3 it is seen that after 5 minutes of exposure to $> 200nm$, above $1100\frac{J}{m_2}$, the survival rate is reduced from 100% to less than 0.5%. The UV flux from 295-400nm (UVB and UVA), although lethal to the organism, improves viability exposure time, with minimal survival, less than 0.05% viable, after 60 minutes. Here we see critically lethal exposure from 200-295nm as expected from DNA sensitivity with a sharp increase in survivability when these wavelengths were removed.

Nair model results for the 6mbar Martian atmosphere, Tables 10.1, 10.2, and 10.3 show insufficient change to the incident UV flux with the introduction of SO_2

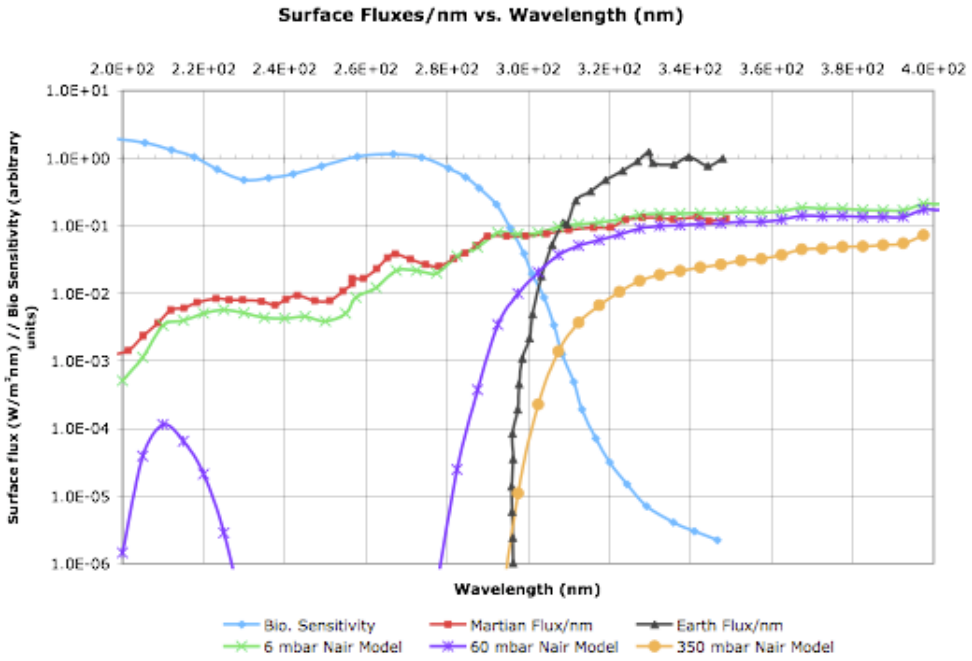

Figure 10.1: Recreated from Rettberg *et al.*, [12] with additional Martian model results from Nair Model for 6, 60 and 350 mbar atmospheres

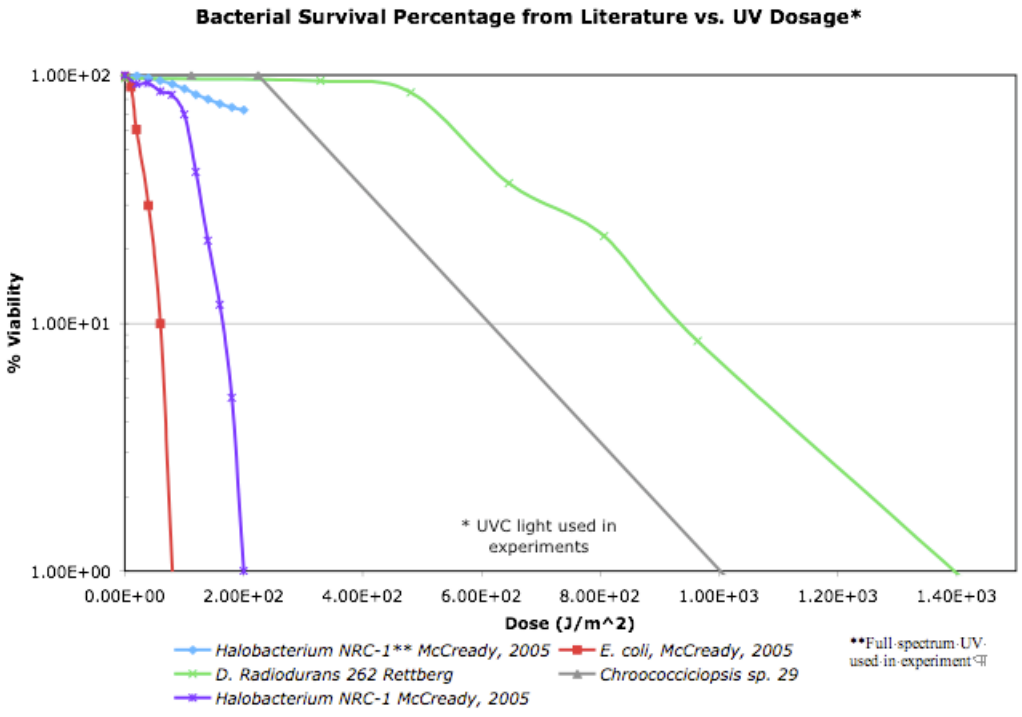

Figure 10.2: UV viability for several test microorganisms

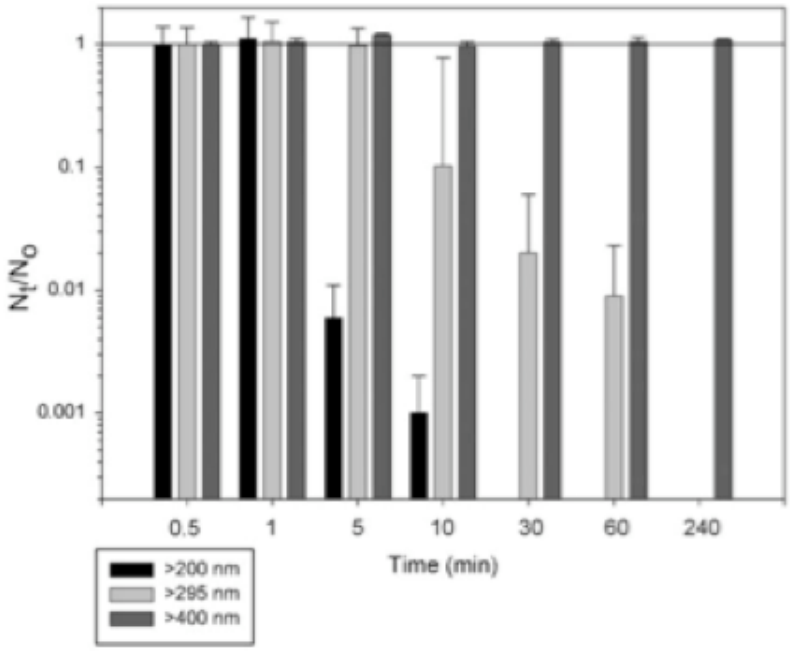

Figure 10.3: Loss of Viability of cyanobacteria under simulated Martian light flux (>200nm), simulated terrestrial flux (>295nm), and all UV radiation removed (>400nm) Numbers are expressed as colony counts in treated cells vs. control cells (Nt/No). reproduced from Cockell *et al.* [15].

Table 10.4: Fluence by UV range and % Survival of *Chroococcidiopsis sp. 029* after exposure to >200nm radiation in Figure 10.3

Time (min.)	**0.5**	**1.0**	5.0	10.0	30.0	60.0	240.0
UVC ($\frac{J}{m^2}$)	**112**	**224**	1,120	2,238	6,714	13,428	53,712
UVB ($\frac{J}{m^2}$)	**248**	**496**	2481	4962	14,886	29,772	119,088
UVA ($\frac{J}{m^2}$)	**1130**	**2260**	11,301	22,602	67,806	135,612	542,448
% Survival	**100**	**100**	0.004	0.0006	0	0	0

in the atmosphere. The total UV flux was lowered by approximately 4% with the introduction of SO_2. Little improvement to the viability is found and the likelihood of survival for this organism on the surface is small on present day Mars. Note though that the UV range fluence distribution, shown in Table 10.5, does vary from the results of the data results, shown in Table 10.4. This stems from the differences in the model Martian atmospheres. Although UVC exposure times would lengthen using the Nair model results, UVB and UVA would decrease. These differences in the 6mbar atmosphere results are not great enough to allow for extended viability beyond minutes and is therefore unimportant when discussing viability of the cyanobacteria in the 6mbar model atmosphere regardless of the presence of SO_2.

Table 10.5: Nair Model Results shown for selected time increments for modeled 6mbar atmosphere

Nair Model Results				
6mbar		No SO_2 flux		
	UVC	UVB	UVA	Total Fluence
Time (min)	$(\frac{J}{m^2})$	$(\frac{J}{m^2})$	$(\frac{J}{m^2})$	$(\frac{J}{m^2})$
0.5	32.1	5.34E+02	4.53E+02	1.02E+03
1	64.2	1.07E+03	9.06E+02	2.04E+03
5	321	5.34E+03	4.53E+03	1.02E+04
10	642	1.07E+04	9.06E+03	2.04E+04
30	1926	3.20E+04	2.72E+04	6.11E+04
60	3852	6.40E+04	5.44E+04	1.22E+05
240	15408	2.56E+05	2.17E+05	4.89E+05
Nair Model Results				
6mbar		High $SO_2 = 1.06x10^{+11}\frac{1}{cm^2 s}$		
	UVC	UVB	UVA	Total Fluence
Time (min)	$(\frac{J}{m^2})$	$(\frac{J}{m^2})$	$(\frac{J}{m^2})$	$(\frac{J}{m^2})$
0.5	14.7	5.26E+02	4.53E+02	9.93E+02
1	29.4	1.05E+03	9.05E+02	1.99E+03
5	147	5.26E+03	4.53E+03	9.93E+03
10	294	1.05E+04	9.05E+03	1.99E+04
30	882	3.15E+04	2.72E+04	5.96E+04
60	1764	6.31E+04	5.43E+04	1.19E+05
240	7056	2.52E+05	2.17E+05	4.77E+05

When comparing viability results to the 60mbar model data over the wavelength range from 200-400nm similar UV flux values are found for all model results with an approximate 6-fold decrease in surface UV flux. Here though the UVC is more drastically decreased compared to the UVB or UBA ranges. This makes individual UV range comparisons difficult because viability in Table 10.4 was tested as a whole, UVC, UVB, and UVA combined. Thus, one must not only look at the total fluence for each time period but also compare the lethal fluence from the initial experiment by UV range. This scaling by UV range can be accomplished by using the biological sensitivity multiplier obtained from Action Spectra analysis of UV sensitivity of microorganisms. Here for simplicity I will use an averaged multiplier over the UV ranges. Although this value will not be exact, the focus is on orders of magnitude results and therefore it will suffice. Looking at the DNA sensitivity curve Figure 10.1, the UV ranges show order of magnitude drops, from initial multiplier for UVC range of approximately 1.0 to 1/100th this value for UVB, and finally 1/100,000th for UVA. Using these scalars a new dosage or fluence table can be created, shown in Table 10.6, this new normalized fluence value can be used for comparison. Comparing the newly scaled results, the 60mbar Nair model atmosphere increases the survivability of the cyanobacteria to approximately 20 hours, still insufficient for two Martian days on the surface of ancient Mars using an equatorial location and approximate day length. One must note that the decreased fluence values may lead to greater survivability than this simple scaling implies, this is because of the time that passes to reach fluence levels measured to be lethal. As the time is extended to reach fluence levels, for example 20 hours compared to 4 hours may give an microorganism sufficient time to repair UV damage which in a shorter amount of time would be lethal. Thus, these survival times stand as minimum survival times and it is likely survivability could be extended beyond these minimal values with discrete testing of UVB ranges

Table 10.6: Nair Model Results adjusted for biosensitivity per Setlow shown for selected time increments for modeled 60mbar atmosphere

Nair Model Results				
60mbar		No SO_2 flux		
	UVC	UVB	UVA	Total Fluence
Time (min)	$(\frac{J}{m^2})$	$(\frac{J}{m^2})$	$(\frac{J}{m^2})$	$(\frac{J}{m^2})$
0.5	0.066	0.298	3.34E-04	0.365
1	0.132	0.596	6.67E-04	0.729
5	0.66	2.98	3.34E-03	3.65
10	1.32	5.96	6.67E-03	7.29
30	3.96	17.9	2.00E-02	21.9
60	7.92	35.8	4.00E-02	43.7
240	31.68	143	0.160	175
Nair Model Results				
60mbar		$SO_2 = 1.06x10^{+10}\frac{1}{cm^2 s}$ Faint Sun		
	UVC	UVB	UVA	Total Fluence
Time (min)	$(\frac{J}{m^2})$	$(\frac{J}{m^2})$	$(\frac{J}{m^2})$	$(\frac{J}{m^2})$
0.5	0.0155	0.179	2.49E-04	0.195
1	0.0309	0.358	4.98E-04	0.389
5	0.155	1.79	2.49E-03	1.95
10	0.309	3.58	4.98E-03	3.89
30	0.927	10.73	1.49E-02	11.67
60	1.85	21.46	3.00E-02	23.34
240	7.42	85.82	0.120	93.36
1200	37.08	429.12	0.5976	700.20

survivability independent of UVC ranges.

When CO_2 is increased to 350mbar with the standard SO_2 upward flux value ($1.06x10^{10}cm^{-2}s^{-1}$) UV flux is almost totally in the 300-400nm range, the 200-300nm range makes up less than 0.05% of the UV flux. Because of this viability of the cyanobacteria can be extended to approximately 12 days by inspection of Figure 10.6. But, the initial flux used in the UVA (300-400nm) experiment was increased to mimic the terrestrial Earth UV spectra. Because the Earth is closer to the Sun, the incident flux is increased by 100% by moving the lamp closer to the experimental chamber. Therefore, the viability value of 12 days would be doubled, or approximately 24 days.

But, inspection of UV graphs, see Figure 9.19, the UVB flux in the 350mbar model is almost identical to the UVB flux on Earth. Therefore, it is likely that survivability would be extended past the approximate 1 month with the extension of time to reach sufficient fluence values and the repair that could take place during this time period.

Experiments were also conducted on *Chroococcidiopsis sp. 29* 1mm below the surface in soil mimicking Martian surface soil. Here, viability was not tested directly but esterase activity and autofluorescence were measured. (Autofluorescence has been suggested as tool to search for extremophile extraterrestrial life by Chandran Sabanayagam [95].) After 4 hours of exposure no measurable difference is seen between native soil for the organism or Martian-type soil and no measurable loss of activity is seen at this depth. Cockell *et al.* [96] additionally experimented on the viability of this microorganism in a monolayer in the hyper-arid climate of Atacama Desert, Yungay, Chile and found death for the organism after 1 day of UV exposure without the presence of water to aid in cell repair. Thus, enzymatic repair of UV-induced damage is inhibited. But he also noted that as little as 1mm of soil covering protected microorganisms from UV induced killing. This organisms is typically not found grown in a monolayer and therefore, this is the most extreme result for UV exposure for this cyanobacterium. Thus, a second result where soil cover as small as 1mm would enable this organism to survive Earth-type UV spectra which is predominately UVA. Notice that the 350mbar atmosphere model data was made up of predominately UVA flux, therefore making the results from the Earth-type flux relevant to this model results. Viability of *Chroococcidiopsis sp. 29* could be a viable Martian model candidate seen only with a 350mbar or higher atmosphere and at 1mm or more of soil depth or within rock pores where it is found in deserts on the Earth.

Halophiles are another microorganism to attract attention for likely Martian life homolog because these archaea have the ability to survive high concentrations of NaCl

Table 10.7: Nair Model Results adjusted for biosensitivity per Setlow shown for selected time increments for modeled 350mbar atmosphere

Nair Model Results				
350mbar		No SO_2 flux		
	UVC	UVB	UVA	Total Fluence
Time (min)	$(\frac{J}{m^2})$	$(\frac{J}{m^2})$	$(\frac{J}{m^2})$	$(\frac{J}{m^2})$
0.5	1.182E-07	0.0189	1.04E-04	0.0190
1	2.364E-07	0.0377	2.08E-04	0.0379
5	1.182E-06	0.189	1.04E-03	0.190
10	2.364E-06	0.377	2.08E-03	0.379
30	7.092E-06	1.13	6.23E-03	1.14
60	1.418E-05	2.26	1.25E-02	2.28
240	5.674E-05	9.06	4.98E-02	9.11
960	2.269E-04	36.2	0.199	36.4
3840	9.078E-04	145	0.797	146
5760	1.362E-03	217	1.20	219
Nair Model Results				
350mbar		High $SO_2 = 1.06x10^{+11}\frac{1}{cm^2s}$		
	UVC	UVB	UVA	Total Fluence
Time (min)	$(\frac{J}{m^2})$	$(\frac{J}{m^2})$	$(\frac{J}{m^2})$	$(\frac{J}{m^2})$
0.5	1.499E-08	0.0143	1.04E-04	0.0144
1	2.898E-08	0.0285	2.07E-04	0.0287
5	1.449E-07	0.143	1.04E-03	0.144
10	2.898E-07	0.285	2.07E-03	0.287
30	8.694E-07	0.885	6.21E-03	0.861
60	1.739E-06	1.71	1.24E-02	1.72
240	6.955E-06	6.84	4.97E-02	6.89
7200	2.09E-04	205	1.49	207
17280	5.01E-04	492	3.58	496

on Earth [13] and the layering of salt deposits on several potential seen on the Martian surface [97]. Viewing Figure 10.2 one sees the results of UV experiments on *Halobacterium sp. NRC-1* and *Halobacterium salinarum* under UVC flux (200-282nm) and visible light. This addition of visible light greatly adds to the microorganisms ability to combat the UVC flux [13]. The model results indicate UV exposure for the 6mbar be lethal to *NRC-1* on the order of minutes. Thus, the 6mbar model does not demonstrate a viable atmosphere for *NRC-1*.

Data for viability of *halobacterium sp. NRC-1* in experiments conducted have tested survival over 200 $\frac{J}{m^2}$ or 75% survivability in UVC and ambient Earth light. Since surface UVC flux values reach higher values in the 60mbar model atmosphere, additional data for higher UVC fluxes needs to be estimated through curve fitting of available data. *Halobacterium sp. NRC-1* viability curve differs greatly from the drop off curve seen for *D. radiodurans*. Thus, Sutherland's partial gamma function analysis is not relevant. The polynomial fit was employed and the results are seen in Figure 10.5. Since the curve fitted data parameters used for analysis are extrapolated, caution must be used when interpreting results. Data is shown in Table 10.8 for the curve fitting. The lifetime of the *Halobacterium sp. NRC-1* is found to be approximately 3 weeks when UVC faint Sun 60mbar model data is compared with UVC and ambient light data results by McCready [13]. This would indicate that this halobacterium could have survived the UVC flux in a less dense atmosphere if some surface UV protection decreased the incident UVC flux. Care must be taken when making conclusions for UVB and UVA as these wavelengths were not part of the experiment by McCready *et al.* [13]. An estimate can be made using the DNA sensitivity scale between approximately 300-303nm, the multiplier larger than the overall averaged value of $\frac{1}{10}^{th}$, to approximately $\frac{3}{10}^{th}$. If the theoretical DNA sensitivity is reliable for this microorganism then the viability is greatly reduced from three

weeks to approximately one day. Thus, the sensitivity of *Halobacterium NRC-1* to UVB spectra is needed for definitive analysis indicating whether viability would be reduced to one day and at this time no studies are available. Due to the difference of the Nair model results in the UVB part of the spectrum when compared with the flux on the Earths surface further experimentation is indicated. Therefore again, UVB resistance data for *halobacterium sp. NRC-1* is needed before lifetimes can be resolved. UVB and UVA were not included in the UV flux shown for these halophiles but an experiment with *halobacterium salinarum* indicated less sensitivity to UVB and UVA radiation. If comparisons are made with the results of Martin *et al.* [16] in Figure 10.4 with respect to another extreme halophile, *Halobacterium salinarum*, then lifetimes for UVB likely increase with viability still strongly seen after 72 days with no loss of viability. *Halobacterium sp. NRC-1* is also a *Halobacterium salinarum* but a different species as Martin used the strain *ATCC 43214*. It is likely these two extreme halophiles would show a similar reaction to UVB and UVA but without specific data for *Halobacterium NRC-1*, *Halobacterium ATCC 43214* data will be used in its place. Both molarity NaCl concentrations 3.0M and 4.3M NaCl appear to have an almost horizontal survivability curve indicating likely survivability well beyond the 72 days indicated by the maximum UVB/UVA dosage shown to the halophile of $39.3 kJ/m^2$ since UVC viability curves appear to follow a more polynomial rather then sharp edged decline. It is known that this halophile survives Earths UV surface flux. Looking at Figure 10.1 it is noticed that UVA Earth flux is larger than UVA flux of any of the Nair Martian models. Thus, using the Nair models, UVA is not a factor in determining survivability on ancient Mars. It should also be noted that lifetimes were greatly extended in experiments by Fendrihan *et al.* [98] when halophiles (including *halobacterium sp. NRC-1*) were exposed to UV doses when embedded in halite crystals grown with fluid inclusion with a 2 order of magnitude increase in the

UV dose 37% survival level. Thus, where the microorganism is located in the salt crystal or liquid medium greatly influences survivability due to UV stressors. This lower CO_2 environment would likely be traced to after the global change at the end of the Phyllocian and thus be indicative of atmospheres likely during the Theiikian.

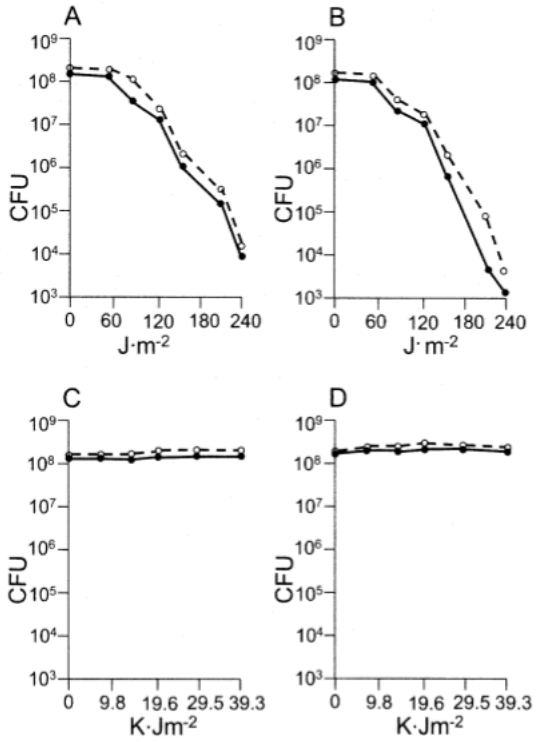

Figure 10.4: Survival of extreme halophile *H. salinarum* reproduced from Martin *et al.* [16]. Figure A, B, and C represent survival of halophile exposed to UVC radiation at 0.05M NaCl, 1.37M NaCl, and 4.3M NaCl respectively. Figures D, E, and F represent survival of halophile in mixed UVB and UVA at 0.05M NaCl, 1.37M NaCl, and 4.3M NaCl respectively.Dashed lines represent incubation in light.

If a direct comparison is made between the UVC dosage and the UVC flux model results for the 350mbar atmosphere, one would say that in the presence of sunlight the *Halobacterium sp. NRC-1* archaeon could have survived on the surface of Mars if other requirements were met as UVC model flux is very low allowing for dosage times in the hundreds to ten thousand years for a 75% survival rate. UVB and UVA were

not included in the UV flux shown for these halophiles but again experiments with *halobacterium salinarum* indicate less sensitivity to UVB and UVA radiation. If this result can be extended to UV resistant halophiles including *halobacterium sp. NRC-1*, then by inspection of Figure 10.4 survivability depends more upon the UVC dosages than UVB or UVA dosages. An estimate can be made using the DNA sensitivity scale between approximately 300-303nm, the multiplier larger than the overall averaged value of $\frac{1}{10}^{th}$, to approximately $\frac{3}{10}^{th}$. If the theoretical DNA sensitivity is reliable for this microorganism then the viability is greatly reduced from thousands of years to approximately $\frac{1}{2}$ a year but could be much longer if UVB sensitivity curves mimic curves for *halobacterium salinarum*. Thus, the sensitivity of *halobacterium NRC-1* to UVB spectra is needed for definitive analysis but using another extreme halophile *H. salinarum sp. ATCC 43214* the likelihood of UV survivability appears high. Comparisons can be made initially for possible viability on the surface of ancient Mars by examination of Martian surface mineralization and locations for viable halophilic life. Because of the high CO_2 atmospheric content needed to provide adequate shielding, it is likely to look for this microorganism in areas with possible early signs of water in the Phyllocian epoch or early Theiikian before the majority of the atmosphere was lost.

Radiodurans have long been studied for their strong UVC resistance and therefore many studies were reviewed when finding the survivability of this microorganism to substantiate independence of specific experimental methodology. From Figure 10.1 it is seen that the *D. radiodurans* are more resistant to UVC flux than the *halobacterium sp. NRC-1*. Thus, a reexamination of the 6mbar and 60mbar atmospheres is required. For analysis data used are for *D. radioduran 262* (UVC resistant strain). In Figure 10.6 *D. radioduran 262* exposured to full spectrum light is compared to exposure to monochromatic 254nm light. Both exposures showed similar results indicating

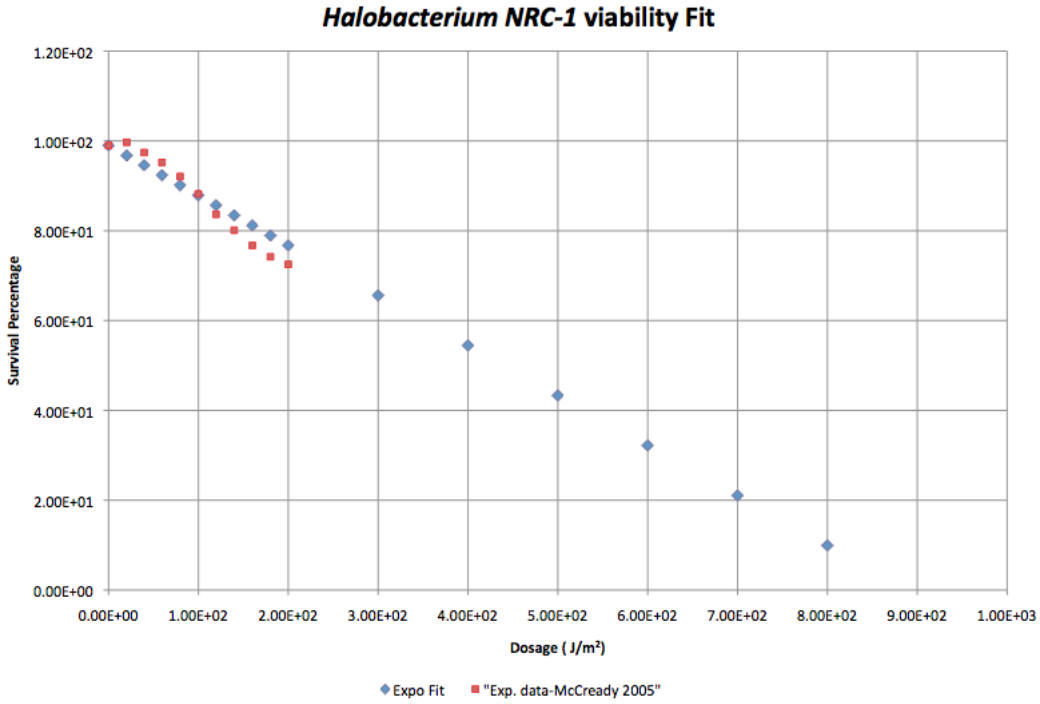

Figure 10.5: Viability Curve Fitting Results for *Halobacterium sp. NRC-1*

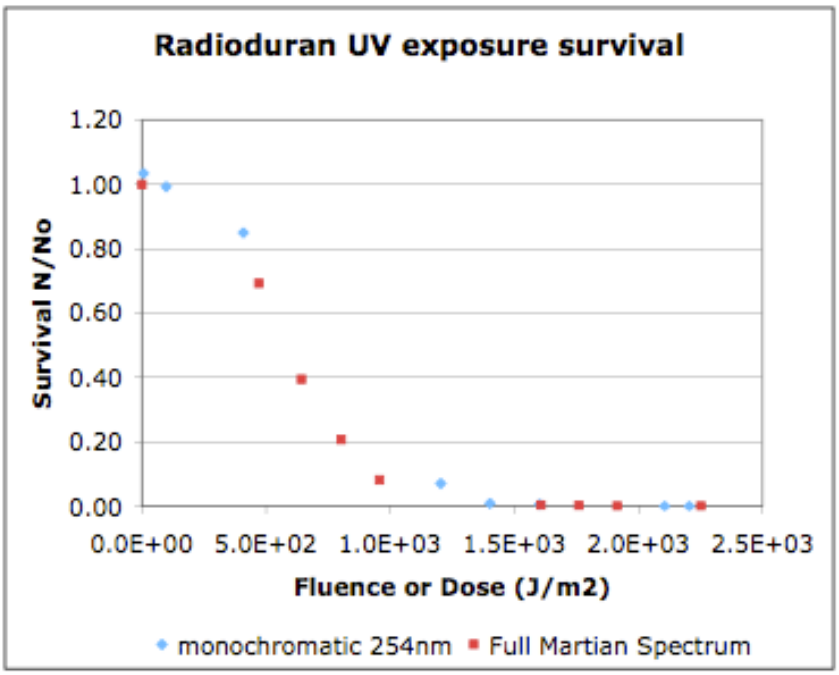

Figure 10.6: Monochromatic 254nm UV exposure and model UV Martian spectrum versus survival, recreated from Rettberg *et al.* [12] (note: error bars omitted)

Table 10.8: Curve Fitted data results for *Halobacterium sp. NRC-1*

Dosage ($\frac{J}{m^2}$)	**Fitted Data Survival %**
0.00	99.1
20	96.8
40	94.6
60	92.4
80	90.1
100	87.9
200	76.7
300	65.6
400	54.5
500	43.3
600	32.2
700	21.1
800	9.93

little DNA sensitivity to UVB and UVA wavelengths. In fact, in additional studies UVB and UVA sensitivity is shown to increase dosage (or fluence) survival by a factor of 100 before death is seen [99]. Therefore, surface exposure to the most lethal UVC would not be lethal to *D. radioduran 262* if other criteria could be met on the surface of Mars today, if only for approximately 15 minutes. When looking at survival rates for Nair model results for 60mbar and 350mbar atmospheres, survivability rates increase from 1 month to thousands of years respectively. Therefore, UV survival is demonstrated for Nair 350mbar model results. Additional experimentation was completed by de la Vega *et al.* [100] and it was found that the combination of present surface UV flux and other climate conditions on the surface of Mars such a soil make up, temperature day/night flux, and surface pressure were lethal to the *D. radiodurans* tested. Removing the UV flux but keeping other physical Martian surface criteria survivability of the microorganism was found, see Figure 10.7. Since the 350mbar Nair model atmosphere has extremely low UVC flux, the other climate conditions present on the surface of Mars today would not limit survival. Thus, an

increased pressure of 350 mbar also would not likely impact survivability in a negative manner as well as increased temperature since this microorganism typically is found at higher Earth surface temperatures and pressures.

E. coli, a non-UV resistant bacterium used as a standard for experimental comparisons is found to not survive in any of the three Martian surface scenarios. A value of 80 $\frac{J}{m^2}$ of UVC with visible light shows no survival of the bacteria in tests conducted by McCready *et al.* [13] and substantiated by multiple additional tests conducted by Diaz and Schulze-Makuch [101]. This eliminates survival when exposed to the 6mbar Martian model atmosphere within 5 minutes as seen in Table 10.1. It is also seen in Table 10.1 that the UVC exposure is lethal to *E. coli* within 10 minutes when exposed to the 60mbar atmosphere. Finally, UVC in the 350mbar atmospheric model exposure is non-lethal to the *E. coli* within this time period, but the UVB and UVA must also be taken into account again. UVB and UVA death is seen at approximately 40 $\frac{W}{m^2}$ for both ranges [102]. Therefore, even the Nair model results for the 350mbar atmosphere would be lethal to *E. coli* within 20 minutes of exposure even with the extremely low UVC radiation flux.

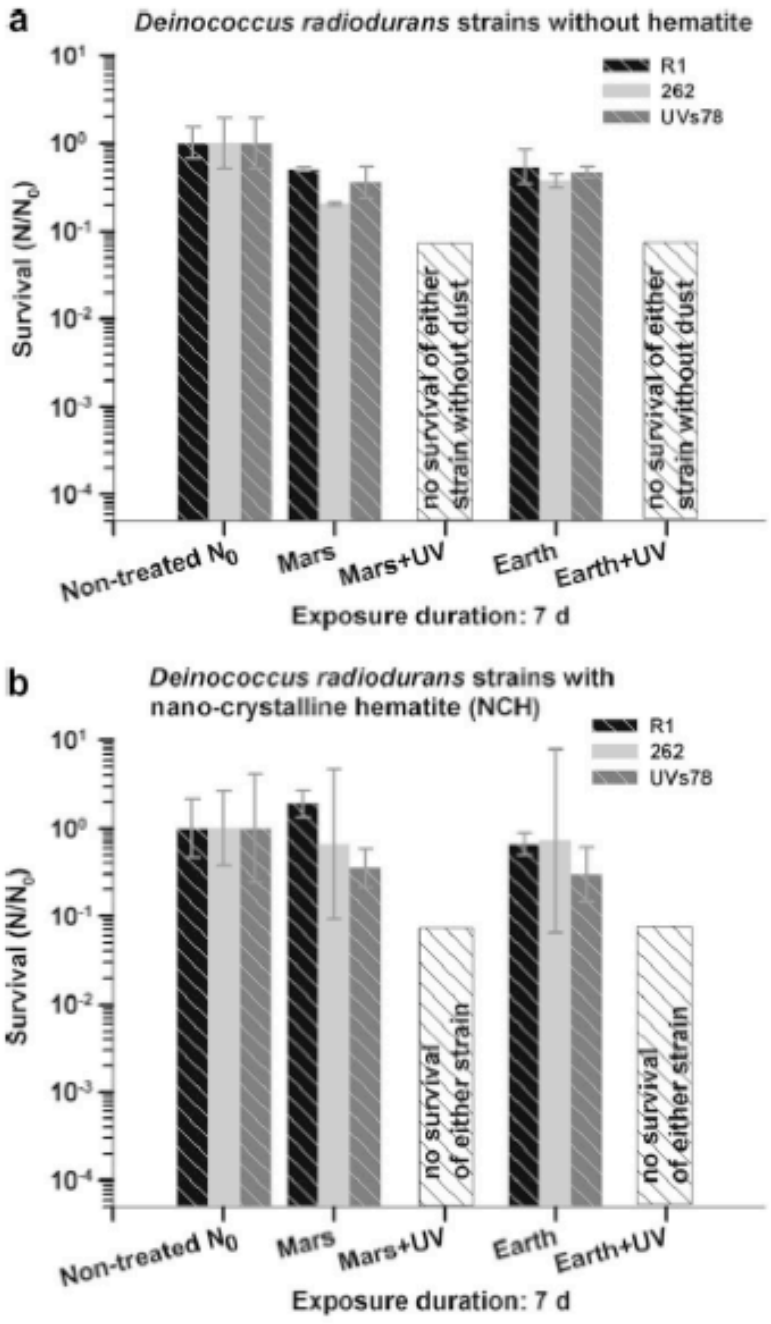

Figure 10.7: Results of *D. Radiodurans* strains to Mars present day climate exposure with and without hematite, reproduced from de la Vega *et al.* [17]

Chapter 11: Conclusions and Future Work

Sulfur Species Modeling and implications for Ancient Mars:

The effects of SO_2 were modeled in atmospheres with limited CO_2 to inhibit cloud formation. The UV surface flux results of model runs were used to infer the likelihood of survivability of selected microorganisms in varying atmospheric scenarios. Finally, analyses need to be synthesized with surface geologic data to elucidate the most likely locations on the surface of Mars to search for such extinct or possible extant life.

SO_2 was shown to have differing effects on the surface UV flux dependent upon the amount of CO_2 in the atmosphere. This is expected as the introduction of SO_2 largely impacts the UVC and UVB absorption spectra which are reduced in higher CO_2 atmospheres with water vapor due to the increased oxygen species and UV photolysis. Thus, even though UVC is reduced by 50% in a 6mbar modeled atmosphere, the SO_2 UVC flux sees only a approximate 30% reduction in a 60mbar atmosphere and finally a more modest 12% reduction for the 350mbar atmosphere. Therefore, SO_2 is a factor in reducing the UV flux but the upward flux rates of SO_2 used in this model were not sufficient reduce surface UV flux without additional CO_2. It is important to note that the most effective concentration scenario for the introduction of SO_2 is seen in the 60mbar atmosphere where the UVC and UVB reduction is vital to the survival of extremophiles chosen for Martian homologs. Therefore, the influence of the introduction of SO_2 is seen most keenly in thinner atmospheres where CO_2 opacity and O_3 photolysis are insufficient UV flux inhibitors alone. Since the amount of SO_2 proposed was not sufficiently large to effect the UV flux in higher CO_2 atmospheres,

it is seen as a possible component with the presence of CO_2 of most importance for possible survival of life in the early to mid-Phyllocian. Changes in the amount of SO_2 would impact these results if the global value estimated by Levine is found to be low.

Since pulsed scenarios show longer lifetimes of SO_2 compared to the averaged outputs used in this model, on the order of years, additional models should be completed to compare results and calculate total sulfur output for repeated pulsed inputs and the length of time possible for these sustained outputs. Comparisons could then be made to overall output calculated by Levine and estimated length of volcanic output on Mars. The same computer model should be used for both deposition methods to see impact of input modeling into the atmosphere for sulfur species lifetimes and reduced UV flux. Finally, pulsed output model runs should be conducted in thinner atmospheres to mimic volcanic output of gases after the global loss of atmosphere that is proposed to have occurred between the Phyllocian and the Theiikian. No pulsed output model data exists at the time of writing of this paper for a thinner CO_2 atmosphere. The SO_2 lifetimes found in these scenarios need to be compared with the averaged models results of approximately days, shown in chapter 10. Both scenarios should also be modeled simultaneously, using a small upward flux for SO_2 and populated lower altitude levels with SO_2 to mimic volcanic outgassing. This could mimic the active Theiikian where outgassing and eruptions were likely common events. With combined modeling techniques a more complete picture could be formed for various times in ancient Martian history dependent upon the level of volcanic activity and density of the CO_2 atmosphere as pulsed could supply a large, longer lived, supply of SO_2 and the surface level upward flux, a smaller constant SO_2 supply.

The Nair model used in this study limited water vapor amounts to saturation levels for the three temperature curves used. The results showed little sensitivity to additional amounts of H_2O in the atmosphere. Even when the model amounts of H_2O

were increased to 100 times the saturation limit, change in atmospheric concentrations of sulfur species was seen to either show little change or change is seen to follow in a predictive fashion. Since the saturation of water is dependent upon atmospheric temperature, additional temperature scenarios should be explored. Temperature curves depend upon greenhouse gas content and therefore increased CO_2 scenarios need updated temperature curves. Another greenhouse gas to be explored is CH_4 in the model as no sensitivity runs were performed for this constituent.

The loss rate of H_2SO_4 is found to be approximately equal the production rate of SO_2 into the atmosphere indicating that almost all of the SO_2 in the atmosphere ends up as H_2SO_4 which is deposited upon the surface. This is seen because of the inefficiency of H2SO4 photolysis and the rapid loss of H_2SO_4 after production in the atmosphere. Sulfuric acid was found to be higher than saturation for all model runs in the first 50km above the surface of Mars indicating precipitation out of the atmosphere. It is also noted that due to the increase in molecules to interact with the H_2SO_4 precipitation (pseudo-reaction rate calculation) is increased as the overall atmospheric concentration is increased. This implies that the total production of sulfuric acid in the atmosphere would be deposited onto the surface of Mars. During times of high atmospheric sulfur content and higher overall atmospheric concentrations this would infer a larger acidic deposition onto the surface. Although the lifetime of SO_2 is sufficiently long for atmospheric mixing, the completeness of atmospheric mixing in hemispheres is unknown. It is known that some surfaces do not show significant sulfuric acid alterations with strong phyllosilicate signals. This may imply that the mixing was incomplete or that sulfuric acid deposition was not sufficient to make measurable alterations. Since most of the volcanic activity on Mars was during the late Phyllocian and throughout the Theiikian, this indicates a change in

surface deposition of H_2SO_4 because of the increase in volcanic activity but also a decrease in overall surface pressure. Future work should reevaluate the pseudo-reaction rate approximation for the condensation time constant of H_2SO_4. Assumptions were made to perform the approximation used in this model. More rigorous calculations of the condensation rate for H_2SO_4 onto aerosols should be calculated and compared with the pseudo-reaction rate to verify this approximation was adequate for use in the model. Finally, because of the discontinuity of the downward flux of H_2SO_4 at the surface, the downward surface flux value should be reevaluated once direct calculations of condensation rate have been performed and model runs completed to determine if this discontinuity still exists.

Proposed life and its survival in modeled atmospheres:

Microorganisms surviving in the early Phyllocian would need to survive in a basic to neutral water environment required for phyllosilicate growth initially during this period. Extreme halophiles, such as *Halobacterium NRC-1*, grow fastest in 2.5 to 5.3M NaCl buffered to a 6-7 pH. Thus, these microorganisms cannot be ruled out because of the high salinity requirement as surfaces on Mars show signs of previous brine filled paleolakes or near subsurface reservoirs [18,103,104]. *Halobacterium NRC-1* is known to survive freezing to -15°C (258K) could have likely survived in ancient Mars during a higher CO_2 content atmosphere. *Halobacterium NRC-1* has also been seen to survive desiccation and live in halite (NaCl) crystal brine filled inclusions, and that this location offers added UVC protection. This makes this halophile a likely candidate to have survived in the Phyllocian in areas showing signs of past water and high salinity.

During this same period *D. radiodurans* and the cyanobacterium *Chroococcidiopsis sp. 29* examined could survive the UV flux. As areas dried up during the loss of water either to the atmosphere or the subsurface, both of these desiccation resistant microorganisms could have survived in rock pours as cyanobacteria do in the Atacama desert [15]. Testing done with both radiodurans and cyanobacteria show the ability to withstand reduced surface pressures (pressures as low as 6mbar) and Martian type soils [15, 100]. Both of these microorganisms have been tested in sub-freeing temperatures [16, 19]. Thus, it is seen that these microorganisms have tolerated Martian-like soils while still remaining viable without the added stressor of UVC which is absent in the 350mbar modeled environment. Care must be taken as today's surface soil content has been altered by oxides and therefore differ from ancient surface environment on Mars. It is likely though that ancient surface geology would have favored life more than the oxides which populate the surface today.

During the global atmospheric change Mars saw not only a loss of CO_2 but likely a change in surface acidity. If this initial global loss of CO_2 changed the atmospheric concentration to as low as 60mbar then possible survivability would be seen for only *Halobacterium NRC-1* and *D. radiodurans* from UV flux alone. With the lifetime seen from averaged model outputs of SO_2 reduced to days rather than years it would be important during this time to have almost continual degassing of volcanic gases. No pulsed SO_2 data from Johnson *et al.* exists for a reduced CO_2 atmospheric content, thus no e-folding times for SO_2 exist for pulsed output for comparison. Since this pulsed output model is as relevant to the most active volcanic period during the Theiikian, it could aid in the estimation of lifetimes for SO_2 this period where the SO_2 sharply decreases UVC flux and is most relevant to life scenarios on ancient Mars.

Mapping the model results and the requirements for survivability of the microorganisms to specific surfaces on Mars, selections for future missions can be made.

These missions should investigate possible life extant or extinct. Since many valley systems exist, selections should be based upon a lander's ability to test multiple geological surfaces in one landing if possible. Thus, surfaces which show multiple water scenarios would be preferred to surfaces with one possible water alteration. For example, Sinus Meridiani shows signs of phyllosilicate-bearing and hydrated sulfate deposits [105]. Thus, this area located near the equator of Mars would offer likely both Phyllocian and Theiikian geological pasts in one location since it bears signs of multiple water scenarios if landers could sufficiently navigate this terrain and other technological barriers could be met.

Locations for Possible Search for Extinct and Extant life on Mars:

Hynek *et al.* [18] completed a review of valley networks through a manual mapping of data from orbital based measurements "including infrared, visible, and topographical data." [1] This mapping has increased the number of valley formations by a factor of eight with formations clustered mainly in the southern hemisphere, see Figure 11.1, within the dated terrain from 3.6-3.8 Ga continuing in a diminished capacity through Martian history until approximately 2.8 Ga ago. These authors go further in concluding that this re-evaluation of surface mapping with improved resolution from orbiters' various measuring devices (list all devices here) infer the surface to be more dominated by precipitation and runoff water scenarios for Ancient Mars than groundwater scenarios. Groundwater sapping is seen as a later development toward the end of a more complete hydrological system. This differs from conclusions made with Viking data which favored ground water sapping scenarios [33].

Water likely was on the surface and/or present as ground water in two distinct

[1] from Hynek *et al.* [18]

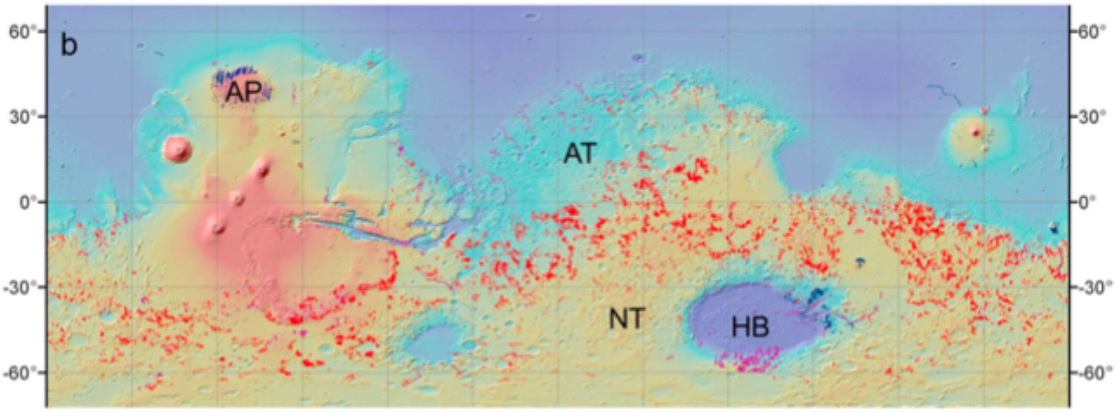

Figure 11.1: Updated Valley locations (shown by red dots) conducted by Hynek *et al.* [18] using THEMIS data on top of MOLA shaded relief map and MOLA topography (high = red and low = blue).

periods in Martian history. The oldest valley systems show geology which requires basic to neutral pH of water and are made up of phylosillocates. Some of these valley systems may have been overlain by more recent deposits. This introduces a problem with the phyllosilicates survival for measuring purposes. It is found through experimentation in acidic environments that the signal of many phyllosilicates is decreased as acidity is increased on their surfaces[106]. Some of these newer aged surfaces showing signs of a second episode of past water which through surface geology appear to be acidic in origin and linked to the increase in volcanism in ancient Mars. Because of the theorized atmospheric loss between the Phyllocian and the Theiikian, the acidity of the water leads to differing CO_2 abundances in the atmosphere. Here, the highest modeled 350mbar atmosphere is associated with the Phyllocian. Thus, the early Phyllocian is associated with basic to neutral waters that would tend toward acidity during the end of this epoch. Then, in a less dense atmosphere during the late Phyllocian and early Theiikian waters appear to be acidic in nature and would for this study be mapped to the 60mbar model runs.

For halophiles an additional requirement to survival are salts. Osterloo *et al.*

[97] have interpreted data from Odssey THEMIS and the MGS–TES instruments to be consistent with the presence of chloride-rich salt deposits dispersed throughout Phyllocian-aged southern highlands with a few results in the Theiikian-aged terrains. These salts generally occur in lowlands such as crater floors and channel beds. Authors also note that on Earth chloride salts can form in varying settings, from saline lakes and groundwater to hydrothermal brines and fumaroles (a hole in a volcanic area where gasses and smoke are expelled) and finally by efflorescence (to become a powder by losing water to crystallization, as when hydrated crystal is exposed to air)[107]. Authors favor precipitation from near-surface brines for the source for depositional origin and suggest that the number and frequency of deposits on Phyllocian aged terrain suggest climates which allow these waters.

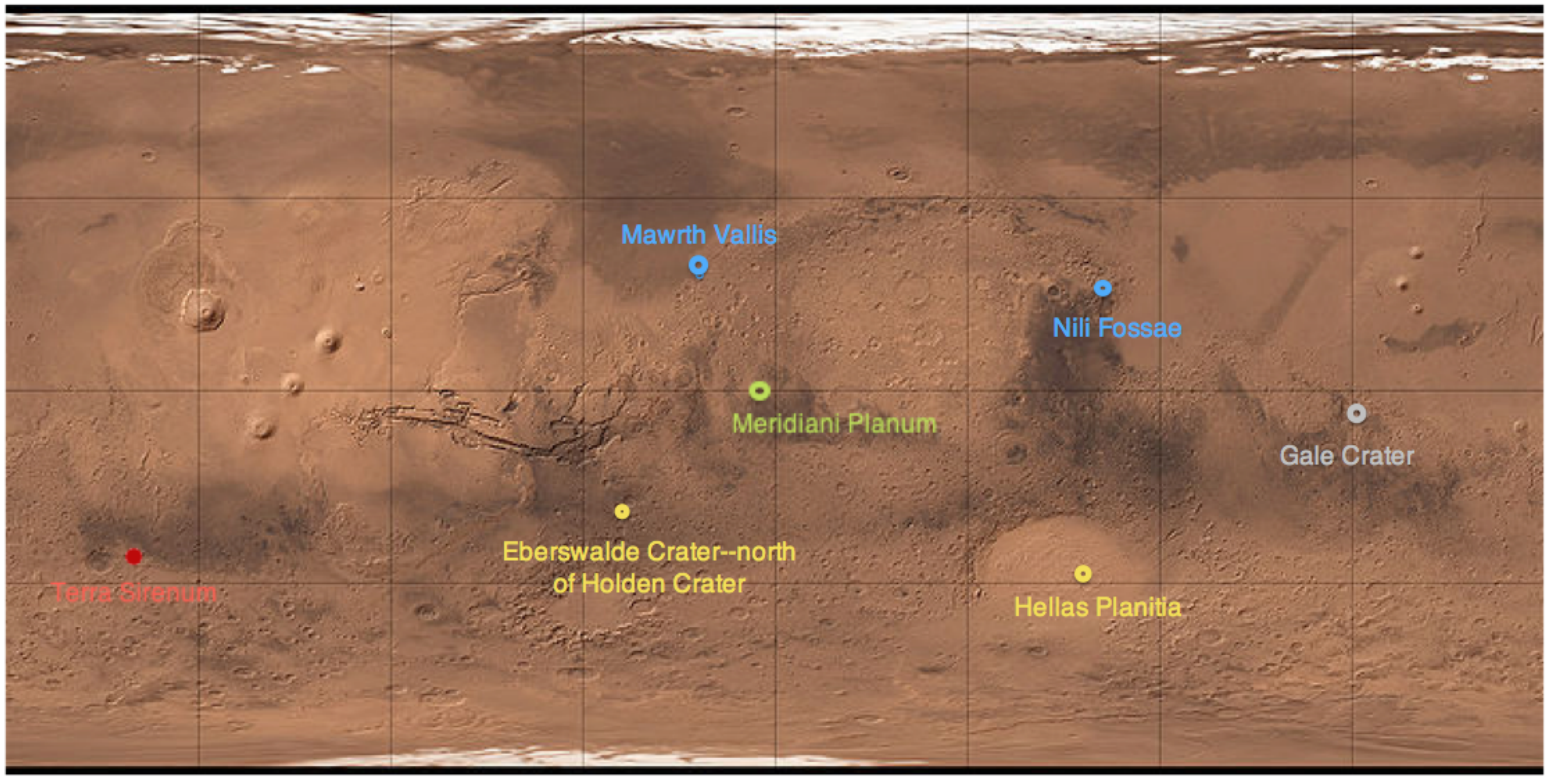

Figure 11.2: Locations on Mars of water signatures discussed as locations of possible extant or extinct life

These chloride salt deposits also show similarities to salt deposits found at Atacama Desert where the cyanobacterium *Chroococcidiopsis sp. 29* was found. Thus, sites with chloride salts could be viable to both *halobacterium sp. NRC-1* and cyanobacterium *Chroococcidiopsis sp. 29*. Terra Sirenum (39.7°S 150°W) has the largest regional chloride deposit on Mars as well as phyllosilicates deposit which appear to pre-date the salt deposits [108]. Thus, an interesting candidate for future missions searching for life.

The Mars Science Laboratory due to launch 2011 is not specifically a life searching mission, but a mission to examine surfaces presumed to be altered by water to enhance geological understanding of processes which acted upon the Martian surface. The final location has not been announced but the mission will investigate one or more of the following areas: Eberswalde Crater (formally known as Holden Crater NE), Gale Crater, Holden Crater, and Mawrth Vallis. These areas would be of interest for life investigations as well since Holden Crater and Mawrth Vallis show signs of two fluvial episodes as seen on Sinus Meridiani (Meridiani Planum is in the western portion and the landing site of the rover Opportunity, it is here hematite and jarosite were found), and Ederswalde crater show signs of a delta and iron/magnesium smectites (phyllosilicates) needing water to form have been inferred through measurements by the Mars Reconnaissance Orbiter. The formation of smectites is important as it is favored in neutral waters and thus not associated with acidic waters. Another location which shows signs of early water and a neutral pH is located in Nili Fossae [109]. Also found in this area of signs of chlorites (ClO_2^-) and carbonates. This indicates that the ancient environment here was not acidic. This may make Nili Fossae especially attractive for the search for life since a very acidic environment could be lethal to the halophiles and possibly cyanobacteria. Nili Fossae is also a source of methane gas release to the present atmosphere and therefore of even more

interest as a possible location for extant methane releasing bacteria [109]. Figure 11.2 indicates the approximate locations of each of locations to search for potential life.

The surface of Mars has not only seen incident UV radiation but also cosmic rays. Mar's ancient magnetic dynamo has been modeled to have produced a magnetic field only in the southern highlands, allowing for atmospheric escape as well as a record of a magnetic field which is seen only in the southern highlands. Because of this cosmic ray influx, the depth of potential life if it exists should be reasoned. Model results by Dartnell *et al.* [110] indicates that cosmic rays incident on the surface of Mars would reduce survivability to depths of 2m today. This indicates that viability is reduced from tests conducted, for example, by de la Vega *et al.* [94] for *D. radiodurans* and excavation would be necessary in future mission with the hope of discovering living organisms. If this depth was exposed, time is vital, as most organisms would die within minutes of excavation when exposed to today's Martian UV flux. Here, studies into biological mechanisms which survive after viability are vital. Cockell *et al.* [15] conducted studies showing certain esterase activity and autofluorescence survived longer than viability but would show signs of recent life even if viability is lost due to UV exposure during excavation. Strategies which included detection of specific biologic activities may be needed if excavation leads to loss of viability for possible extant microorganisms.

Today as more data are arriving and being interpreted from Martian orbiters' instruments, questions can be better addressed as to Mar's ancient history and the possibility of extant or extinct life. Continued work with microorganisms is needed for survivability and viability of extremophiles in various niches available to life on ancient Mars and present day Mars, if only in the subsurface today. Ancient Mars shows signs of habitability during the Phyllocian and possibly during the Theiikian

although the acidic environment is less hospitable for life. A resolution to the question of groundwater pH is needed before Theiikian habitability can be addressed for many microorganisms since high acidity is not tolerable to many Earth-UV resistant microorganisms.

Appendix A: Orbiters and their Instruments

Many orbiters have been to Mars and offer data in various forms from instruments aboard. Below is a list of orbiters with their associated instruments and typical abbreviations used in literature. Information for this listing was gathered from mission websites.

Mars Express (ME)

HRSC – High Resolution Stereo Camera – full color 3D camera with resolution of about 10m with select area resolution to 2m

OMEGA – Visible and Infrared Mineralogical Mapping Spectrometer – 0.5-5.2 micron wavelength range

MARSIS – Sub-surface Sounding Radar Altimeter

PFS – Planetary Fourier Spectrometer

SPICAM – Ultraviolet and Infrared Atmospheric Spectrometer

ASPERA – Energetic Neutral Atoms Analyser

MaRS – Mars Radio Science Experiment

Mars Global Surveyor (MGS)

Instruments:

MOC – Mars Orbiter Camera

MOLA – Mars Orbiter Laser Altimeter

TES – Thermal Emission Spectrometer

MAG/ER – Magnetometer

USO/RS – Ultrastable Oscillator for Doppler measurements

MRSR – Mars relay signal receiver

Mars Reconnaissance Orbiter (MRO)

Instruments:

HiRISE (camera) – High Resolution Imaging Science Experiment camera (resolution 0.3m from an altitude of 300km. Colorbands 400 to 600 nm, 550 to 850 nm and 800 to 1000 nm.

CTX (camera) – Context Camera grayscale images colorbands 500 to 800 nm with resolution of 6m.

MARCI (camera) – Mars Color Imager wide-angle low-resolution camera colorbands 5 visible and 2 ultraviolet wavelengths

CRISM (camera) – Compact Reconnaissance Imaging Spectrometer visible and near-infrared spectromenter used for surface mineralogy

MCS (camera) – Mars Climate Sounder spectrometer with 1 visible/near infrared and 8 far infrared to measure temperature, pressure, water vapor, and dust levels

SHARAD (radar) – Shallow Subsurface Radar probe internal structure of polar caps

Mars Odyssey (MO)

THEMIS – Thermal Emission Imaging System

GRS – Gamma Ray Spectrometer

MARIE – Mars Radiation Environment Experiment

Bibliography

Bibliography

[1] H. H. Kieffer, B. M. Jakosky, C. W. Snyder, and M. S. Matthews, Eds., *Mars (A93-27852 09-91)*. Tuscson: The University of Arizona Press, 1992, ch. 11, pp. 345–382, authors:Tanaka, Kenneth L., Scott, David H., and Greeley, Ronald.

[2] R. Symonds, W. Rose, G. Bluth, and T. Gerlach, *Volatiles in Magmas*. Washington D.C.: Mineralogical Society of America, 1994, pp. 1–66, volcanic Gas Studies - Methods, Results, and Applications.

[3] USGS, "Volcanic gases and their effects," June 2010, last updated. [Online]. Available: http://volcanoes.usgs.gov/hazards/gas/index.php

[4] V. Moroz, "Chemical composition of the atmosphere of Mars," *Advances in Space Research*, vol. 22, pp. 449–457, 1998.

[5] V. Formisano, S. Atreya, T. Encrenaz, N. Ignatiev, and M. Giuranna, "Detection of methane in the atmosphere of Mars," *Science*, vol. 306, pp. 1758–1761, 2004.

[6] H. Nair, M. Allen, A. Anbar, Y. Yung, and R. Clancy, "A photochemical model of the Martian atmosphere," *Icarus*, vol. 111, pp. 124–150, 1994.

[7] H. Holland, *The Chemistry of the Atmosphere and Oceans*. New York, NY: Wiley, 1978.

[8] J.-P. Bibring *et al.*, "Mars surface diversity as revealed by the OMEGA mars express observations," *Science*, vol. 312, pp. 400–404, 2006.

[9] A. Wong, S. Atreya, and T. Encrenaz, "Correction to chemical markers of possible hot spots on Mars," *Journal of Geophysical Research*, vol. 109, 2004, doi:10.1029/2003JE002210.

[10] Y. L. Yung and W. B. DeMore, *Photochemistry of Planetary Atmospheres*. New York: Oxford University Press, 1999.

[11] H. R. Shahmohammadi, E. Asgarani, H. Terato, H. Ide, and O. Yamamoto, "Effects of ^{60}Co gamma-rays, ultraviolet light, and mitomycin c on *Halobacterium salinarium* and *Thiobacillus intermedius*," *Journal of Radiation Research*, vol. 38, pp. 37–43, 1997.

[12] P. Rettberg, E. Rabbow, and G. Horneck, "Biological space experiments for the simulation of martian conditions: Uv radiation and martian soil analogues," *Advances in Space Research*, vol. 33, no. 8, pp. 1294–1301, 2004.

[13] S. McCready, J. A. Muller, I. Boubriak, B. R. Berquist, W. L. Ng, and S. DasSarma, "Uv irradiation induces homologous recombination genes in the model archaeon, *Halobacterium sp. NRC-1*," *Saline Systems*, vol. 1, no. 3, 2005, doi:10.1186/1746-1448-1-3.

[14] G. Weidler, S. Leuko, and H. Stan-Lotter, "Survival and growth of *Halobacterium sp. NRC-1* following incubation at -15 degrees c, freezing or freeze-drying, and the protective effect of cations," ESA, Madrid, Spain, pp. 117–118, 2004, 18-20 November 2003. ESA SP-545, March 2004.

[15] C. S. Cockell, A. C. Schuerger, D. Billi, E. I. Friedmann, and C. Panitz, "Effects of simulated Martian uv flux on the cyanobacterium, *Chroococcidiopsis,sp. 29*," *Astrobiology*, vol. 5, no. 2, pp. 127–140, 2005.

[16] E. Martin, R. Reinhardt, L. Baum, M. Becker, J. Shaffer, and T. Kokjohn, "The effects of ultraviolet radiation on the moderate halophile *Halomonas elongata* and the extreme halophile *Halobacterium salinarum*," *Canadian Journal of Microbiology*, vol. 46, no. 2, pp. 180–187, 2000.

[17] U. P. de la Vega, P. Rettberg, and G. Reitz, "Simulation of the environmental climate conditions on Martian surface and its effect on *Deinococcus radiodurans*," *Advances in Space Research*, vol. 40, pp. 1672–1677, 2007.

[18] B. M. Hynek, M. Beach, and M. R. T. Hoke, "Updated global map of Martian valley networks and implications for climate and hydrologic processes," *Journal of Geophysical Research*, vol. 115, 2010, e09008, doi:10.1029/2009JE003548.

[19] R. Mancinelli, T. Fahlen, R. Landheim, and M. Klovstad, "Brines and evaporites: analogs for martian life," *Advances in Space Research*, vol. 33, no. 8, pp. 1244–1246, 2004.

[20] B. Clark *et al.*, "Chemistry and mineralogy of outcrops at Meridiani Planum," *Earth Planet Sci. Lett.*, vol. 240, pp. 73–94, 2005.

[21] Squyers *et al.*, "In situ evidence for an ancient aqueous environment at Meridiani Planum, Mars," *Science*, vol. 306, pp. 1709–1714, 2004.

[22] A. H. Marcus, "A stochastic model of the formation and survival of lunar craters V. approximate diameter distribution of primary and secondary craters," *Icarus*, vol. 5, no. 1-6, pp. 590–605, 1966.

[23] R. B. Baldwin, "Mars: An estimate of the age of its surface," *Science*, vol. 149, no. 3691, pp. 1498–1499, 1965.

[24] A. H. Marcus, "Martian craters: Number density," *Science*, vol. 160, no. 3834, pp. 1333–1335, 1968.

[25] C. Fassett and J. Head, III, "Valley formation on martian volcanoes in the hesperian: Evidence for melting of summit snowpack, caldera lake formation, drainage and erosion on Ceraunius Tholus," *Icarus*, vol. 189, pp. 118–135, 2007.

[26] O. Popova, I. Nemtchinov, and W. Hartmann, "Bolides in the present and past Martian atmosphere and effects on cratering processes," *Meteoritics and Planetary Science*, vol. 38, pp. 905–925, 2003.

[27] W. Hartmann, "Martian cratering 8: Isochron refinement and the chronology of Mars," *Icarus*, vol. 174, pp. 294–320, 2005.

[28] L. Nyquist, D. Bogard, C.-Y. Shih, A. Greshake, D. Stoffler, and O. Eugster, "Ages and geologic histories of Martian meteorites," *Space Science Reviews*, vol. 96, pp. 105–164, 2001.

[29] T. L. Segura, O. Toon, A. Colaprete, and K. Zahnle, "Environmental effects of large impacts on Mars," *Science*, vol. 298, pp. 1977–1980, 2002.

[30] R. A. Craddock, V. Ansan, A. Howard, and N. Mangold, "Crater modification processes in the aeolis region on Mars," in *39th Lunar and Planetary Science Conference*, League City, Texas, March 2008.

[31] F. Forget, R. Haberle, F. Montmessin, B. Levrard, and J. Head, "Formation of glaciers on Mars by atmospheric precipitation at high obliquity," *Science*, vol. 311, pp. 368–371, 2006.

[32] F. Forget and R. Pierrehumbert, "Warming early Mars with carbon dioxide clouds that scatter infrared radiation," *Science*, vol. 278, pp. 1273–1276, 1997.

[33] V. Gulick, "Origin of the valley networks on Mars: a hydrological perspective," *Geomorphology*, vol. 37, pp. 241–268, 2001.

[34] R. Lundin, H. Lammer, and I. Ribas, "Planetary magnetic fields and solar forcing: Implications for atmospheric evolution," *Space Science Review*, vol. 129, pp. 245–278, 2007.

[35] J. P. Greenwood, S. Itoh, N. Sakamoto, E. P. Vicenzi, and H. Yurimoto, "Hydrogen isotope evidence for loss of water from Mars through time," *Geophysical Research Letters*, vol. 35, 2008, doi:10.1029/2007GL032721.

[36] L. E. Borg, J. N. Connelly, L. E. Nyquist, C.-Y. Shih, and H. Wiesmann, "The age of the carbonates in Martian meteorite alh84001," *Science*, vol. 286, pp. 90–94, 1999.

[37] M. Bullock and J. Moore, "Atmospheric conditions on early mars and the missing layered carbonates," *Geophysical Research Letters*, vol. 34, 2007, l19201, doi: 10.1029/2007GL030688.

[38] H. Lammer, F. Selsis, T. Penz, U. Amerstorfer, H. I. Lichtenegger, C. Kolb, and I. Ribas, "Atmospheric evolution and the history of water on Mars," *Advances in Astrobiology and Biogeophysics*, vol. 4, pp. 23–43, 2005.

[39] D. E. Shean and J. W. Head, "Origin and evolution of a cold-based tropical moutain glacier on Mars: The Pavonis Mons fan-shaped deposit," *Journal of Geophysical Research*, vol. 110, 2005, doi:10.1029/2004JE002360.

[40] J. Laskar, A. Correia, M. Gastineau, F. Joutel, B. Levrard, and P. Robutel, "Long term evolution and chaotic diffusion of the insolation quantities of Mars," *Icarus*, vol. 170, pp. 343–364, 2004.

[41] A. Yen, S. Kim, M. Hecht, M. Frant, and B. Murray, "Evidence that the reactivity of the Martian soil is due to superoxide ions," *Science*, vol. 289, pp. 1909–1912, 2000.

[42] S. K. Atreya, A.-S. Wong, N. O. Renno, W. M. Farrell, G. T. Delory, D. D. Sentman, S. A. Cummer, J. R. Marshall, S. C. Rafkin, and D. C. Catling, "Oxidant enhancement in Martian dust devils and storms: Implications for life and habitability," *Astrobiology*, vol. 6, pp. 439–450, 2006.

[43] Y. Moudden, "Simulated seasonal variations of hydrogen peroxide in the atmosphere of Mars," *Planetary and Space Science*, vol. 55, pp. 2137–2143, 2007.

[44] T. Encrenaz, B. Bezard, T. Greathouse, M. Richter, J. Lacy, S. Atreya, A. Wong, S. Lebonnois, F. Lefevre, and F. Forget, "Hydrogen peroxide on mars: evidence for spatial and seasonal variations," *Icarus*, vol. 170, pp. 424–429, 2004.

[45] F. Poulet, J.-P. Bibring, J. Mustard, A. Gendrin, N. Mangold, Y. Langevin, R. Arvidson, B. Gondet, and C. Gomez, "Phyllosilicates on mars and implications for early martian climate," *Nature*, vol. 438, no. 7068, pp. 623–627, 2005.

[46] M. B. McElroy and T. M. Donahue, "Stability of the Martian atmosphere," *Science*, vol. 177, pp. 986–988, 1972.

[47] T. Parkinson and D. Hunten, "Spectroscopy and acronomy of O_2 on Mars," *Journal of Atmospheric Science*, vol. 29, pp. 1380–1390, 1972.

[48] V. Krasnopolsky, "Photochemistry of the Martian atmosphere (mean conditions)," *Icarus*, vol. 101, pp. 313–332, 1993.

[49] M. E. Summers, B. J. Lieb, E. Chapman, and Y. L. Yung, "get title," *Geophysical Research Letters*, vol. 29, p. 2171, 2002, doi:10.1029/2002GL015377.

[50] A. Wong, S. Atreya, and T. Encrenaz, "Chemical markers of possible hot spots on Mars," *Journal of Geophysical Research*, vol. 108, pp. 5026–5037, 2003.

[51] W. B. DeMore, S. Sander, D. Golden, R. Hampson, M. Kurylo, C. Howard, A. Ravishankara, C. Kolb, and M. Molina, "Chemical kinetics and photochemical data for use in stratospheric modeling, Evalution 12, JPL publication 97-4," NASA, Jet Propulsion Laboratory, California Institute of Technolgy, Pasadena, CA, Tech. Rep., 1997, temperature range 200-300K.

[52] ——, "Chemical kinetics and photochemical data for use in stratospheric modeling, Evalution 11, JPL publication 94-26," NASA, Jet Propulsion Laboratory, California Institute of Technolgy, Pasadena, CA, Tech. Rep., 1994, temperature range 200-300K.

[53] H.-G. Yu and G. Nyman, "Quantum dynamics of the $O(^3P)+CH_4 \rightarrow OH + CH_3$ reaction: An application of the rotating bond umbrella model and spectral transform subspace iteration," *Journal of Chemical Physics*, vol. 112, pp. 238–247, 2000.

[54] R. Zellner, D. Hartmann, J. Karthauser, D. Rhasa, and G. Weibring, "A laser photolysis/lif study of the reactions of $O(^3P)$ atoms with CH_3 and CH_3O_2 radicals," *Journal of the Chemical Society, Faraday Transaction 2: Molecular and Chemical Physics*, vol. 84, pp. 549–568, 1988.

[55] R. Atkinson, D. Baulch, R. Cox, J. Crowley, R. Hampson, R. Hynes, M. Jenkin, M. Rossi, and J. Troe, "Evaluated kinetic and photochemical data for atmospheric chemistry: Volume i gas phase reactions of O_x, H_{ox}, N_{ox} and S_{ox} species," *Atmospheric Chemical Physics*, vol. 4, pp. 1461–1738, 2004.

[56] W. B. DeMore, S. Sander, D. Golden, R. Hampson, M. Kurylo, C. Howard, A. Ravishankara, C. Kolb, and M. Molina, "Chemical kinetics and photochemical data for use in stratospheric modeling, Evalution 13, JPL publication 00-3," NASA, Jet Propulsion Laboratory, California Institute of Technolgy, Pasadena, CA, Tech. Rep., 2000, temperature range 200-300K.

[57] D. Baulch, C. Cobos, R. Cox, C. Esser, P. Frank, T. Just, J. Kerr, M. Pilling, J. Troe, R. Walker, and J. Warnatz, "Evaluated kinetic data for combustion modeling," *Journal of Physical Chemistry Reference Data*, vol. 21, pp. 411–429, 1992.

[58] R. Atkinson, D. Baulch, R. Cox, J. Hampson, R.F., J. Kerr, M. Rossi, and J. Troe, "Evaluated kinetic, photochemical and heterogeneous data for atmospheric chemistry: supplement V, IUPAC subcommittee on gas kinetic data

evaluation for atmospheric chemistry," *Journal of Physical Chemistry Reference Data*, vol. 26, pp. 521–1011, 1997.

[59] S. Sander, D. Golden, R. Hampson, M. Kurylo, C. Howard, A. Ravishankara, C. Kolb, and M. Molina, "Chemical kinetics and photochemical data for use in stratospheric modeling, Evalution 15, JPL publication 06-02," NASA, Jet Propulsion Laboratory, California Institute of Technolgy, Pasadena, CA, Tech. Rep., 2006, temperature range 200-300K.

[60] T. Reiner and F. Arnold, "Laboratory investigations of gaseous sulfuric acid formation via SO_3+H_2O + M $\rightarrow$ H_2SO_4 + M: measurement of the rate constant and product identification," *Journal of Physical Chemistry*, vol. 101, pp. 7399–7407, 1994, measurements at 298K.

[61] V. C. Gulick and V. R. Baker, "Fluvial valleys and Martian palaeoclimates," *Nature*, vol. 341, pp. 514–516, 1989.

[62] J. Pollack, J. Kasting, S. Richardson, and K. Poliakoff, "Fluvial valleys and Martian palaeoclimates," *Icarus*, vol. 71, no. 2, pp. 203–204, 1989.

[63] G. Plumlee, "Implications for volcanogenic volatile release on the weathering of mars," in *Lunar and Planetary Institute MSATT Workshop on Chemical Weathering on Mars*, Houston, Texas, 1992.

[64] J. Kasting, "Co_2 condensation and the climate of early Mars," *Icarus*, vol. 94, no. 1, pp. 514–516, 1991.

[65] M. Mischna, J. Kasting, A. Pavlov, and R. Freedman, "Influence of carbon dioxide clouds on early martian climate," *Icarus*, vol. 145, pp. 546–554, 2000.

[66] Y. L. Yung, H. Nair, and M. Gerstell, "Co_2 greenhouse in the early Martian atmosphere: SO_2 inhibits condensation," *Icarus*, vol. 130, pp. 222–224, 1997.

[67] F. Tian, M. W. Claire, J. D. Haqq-Misra, M. Smith, D. C. Crisp, D. Catling, K. Zahnle, and J. F. Kasting, "Photochemical and climate consequences of sulfur outgassing on early Mars," *Earth and Planetary Science Letters*, vol. 295, pp. 412–418, 2010.

[68] N. Mangold, A. Gendrin, B. Gondet, S. LeMouelic, C. Quantin, V. Ansan, J.-P. Bibring, Y. Langevin, P. Masson, and G. Neukum, "Spectral and geological study of the sulfate-rich region of West Candor Chasma, Mars," *Icarus*, vol. 194, pp. 519–543, 2008.

[69] E. Noe Dobrea, F. Poulet, and M. M.C., "Correlations between hematite and sulfates in the chaotic terrain east of Valles Marineris," *Icarus*, vol. 193, pp. 516–534, 2008.

[70] M. Settle, "Formation and deposition of volcanic sulfate aerosols on Mars," *Journal of Geophysical Research*, vol. 84, 1979, b14.

[71] S. S. Johnson, A. A. Pavlov, and M. A. Mischna, "Fate of so_2 in the ancient Martian atmosphere: Implications for transient greenhouse warming," *Journal of Geophysical Research*, vol. 114, 2009, e11011, doi:10.1029/2008/JE003313.

[72] I. Halevy, M. T. Zuber, and D. P. Schrag, "Sulfur dioxide climate feedback on early Mars," *Science*, vol. 318, pp. 1903–1907, 2007.

[73] P. Archer Jr., A. Pavlov, and P. Smith, "Atmospheric methane and Martian climate," in *Seventh International Conference on Mars*, Pasadena, California, July 2007.

[74] R. Navarro-Gonzalez, K. F. Navarro, J. de la Rosa, E. Iniguez, P. Molina, L. D. Miranda, P. Morales, E. Cienfuegos, P. Coll, F. Raulin, R. Amils, and C. P. McKay, "The limitations on organic detection in Mars-like soils by thermal volatilization–gas chromatography–MS and their implications for the Viking results," *Proceedings of the National Academy of Sciences*, vol. 103, no. 44, pp. 16 089–16 094, 2006, physical Sciences, Chemistry.

[75] D. Schulze-Makuch, L. Irwin, J. Lipps, D. LeMone, J. Dohm, and A. Fairen, "Scenarios for the evolution of life on Mars," *Journal of Geophysical Research-Planets*, vol. 110, 2005, article Number: E12S23.

[76] J. Wierzchos, C. Ascaso, and C. P. McKay, "Endolithic cyanobacteria in halite rocks from the hyperarid core of the atacama desert," *Astrobiology*, vol. 6, no. 3, pp. 415–422, 2006.

[77] G. Landis, "Martian water: Are there extant halobacteria on Mars?" *Astrobiology*, vol. 1, no. 2, pp. 161–164, 2001.

[78] J. M. Houtkooper and D. Shulze-Makuch, "A possible biogenic origin for hydrogen peroxide on Mars: the Viking results reinterpreted," *International Journal of Astrobiology*, vol. 6, pp. 147–152, 2007.

[79] A. Shapiro, D. D., L. M.C., K. D.E., and H. S.H., "Minimal requirements in defined media for improved growth of some radio-resistant pink *tetracocci.*" *Applied Environmental Microbiology*, vol. 33, p. 11291133, 1977.

[80] J. Battista, "Against all odds: The survival strategies of *Deinococccus radiodurans*," *Annual Review of Microbiology*, vol. 51, pp. 203–224, 1997.

[81] R. H. Vreeland, J. Jones, A. Monson, W. D. Rosenzweig, T. K. Lowenstein, M. Timofeeff, C. Satterfield, B. C. Cho, J. S. Park, A. Wallace, and W. D. Grant, "Isolation of live cretaceous (121–112 million years old) halophilic Archaea from primary salt crystals," *Geomicrobiology Journal*, vol. 24, pp. 275–282, 2007.

[82] W.-A. Joo and C.-W. Kim, "Proteomics of halophilic archaea," *Journal of Chromatography B*, vol. 815, no. 1–2, pp. 237–250, 2004.

[83] S. Squyres, J. Grotzinger, R. Arvidson, J. Bell III, W. Calvin, P. Christensen, B. Clark, J. Crisp, W. Farrand, K. Herkenfoff, J. Johnson, G. Klingelhofer, A. Knoll, S. McLennan, H. McSween Jr., R. Morris, J. Rice Jr., R. Rieder, and L. Soderblom, "In situ evidence for an ancient aqueous environment at Meridiani Planum, Mars," *Science*, vol. 306, pp. 1709–1715, 2004.

[84] C. Marnocha, V. Chevrier, and D. Ivey, "Sulfate-reducing bacteria as a model for life in the Martian subsurface," LPI, The Woodlands, Texas, p. 1536, 2010, contribution No. 1533.

[85] A. Wargin, K. Olanczuk-Neyman, and M. Skucha, "Sulfate-Reducing bacteria, their properties and methods of elimination from groundwater," *Polish Journal of Environmental Studies*, vol. 16, pp. 639–644, 2007.

[86] N. Shpigel, S. Elazar, and I. Rosenshine, "Mammary pathogenic *Escherichia coli*," *Curr. Opin. Micro.*, vol. 11, pp. 60–65, 2008.

[87] J. F. Kasting, "Climatic effects of enhanced CO_2 levels in Mars early atmosphere," pp. 64–66, 1987, lunar and Planetary Institute, MECA Symposium on Mars: Evolution of its Climate and atmosphere, see N89-10780 01-91.

[88] M. Summers and D. Strobel, "Photochemistry of the atmosphere of Uranus," *Astrophysical Journal*, vol. 346, pp. 495–508, 1989.

[89] B. M. Jakosky and R. J. Phillips, "Mars' volatile and climate history," *Nature*, vol. 412, no. 6843, pp. 237–244, 2001.

[90] B. Moseley, "Repair of ultraviolet radiation damage in sensitive mutants of *Micrococcus radiodurans*," *Journal of Bacteriology*, vol. 97, no. 2, pp. 647–652, 1969.

[91] J. K. Setlow and M. Boling, "The resistance of *Micrococcus radiodurans* to ultraviolet radiation," *Biochimica et Biolphysica Acta*, vol. 108, pp. 259–265, 1965.

[92] J. C. Sutherland, "Repair dependent radiation survival: a stocastic model with Euler gamma function solutions," *Physical Medical Biology*, vol. 51, pp. 4883–4901, 2006.

[93] G. Horneck, "The microbial case for Mars and its implication for human expeditions to Mars," *Acta Astronautica*, vol. 63, pp. 1015–1024, 2008.

[94] U. P. D. L. Vega, P. Rettberg, T. Douki, J. Cadet, and G. Horneck, "Sensitivity to polychromatic UV-radiation of strains of *Deinococcus radiodurans* differing in their DNA repair capacity," *International Journal of Radiation Biology*, vol. 81, no. 8, pp. 601–611, 2005.

[95] C. Sabanayagam, "Searching for life in our solar system with light microscopy," August 2010. [Online]. Available: http://spie.org/x41212.xml?ArticleID=x41212

[96] C. S. Cockell, C. P. McKay, K. Warren-Rhodes, and G. Horneck, "Ultraviolet radiation–induced limitations to epilithic microbial growth in arid deserts – dosimetric experiments in the hyperarid core of the Atacama Desert," *Journal of Photochemistry and Photobiology B: Biology*, vol. 90, no. 2, pp. 79–87, 2008.

[97] M. Osterloo, V. Hamilton, J. Bandfield, T. Glotch, A. Baldridge, P. Christensen, L. Tornabene, and F. Anderson, "Chloride-bearing materials in the southern highlands of Mars," *Science*, vol. 39, pp. 1651–1654, 2008.

[98] S. Fendrihan, A. Berces, H. Lammer, M. Musso, G. Ronto, T. Polacsek, A. Holzinger, C. Kolb, and H. Stan-Lotter, "Investigating the effects of simulated Martian ultraviolet radiation on *Halococcus dombrowskii* and other extremely halophilic archaebacteria," *Astrobiology*, vol. 9, no. 1, pp. 104–112, 2009.

[99] U. P. de la Vega, P. Rettberg, T. Douki, J. Cadet, and G. Horneck, "Sensitivity to polychromatic UV-radiation of strains of *Deinococcus radiodurans* differing in their dna repair capacity," *International Journal of Radiation Biology*, vol. 81, no. 8, pp. 601–611, 2005.

[100] U. P. D. L. Vega, P. Rettberg, and G. Reitz, "Simulation of the envrionmental climate conditions on Martian surface and its effect on *Deinococcus radiodurans*," *Advances in Space Research*, vol. 40, pp. 1672–1677, 2007.

[101] B. Diaz and D. Schulze-Makuch, "Microbial survival rates of *Escherichia coli* and *Deinococcus radioduans* under low termperature, low pressure, and UV–radiation conditions, and their relevance to possible Martian life," *Astrobiology*, vol. 6, pp. 332–347, 2006.

[102] A. Benabbou, Z. Derriche, C. Felix, P. Lejeune, and C. Guillard, "Photocatalytic inactivation of escherischia coli effect of concntration of TiO_2 and microorganism, nature, and intensity of UV irradiation," *Applied Catalysis B: Environmental*, vol. 76, pp. 257–263, 2007.

[103] G. D. Achille, B. M. Hynek, and M. L. Searls, "Positive identification of lake strandlines in Shalbatana Vallis, Mars," *Journal of Geophysical Research Letters*, vol. 36, 2009, L14201, doi:10.1029/2009GL038854.

[104] K. R. Stockstill, J. E. Moersch, H. Y. M. Jr., J. Piatek, and P. R. Christensen, "TES and THEMIS study of proposed paleolake basins within the Aeolis quadrangle of Mars," *Journal of Geophysical Research*, vol. 112, 2007, e01001, doi:10.1029/2005JE002517.

[105] S. M. Wiseman, R. E. Arvidson, R. V. Morris, F. Poulet, J. C. Andrews-Hanna, J. L. Bishop, S. L. Murchie, F. P. Seelos, D. D. Marais, and J. L. Griffes, "Spectral and stratigraphic mapping of hydrated sulfate and phyllosilicate–bearing deposits in northern Sinus Meridiani, Mars," *Journal of Geophysical Research*, vol. 115, 2010, e00D18, doi:10.1029/2009JE003354.

[106] T. Altheide and V. Chevrier, "Acidic weathering of Martian-relevant phyllosilicates," in *Proceedings from the 2009 40th Lunar and Planetary Science Conference*, The Woodlands, Texas, March 2009.

[107] Http://www.thefreedictionary.com/.

[108] T. D. Glotch, J. L. Bandfield, L. L. Tornabene, H. B. Jensen, and F. P. Seelos, "Distribution and formation of chlorides and phyllosilicates in Terra Serenum, Mars," *Geophysical Research Letters*, vol. 37, 2010, l16202, doi:10.1029/2010GL044557.

[109] V. Chevrier, "Phyllosilicates, carbonates, methane and the habitability of Nili Fossae on early Mars," in *Astrobiology Science Conference 2010*, League City, Texas, April 2010.

[110] L. R. Dartnell, L. Desorgher, J. M. Ward, and A. J. Coates, "Modelling the surface and subsurface Martian radiation environment: Implications for astrobiology," *Geophysical Reseearch Letters*, vol. 34, 2006, L02207, doi:10.1029/2006GL027494.

Curriculum Vitae

Mary Ewell received her Bachelor of Science in Physics and Mathematics in 1994 from George Mason University. She received the Gayle Solomon's award that year as the outstanding senior in Physics and Mathematics. She received her Masters of Science in Engineering and Applied Physics in 2000 from George Mason University. She has been employed since 1995 by the department of Physics and Astronomy at George Mason University teaching undergraduate laboratories. She presently coordinates instructors for the University Physics Lab II.